

OMEN-SED 1.0: A new, numerically efficient sediment module for the coupling to Earth System Models

Dominik Hülse¹, Sandra Arndt^{1,2}, Stuart Daines³, Pierre Regnier², and Andy Ridgwell^{1,4}

¹School of Geographical Sciences, University of Bristol, Clifton, Bristol BS8 1SS, UK

²Department of Earth and Environmental Sciences, Université Libre de Bruxelles, Brussels, Belgium

³Earth System Science, University of Exeter, North Park Road, Exeter EX4 4QE, UK

⁴Department of Earth Sciences, University of California, Riverside, CA 92521, USA

Correspondence to: Dominik Hülse (Dominik.Huelse@bristol.ac.uk)

Abstract. Here we describe the first version of a new, analytical early diagenetic model resolving organic matter cycling and associated biogeochemical dynamics in marine sediments called OMEN-SED (Organic Matter ENabled SEDiment model). Most biogeochemical cycles and reactions in the surface sediments can be related either directly or indirectly to the degradation of organic matter.

- Despite its fundamental importance, an appropriate Earth system model of the coupled atmosphere-ocean-sediment system which is able to model all relevant processes and feedbacks over geological time-scales currently does not exist. The major problem is the high computational cost of simulating the essential redox reactions in marine sediments which are important to calculate burial of organic matter and benthic recycling fluxes of chemical compounds. In most Earth system models sediment-water dynamics are either neglected or treated in a very simplistic way. To provide a more realistic description of organic matter degradation and nutrient cycles in marine sediments we have developed OMEN-SED, a new, one-dimensional, numerically efficient reactive transport model. OMEN-SED is the first analytical model to explicitly describe organic matter cycling as well as associated dynamics of the most important terminal electron acceptors (i.e. O₂, NO₃, SO₄), related reduced substances (NH₄, H₂S), the full suite of secondary-redox reactions, macronutrients (PO₄) and associated pore water quantities (ALK, DIC). To represent a redox-dependent sedimentary P cycle we consider the formation and burial of Fe-bound P and authigenic Ca-P minerals. Thus, OMEN-SED captures most of the features of a complex, numerical diagenetic model, however, its computational efficiency allows the coupling to global Earth System models and therefore the investigation of coupled global biogeochemical dynamics over different timescales. This paper provides a detailed description of

the new sediment model, **tested with observations, SA and global observations** and describes it's coupling to the Earth System model cGENIE.

Contents

1	Introduction	4
25	2 Model Description	9
2.1	General Model Approach	10
2.2	Conservation Equations and Analytical Solution	13
2.2.1	Organic matter or Particulate Organic Carbon (POC)	13
2.2.2	Oxygen	14
30	2.2.3 Nitrate and Ammonium	16
2.2.4	Sulfate and Sulfide	17
2.2.5	Phosphate	19
2.2.6	Dissolved Inorganic Carbon (DIC)	22
2.2.7	Alkalinity	23
35	2.3 Determination of Integration Constants	25
2.3.1	Generic Boundary Condition Matching (GBCM)	25
2.3.2	Abstracting out the bioturbation boundary	26
2.4	Model Parameters	28
2.4.1	Transport Parameters	28
40	2.4.2 Reaction Parameters and Stoichiometries	29
3	Stand-alone sensitivity analysis and case studies	31
3.1	Sensitivity Analysis	31
3.1.1	Methodology	31
3.1.2	Results	33
45	3.2 Case study: Simulations of sediment cores	36
3.2.1	Methodology	36
3.2.2	Results	37
3.3	Case study: Stand-alone simulations of global ocean transect	39
3.3.1	Methodology	39
50	3.3.2 Results	41
4	Coupled pre-industrial Earth system model simulations	43
4.1	Coupling to the cGENIE Earth system model	43
4.2	Coupled pre-industrial simulations	45
4.2.1	Methodology	45

55	4.2.2 Results	47
5 Scope of applicability and model limitations		51
6 Conclusions		53
7 Code Availability		54
A Reaction Network		54
60 B Sensitivity Analysis		54
B1		54

1 Introduction

Dominik: Introduction needs polishing, this is my first draft

DH: Will delete the sub-headings!

65 Role of marine sediments for climate and global biogeochemical cycles:

Marine surface sediments are key components in the Earth system. They host the largest carbon reservoir within the surficial Earth system, provide the only long term sink for atmospheric CO₂, recycle nutrients and represent the most important geochemical archive used for deciphering past changes in biogeochemical cycles and climate (e.g. Berner, 1991; Archer and Maier-Reimer, 1994; Ridgwell and Zeebe, 2005; Arndt et al., 2013). Physical and chemical processes in sediments (i.e. diagenetic processes) depend on the water column and vice versa: Diagenesis is controlled by the external supply of solid material (e.g. organic matter, calcium carbonate, opal) from the water column and is affected by overlying bottom water concentrations of solutes. At the same time, sediments impact the water column directly either by short- and long-term storage of deposited material or diagenetic processing of deposited material and diffusion of some of the resulting products (e.g. nutrients, DIC) to the overlying bottom waters. This so-called benthic-pelagic coupling is essential for understanding global biogeochemical cycles and climate (e.g. Archer and Maier-Reimer, 1994; Archer et al., 2000; Soetaert et al., 2000; Mackenzie, 2005).

80 Biological primary production of organic matter (OM, CH₂O in equation R1) and the reverse process of degradation can be written in a greatly simplified reaction as:



On geological timescales production of OM is generally greater than degradation which results in some organic matter being buried in marine sediments and oxygen accumulating in the atmosphere. Thus burial of OM leads to net oxygen input to, and CO₂ removal from the atmosphere (Berner, 2004). On shorter timescales, the upper few meters of the sediments where early diagenesis occurs are specifically important as this zone controls whether a substance is recycled to the water column or buried for a longer period of time in the deeper sediments (Hensen et al., 2006). Most biogeochemical cycles and reactions in this part of marine sediments can be related either directly or indirectly to the degradation of organic matter (Arndt et al., 2013). Oxygen and nitrate for instance, the most powerful electron acceptors, are consumed in the course of the degradation of organic matter, resulting in the release of ammonium and phosphorus to the pore water. As such, degradation of OM in the sediments can profoundly affect the oxygen and nutrient inventory of the ocean and thus primary productivity (Van Cappellen and Ingall, 1994; Lenton and Watson, 2000). Furthermore, organic matter degradation releases metabolic CO₂ to the pore water, causing it to have a lower pH and provoking the dissolution of CaCO₃ (Emerson and Bender, 1981).

Nutrient recycling from marine sediments has been suggested to play a key role for climate and ocean biogeochemistry for different events during Earth history. For example, feedbacks between

phosphorus storage and erosion from shelf sediments and marine productivity have been hypothesised to play an important role for glacial/interglacial atmospheric CO₂ changes (Broecker, 1982; 100 Ruttenberg, 1993). Furthermore, nutrient recycling from anoxic sediments has been invoked to explain the occurrence of more extreme events in Earth history, for instance Oceanic Anoxic Events (OAEs, e.g. Mort et al., 2007; Tsandev and Slomp, 2009). OAEs represent severe disturbances of the global carbon, oxygen and nutrient cycles of the ocean and are usually characterized by widespread bottom water anoxia and photic zone euxinia (Jenkyns, 2010). One way to explain the genesis and 105 persistence of OAEs is increased oxygen demand due to enhanced primary productivity. Increased nutrient inputs to fuel primary productivity may have come from marine sediments as the burial efficiency of phosphorus declines when bottom waters become anoxic (Ingall and Jahnke, 1994; Van Cappellen and Ingall, 1994). The recovery from OAE like conditions is thought to involve the permanent removal of excess CO₂ from the atmosphere and ocean by burying carbon in the form 110 of organic matter in marine sediments (e.g. Arthur et al., 1988; Jarvis et al., 2011), which is consistent with the geological record of widespread black shale formation (Stein et al., 1986). However, the overall amount, exact timing and the rate of organic matter burial remain a topic of an ongoing debate. Therefore, globally quantifying the burial and degradation of organic matter in marine sediments and related biogeochemical dynamics is important for understanding climate and the cycling 115 of many chemical elements on various timescales.

Diagenetic Models:

Quantifications of diagenetic processes are possible through the application of idealised mathematical representations of diagenesis, or so-called diagenetic models (see e.g. Berner, 1980; Boudreau, 1997). The number of research questions that can be addressed with diagenetic models is infinite 120 and a plethora of different approaches have been developed, mainly following two distinct directions (Arndt et al., 2013). First, state-of-the art vertically resolved numerical models simulating the entire suite of essential coupled redox and equilibrium reactions within marine sediments (e.g. BRNS, Aguilera et al., 2005; CANDI, Boudreau, 1996; MEDIA, Meysman et al., 2003; STEADYSED, Van Cappellen and Wang, 1996). These “complete”, non-steady-state models, thus resolve the resulting characteristic redox-zonation of marine sediments through explicitly including oxic OM 125 degradation, denitrification, oxidation by manganese and iron (hydr)oxides, sulfate reduction and methanogenesis as well as the reoxidation of reduced byproducts (i.e. NH₄, Mn²⁺, Fe²⁺, H₂S, CH₄, see e.g. Regnier et al., 2011; Arndt et al., 2013). Furthermore, they incorporate various mineral dissolution and precipitation reactions, as well as fast equilibrium sorption processes for example of NH₄, PO₄ and metal ions (i.e. Mn²⁺, Fe²⁺ and Mg²⁺, compare Van Cappellen and Wang, 1996; Meysman et al., 2003). Modelled, depth-dependent, transport processes usually comprise advection, diffusion, bioturbation and bio-irrigation. This group of diagenetic models generally uses a so-called multi-G approach (Jørgensen, 1978; Berner, 1980), thus dividing the bulk organic matter pool into a number of compound classes that are characterised by different degradabilities k_i ,

135 which are generally dependent on the type and concentration of the specific terminal electron acceptor (TEA). Alternative approaches, in particular reactive continuum models (Boudreau and Ruddick, 1991), assume a continuous distribution of reactive types but are much less often used. These complex, “complete” models have a great potential for quantifying OM degradation dynamics for sites where enough observations are available to constrain its model parameters (see e.g. Boudreau et al.,
140 1998; Wang and Van Cappellen, 1996; Thullner et al., 2009, for applications). However, due to the high degree of coupled processes and depth-varying parameters the diagenetic equation needs to be solved numerically, thus resulting in a very high computational demand and consequently rendering their application in an Earth system model framework prohibitive. Additionally, their global applicability is limited by the restricted transferability of model parameters from one site to the global
145 scale (Arndt et al., 2013).

The second group of models solves the diagenetic equation analytically or semi-analytically, thus providing an alternative and computational more efficient approach. However, finding an analytical solution, especially when complex reaction networks are to be considered, is not straightforward and generally requires the assumption of steady state. The complexity of the reaction network can be reduced by dividing the sediment column into distinct zones and accounting for the most pertinent biogeochemical processes within each zone, thus increasing the likelihood of finding an analytical solution. In general, analytical diagenetic models are less sophisticated and comprehensive than numerical models and are used for the coupling to global ESMs (e.g. HAMOCC and NorESM use the model of Heinze et al. (1999)) or box models (e.g. DCESS, Shaffer et al., 2008 or MBM using MEDUSA, Munhoven, 2007). These analytic or semi-analytical models account for the most important transport processes (i.e advection, bioturbation and molecular diffusion) through basic parametrizations and include fewer biogeochemical reactions which are generally restricted to the upper, bioturbated 10 cm of the sediments. They assume that the sedimentary organic matter pool is composed of just a single compound class which is either degraded with a globally invariant
150 degradation rate constant (Munhoven, 2007) or a fixed rate constant depending on local oxygen concentrations (Shaffer et al., 2008; Palastanga et al., 2011). Pore water tracers explicitly represented in DCESS (Shaffer et al., 2008) and the HAMOCC model of Heinze et al. (1999) and Palastanga et al. (2011) are restricted to DIC, TA, PO₄ and O₂. The MEDUSA model (Munhoven, 2007) considers CO₂, HCO₃⁻, CO₃²⁻ and O₂. Other species produced or consumed during OM degradation are neglected. Thus, with oxygen being the only TEA explicitly modelled the influence of reduced species
155 is only implicitly included in the boundary conditions for O₂. A newer versions of the HAMOCC model, being a notable exception, as Ilyina et al. (2013) include NO₃ and denitrification explicitly. Furthermore, the version of Palastanga et al. (2011) represents an redox-dependent explicit sedimentary phosphorus cycle. Yet, reoxidation of reduced byproducts, so-called secondary redox-reactions,
160 or sorption processes are not included in any of the discussed models.

How are sediments resolved in Earth system models:

Earth system models generally track the biogeochemical dynamics of organic and inorganic carbon, essential nutrients (nitrogen, phosphorus) and oxygen with the aim of investigating the evolution of the ocean's redox structure and carbonate system and its feedbacks on global climate. This general
175 aim thus defines a minimum set of state variables and reaction processes that need to be resolved for an efficient representation of the benthic-pelagic coupling in Earth system models. A suitable sediment model has to provide a robust quantification of organic (and inorganic) carbon burial fluxes, as well as benthic uptake/return fluxes of oxygen, growth-limiting nutrients and reduced species. As a consequence, the reaction network must account for the most important primary and secondary
180 redox reactions, equilibrium reactions, mineral precipitation/dissolution and adsorption/desorption, resulting in a complex set of coupled reaction-transport equations.

Even though there are more appropriate sediment representations, in most current ESMs sediment-water dynamics are either neglected or treated in a very simplistic way (Soetaert et al., 2000; Hülse et al., 2017). Most Earth system Models of Intermediate Complexity (EMICs) and also some of
185 the higher resolution global carbon cycle models represent the sediment-water interface either as a reflective or a conservative/semi-reflective boundary (Hülse et al., 2017). Thus, all particulate material deposited on the seafloor is either instantaneously consumed (reflective boundary), or a fixed fraction is buried in the sediments (conservative/semi-reflective boundary). Both highly simplified approaches furthermore completely neglect the exchange of solute species through the sediment-
190 water interface and, therefore, cannot resolve the complex benthic-pelagic coupling. However, due to their computational efficiency, both representations are often used in global biogeochemical models (e.g. Najjar et al., 2007; Ridgwell et al., 2007; Goosse et al., 2010). A superior approach is the vertically integrated dynamic model, which represents the whole sediment column as a single box (Hülse et al., 2017). Here, OM deposited on the seafloor is added to the sediment box where
195 it gets degraded and dissolved species diffuse through the sediment-water interface in accordance with these transformations. This approach thus ignores the vertical extent of the sediments and the temporary storage of dissolved species (Soetaert et al., 2000). Yet, it is computationally efficient and allows differentiating between various fractions of organic matter. Most EMICs incorporate a vertically integrated dynamic model for particulate inorganic carbon only (i.e. mainly CaCO_3) and
200 just a few consider oxic-only sediment degradation of organic matter (Hülse et al., 2017).

The most complex description of diagenetic organic matter degradation in Earth system models is the second group of vertically resolved diagenetic models as discussed above (e.g. Heinze et al., 1999; Munhoven, 2007; Shaffer et al., 2008). These models solve the one-dimensional reaction-transport equation for a number of solid and dissolved species for the upper, bioturbated 10 cm
205 of the sediments. Examples of global ESMs employing a vertically resolved diagenetic model are NorESM (Tjiputra et al., 2013) and HAMOCC (Palastanga et al., 2011; Ilyina et al., 2013), both using a version of Heinze et al. (1999). None of the EMICs reviewed by Hülse et al. (2017) use such a

sediment representation. DCESS (Shaffer et al., 2008) and MBM (Munhoven, 2007) are box models employing a vertically resolved diagenetic model. However, in general oxygen is the only TEA explicitly modelled and secondary redox reactions and reduced species are completely neglected in these approaches. Furthermore, all models represent the bulk OM pool as a single fraction with a fixed degradation rate constant.

Problem with that:

Obviously, such a simplification of the OM pool can neither account for the observed vast structural complexity in natural organic matter and its resulting different degradation rates nor for the rapid decrease in OM degradability in the uppermost centimetres of the sediments (Arndt et al., 2013). It has been suggested that at least a 3G approach is necessary to accurately represent organic matter dynamics in this part of the sediments where most OM is degraded (e.g. Soetaert et al., 1996). Even more restrictive is the use of O₂ as the only TEA and the complete absence of reduced substances and related secondary redox reactions. Even though for the majority of the modern sediments (i.e. in the deep-ocean) O₂ is the primary electron acceptor and Archer et al. (2002) suggested that aerobic degradation accounts for 66% of total organic matter respiration more recent model and data studies have reported that sulfate reduction is the dominant degradation pathway on a global average (with contributions of 55-76% Canfield et al., 2005; Jørgensen and Kasten, 2006; Thullner et al., 2009).

Oxygen becomes progressively less important as TEA with decreasing seafloor depth and sulfate reduction has been shown to account for 83% of OM degradation in coastal sediments (Krumins et al., 2013). In these environments most O₂ is used to reoxidise reduced substances produced during anaerobic degradation (Canfield et al., 2005; Thullner et al., 2009). Thus, the in situ production of e.g. NO₃ and SO₄ through oxidation of NH₄ and H₂S forms an important sink for O₂ which is entirely neglected in current sediment representations in global models. In addition, due to the lack of an appropriate sedimentary P cycle (with the exception of the HAMOCC version of Palastanga et al. (2011), no current global ESM is able to model the redox dependent P release from marine sediments and its implications for primary productivity, global biogeochemical cycles and climate.

Solution presented here:

Analytical approaches with distinct biogeochemical zones were implemented and used in the seventies and eighties to describe observed pore water profiles (e.g. Vanderborght and Billen, 1975; Vanderborght et al., 1977; Billen, 1982; Goloway and Bender, 1982) and later for inclusion into global Earth system models (Tromp et al., 1995). However, in addition to the oxic zone these models only describe one anoxic zone, either a denitrification (Vanderborght and Billen, 1975; Vanderborght et al., 1977; Billen, 1982; Goloway and Bender, 1982) or a sulfate reduction zone (Tromp et al., 1995). Furthermore, the approaches of Vanderborght and Billen (1975), Goloway and Bender (1982) and Tromp et al. (1995) do not explicitly model the produced reduced species (i.e. NH₄ and H₂S, respectively). In addition, the model of Tromp et al. (1995) ignores reoxidation of H₂S produced during sulfate reduction. In order to provide a more realistic description of organic matter

245 degradation and nutrient cycles in marine sediments we have developed the OrganicMatter ENabled
246 SEDiment model (OMEN-SED), a new, one-dimensional, numerically efficient reactive transport
247 model. OMEN-SED is the first analytical model to explicitly describe OM cycling as well as associ-
248 ated dynamics of the most important TEAs (i.e. O₂, NO₃, SO₄), related reduced substances (NH₄,
249 H₂S), the full suite of secondary-redox reactions, macronutrients (PO₄) and associated pore water
250 quantities (ALK, DIC). To represent a redox-dependent sedimentary P cycle we consider the for-
251 mation and burial of Fe-bound P and authigenic Ca-P minerals. Thus, OMEN-SED captures most
252 of the features of a complex, numerical diagenetic model, however, its computational efficiency al-
253 lows the coupling to global Earth system models and therefore the investigation of coupled global
254 biogeochemical dynamics over different timescales. Here, the model is presented as a 2G-approach,
255 however, a third, non-degradable OM fraction can easily be added and OMEN-SED can be further
256 extended to a Multi-G approach.

The first part of the paper provides a detailed description of OMEN-SED (Section 2). This in-
257 cludes descriptions of the general model approach (Section 2.1), of the conservation equations for
258 all explicitly represented biogeochemical tracers (Section 2.2), as well as a summary of global re-
259 lationships used to constrain reaction and transport parameters in OMEN-SED (Section 2.4). In
260 addition, a generic algorithm is described which is used to match internal boundary conditions and
261 to determine the integration constants for the analytical solutions (Section 2.3). In order to validate
262 the stand-alone version of OMEN-SED the second part of the paper performs an extensive sensitivity
263 analysis for the most important model parameters and resulting sediment-water interface fluxes are
264 compared with a global database (Section 3.1). In addition, results of the stand-alone model are com-
265 pared with observed pore water profiles from different ocean depths (Section 3.2) and OMEN-SED
266 simulations of TEA-fluxes along a typical ocean transect are compared with observations and results
267 from a complete, numerical diagenetic model (Section 3.3). Thereafter, the coupling of OMEN-SED
268 to the carbon-centric version of the “GENIE” Earth system model (cGENIE, Ridgwell et al., 2007)
269 is describe (Section 4.1). Sensitivity studies are carried out using this coupled model and modelled
270 organic matter concentrations in the surface sediments are compared to a global database (Seiter
et al., 2004, Section 4.2). Finally, potential applicabilities of OMEN-SED are suggested and model
271 limitations are critically analyzed (Section 5).

2 Model Description

275 OMEN-SED is a new, one-dimensional, computationally efficient reaction-transport model is de-
276 signed for the coupling to regional/global biogeochemical and Earth system models. OMEN-SED
277 is implemented as a Fortran version that can be easily coupled to a pelagic model via the coupling
278 routine **OMEN_SED_main**. In addition, OMEN-SED exists as a stand-alone version implemented
279 in MATLAB and the entire model can be executed on a standard personal computer in less than

280 0.1 seconds. The source code of both, the Fortran and the MATLAB stand-alone version, as well as instructions for executing OMEN-SED and for plotting model results are available as a supplement to this paper. The following section provides a detailed description of OMEN-SED. Tables 1 and 15 summarise the biogeochemical reaction network and Tables 9 and 10 provide a glossary of model parameters along with their respective units.

285 **2.1 General Model Approach**

In OMEN-SED, the calculation of benthic uptake, recycling and burial fluxes is generally based on the vertically resolved conservation equation for solid and dissolved species in porous media (e.g. Berner, 1980; Boudreau, 1997):

$$\frac{\partial \xi C_i}{\partial t} = -\frac{\partial}{\partial z} \left(-\xi D_i \frac{\partial C_i}{\partial z} + \xi w C_i \right) + \xi \sum_j R_i^j \quad (1)$$

290 where C_i is the concentration of biogeochemical species i , ξ equals the porosity ϕ for solute species and $(1 - \phi)$ for solid species. The term z is the sediment depth, t denotes the time, D_i is the apparent diffusion coefficient of species i ($D_i = D_{i,0} + D_{\text{bio}} = D_{\text{mol},i} \cdot f_{ir} + D_{\text{bio}}$ for dissolved species and $D_i = D_{\text{bio}}$ for solid species), w is the burial rate and $\sum_j R_i^j$ represents the sum of all biogeochemical rates j affecting species i .

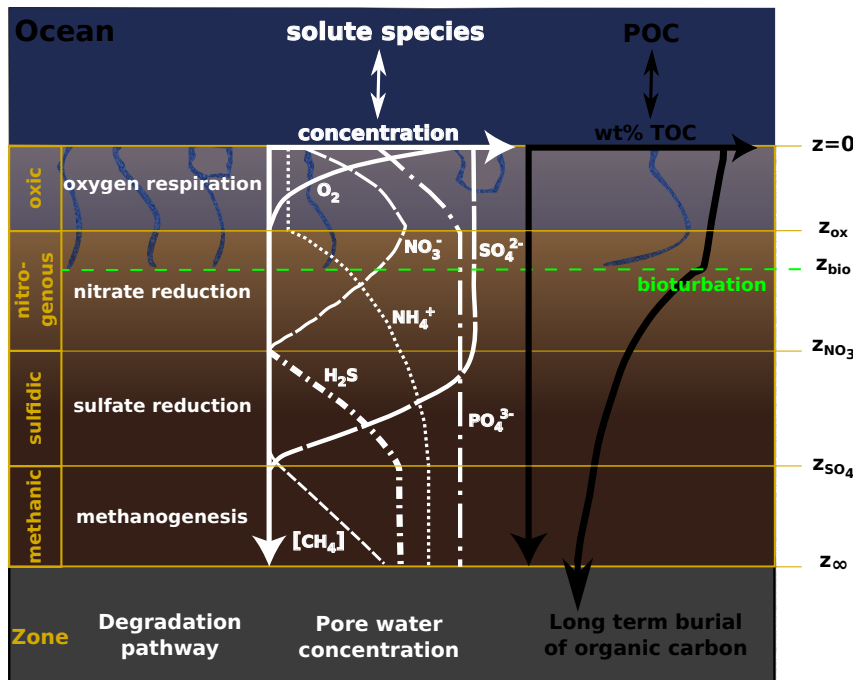


Figure 1. Schematic of the different modelled species and zones in OMEN-SED. Here showing the case $z_{\text{ox}} < z_{\text{bio}} < z_{\text{NO}_3} < z_{\text{SO}_4}$.

SA: maybe include some examples and test figures in supplement?

Table 1. Reactions and biogeochemical tracers implemented in the reaction network of OMEN-SED. The primary and secondary redox reactions are listed in the sequence they occur with increasing sediment depth.

Description	
Primary redox reactions	Degradation of organic matter via aerobic degradation, denitrification, sulfate reduction, methanogenesis (implicit)
Secondary redox reactions	Oxidation of ammonium and sulfide by oxygen, anaerobic oxidation of methane by sulfate
Adsorption/Desorption	Ad-/Desorption of P on/from Fe(OH) ₃ , NH ₄ adsorption, PO ₄ adsorption
Mineral precipitation	Formation of authigenic P
Biogeochemical tracers	Organic matter (2-G), oxygen, nitrate, ammonium, sulfate, sulfide (hydrogen sulfide), phosphate, Fe-bound P, DIC, ALK

295 OMEN-SED accounts for both the advective, as well as the diffusive transport of dissolved and solid species. Solid and dissolved species are buried in the sediment according to a constant burial rate w , thus neglecting the effect of sediment compaction (i.e. $\frac{\partial\phi}{\partial z} = 0$) due to mathematical constraints. The molecular diffusion of dissolved species is described by Fick's law applying a species-specific apparent diffusion coefficient, $D_{\text{mol},i}$. In addition, the activity of infaunal organisms in the
300 bioturbated zone is simulated using a diffusive term (e.g. Boudreau, 1986), with a constant bioturbation coefficient D_{bio} in the bioturbated zone, while D_{bio} is set to zero below the maximum bioturbation depth, z_{bio} . The pumping activity by burrow-dwelling animals and the resulting ventilation of tubes, the so-called bioirrigation, is encapsulated in a factor f_{ir} that enhances the molecular diffusion coefficient (hence, $D_{i,0} = D_{\text{mol},i} \cdot f_{ir}$, Soetaert et al., 1996). The reaction network of
305 OMEN-SED accounts for the most important primary and secondary redox reactions, equilibrium reactions, mineral dissolution and precipitation, as well as adsorption and desorption processes that affect the dissolved and solid species explicitly resolved in OMEN-SED. Tables 1 and 15 provide a summary of the reactions and biogeochemical tracers considered in OMEN-SED together with their respective reaction stoichiometries.

310 All parameters in Eq. (1) may vary with depth and many reaction rate expressions depend on the concentration of other species. Expressing Eq. (1) for a set of chemical species thus results in a non-linear, coupled set of equations that can only be solved numerically. However, OMEN-SED is designed for the coupling to Earth system models and, therefore, cannot afford a computationally expensive numerical solution. Yet, a computationally efficient analytical solution of Eq. (1) can be
315 derived by 1) assuming steady state conditions (i.e. $\frac{\partial C_i}{\partial t} = 0$) and 2) reducing the vertical variability in parameters and reaction rate expressions by dividing the sediment column into a number of functional biogeochemical zones (Fig. 1, compare e.g. Billen, 1982; Goloway and Bender, 1982; Tromp et al., 1995; Gypens et al., 2008, for similar solutions). More specifically, OMEN-SED divides the sediment column into: I) a bioturbated and II) a non-bioturbated zone defined by an imposed, con-

SA: Tab 1 is maybe a bit redundant? **DH:** I still think it's a good summary/overview!? and the other one could go into the appendix!?

stant bioturbation depth z_{bio} (Fig. 1). Furthermore, it resolves the dynamic redox stratification of marine sediments by dividing the sediment into 1) an oxic zone delineated by the oxygen penetration depth z_{ox} ; 2) a denitrification (or nitrogenous) zone situated between z_{ox} and the nitrate penetration depth z_{NO_3} ; 3) a sulfate reduction zone situated between z_{NO_3} and the sulfate penetration depth z_{SO_4} ; and 4) a methanogenic zone situated below z_{SO_4} (Fig. 1). In each of these zones Eq. (1) is applied with depth invariant parameters. Yet, parameter values may differ across zones. The biogeochemical zones are linked by stating continuity in both concentrations and fluxes at the dynamic, internal boundaries ($z_b \in \{z_{\text{bio}}, z_{\text{ox}}, z_{\text{NO}_3}, z_{\text{SO}_4}\}$). These boundaries are dynamic because their depth varies in response to changing ocean boundary conditions and forcings (see Section 2.3.1 for details). Furthermore, the maximum bioturbation depth is not restricted to a specific biogeochemical zone, hence OMEN-SED allows bioturbation to occur in the anoxic zones of the sediment (here all zones $z > z_{\text{ox}}$ combined). In addition, the formulation of the reaction term in Eq. (1) varies between zones and encapsulates the most pertinent reaction processes within the respective zone (see Section 2.2), thus simplifying the mathematical description of the reaction network while retaining most of its biogeochemical complexity.

All consumption or production processes of dissolved species related to the degradation of organic matter are a function of the organic matter concentration and, because first-order decay is assumed in the kinetic expression, can be expressed as a series of exponential terms ($\sum_j \alpha_j \exp(-\beta_j z)$, see Eq. (2)). In addition, slow adsorption/desorption and mineral precipitation processes can be expressed as zero or first order (reversible) reaction (Q or $k \cdot (C_i - \tilde{C})$, in Eq. (2)). Fast adsorption is described as an instantaneous equilibrium reaction using a constant adsorption coefficient K_i . The reoxidation of reduced substances is accounted for implicitly by adding a (consumption/production) flux to the internal boundary conditions (see Sections 2.2.2, 2.2.3 and 2.2.4 **SA: make reference to the section where this is explained in detail**). This simplification has been used previously by Gypens et al. (2008) for nitrate and ammonium and can be justified as it has been shown that the reoxidation mainly occurs within a thin layer at the oxic/anoxic interface (Soetaert et al., 1996). The general reaction-transport equation of OMEN-SED is thus given by:

$$\frac{\partial C_i}{\partial t} = 0 = \frac{D_i}{1 + K_i} \frac{\partial^2 C_i}{\partial z^2} - w \frac{\partial C_i}{\partial z} - \frac{1}{1 + K_i} \left(k \cdot (C_i - \tilde{C}) + \sum_j \alpha_j \exp(-\beta_j z) - Q \right) \quad (2)$$

where $1/\beta_j$ can be interpreted as the length scale and α_j as the relative importance (or the magnitude at $z = 0$) of reaction j (Boudreau, 1997), k is a generic first order reaction rate constant, \tilde{C} is an equilibrium or asymptotic concentration of C and Q is a zeroth-order (or constant) reaction rate.

The analytical solution of Eq. (2) is of the general form:

$$C_i(z) = A \exp(az) + B \exp(bz) + \sum_j \frac{\alpha_j}{D\beta_j^2 - w\beta_j - k} \cdot \exp(-\beta_j z) + \frac{Q}{k} \quad (3)$$

DH: Do you mean these sections? Not discussed in further details anywhere else

with

$$355 \quad a = \frac{w - \sqrt{w^2 + 4 \cdot D \cdot k}}{2 \cdot D}, \quad b = \frac{w + \sqrt{w^2 + 4 \cdot D \cdot k}}{2 \cdot D} \quad (4)$$

where A and B are integration constants that can be determined by applying a set of internal boundary conditions (see Section 2.3).

Based on Eq. (2) and its analytical solution Eq. (3), OMEN-SED returns the fraction of particulate organic carbon (POC) buried in the sediment, f_{POC} , as well as the benthic uptake/return fluxes F_{C_i} 360 of dissolved species C_i (in mol cm $^{-2}$ year $^{-1}$) in response to changing boundary conditions and forcings:

$$f_{\text{POC}} = \frac{\text{POC}(z_\infty)}{\text{POC}(0)} \quad (5)$$

$$F_{C_i} = \phi(0) \left(D_i \frac{\partial C_i(z)}{\partial z} \Big|_{z=0} - w [C_i(0) - C_i(z_\infty)] \right) \quad (6)$$

365 where w is the deposition rate, D_i is the diffusion coefficient and $\text{POC}(0)$, $\text{POC}(z_\infty)$, $C_i(0)$, $C_i(z_\infty)$ denotes the concentration of POC and dissolved species i at the SWI and at the lower sediment boundary, respectively.

2.2 Conservation Equations and Analytical Solution

2.2.1 Organic matter or Particulate Organic Carbon (POC)

370 In marine sediments, particulate organic carbon (POC) is degraded by heterotrophic activity coupled to the sequential utilisation of terminal electron acceptors according to the free energy gain of the half-reaction $(\text{O}_2 > \text{NO}_3^- > \text{MnO}_2 > \text{Fe(OH)}_3 > \text{SO}_4^{2-}$, e.g. Stumm and Morgan, 2012). Here, organic matter degradation is described via a multi G-model approach (Arndt et al., 2013, and references therein), dividing the bulk OM into a number i of discrete compound classes POC_i 375 characterised by class-specific first-order degradation rate constants k_i . The conservation equation for organic matter dynamics is thus given by:

$$\frac{\partial \text{POC}_i}{\partial t} = 0 = D_{\text{POC}_i} \frac{\partial^2 \text{POC}_i}{\partial z^2} - w \frac{\partial \text{POC}_i}{\partial z} - k_i \cdot \text{POC}_i \quad (7)$$

380 with $D_{\text{POC}_i} = D_{\text{bio}}$ for $z \leq z_{\text{bio}}$ and $D_{\text{POC}_i} = 0$ for $z > z_{\text{bio}}$. Integration of equations (7) yields the following general solutions:

I. Bioturbated zone ($z \leq z_{\text{bio}}$)

$$\text{POC}_i^I(z) = A_{1i} \cdot \exp(a_{1i}z) + B_{1i} \cdot \exp(b_{1i}z)$$

which using the boundary condition at $z = 0$ can be rewritten as:

$$385 \quad \text{POC}_i^I(z) \stackrel{\text{BC1}}{=} A_{1i} \cdot [\exp(a_{1i}z) - \exp(b_{1i}z)] + \text{POC}_{0i} \cdot \exp(b_{1i}z) \quad (8)$$

Table 2. OM Boundary conditions applied in OMEN-SED. For the boundaries we define: $z_{\text{bio}}^- := \lim_{h \rightarrow 0} (z_{\text{bio}} - h)$ and $z_{\text{bio}}^+ := \lim_{h \rightarrow 0} (z_{\text{bio}} + h)$.

Boundary	Condition	
$z = 0$	known concentration	1) $\text{POC}_i(0) = \text{POC}_{0i}$
$z = z_{\text{bio}}$	continuity	2) $\text{POC}_i(z_{\text{bio}}^-) = \text{POC}_i(z_{\text{bio}}^+)$ 3) $-D_{\text{bio}} \cdot \frac{\partial \text{POC}_i}{\partial z} \Big _{z_{\text{bio}}^-} = 0$

II. Non-bioturbated zone ($z_{\text{bio}} < z$)

$$\text{POC}_i^{II}(z) = A_{2i} \cdot \exp(a_{2i}z) \quad (9)$$

390 where

$$a_{1i} = \frac{w - \sqrt{w^2 + 4 \cdot D_{\text{POC}_i} \cdot k_i}}{2 \cdot D_{\text{POC}_i}}, \quad b_{1i} = \frac{w + \sqrt{w^2 + 4 \cdot D_{\text{POC}_i} \cdot k_i}}{2 \cdot D_{\text{POC}_i}}, \quad a_{2i} = -\frac{k_i}{w} \quad (10)$$

Determining the integration constants ($A_{1,i}$, $B_{1,i}$, $A_{2,i}$) requires the definition of a set of boundary conditions (Table 2). For organic matter, OMEN-SED applies a known concentration/flux at the sediment-water interface and assumes continuity across the bottom of the bioturbated zone, z_{bio} .

395 See Section 2.3.1 for further details on how to find the analytical solution.

2.2.2 Oxygen

OMEN-SED explicitly accounts for oxygen consumption by the aerobic degradation of organic matter within the oxic zone, as well as the oxidation of reduced species (i.e. NH_4 , H_2S) produced in the anoxic zones of the sediment. In the oxic zone ($z < z_{\text{ox}}$), the aerobic degradation consumes oxygen 400 with a fixed $\text{O}_2 : \text{C}$ ratio (O_2C , Tab. 10). A predefined fraction, γ_{NH_4} , of the ammonium produced during the aerobic degradation of OM is nitrified to nitrate, consuming two moles of oxygen per mole of ammonium produced. In addition, OMEN-SED implicitly accounts for the oxygen consumption due to oxidation of reduced species (NH_4 , H_2S) produced below the oxic zone through the flux boundary condition at the dynamically calculated (**SA:** see section ?? for details) oxygen 405 penetration depth z_{ox} . All oxygen consumption processes can thus be formulated as a function of organic matter degradation. The conservation equation for oxygen is given by: **SA: I'd show the POC substitution in the equations below:**

$$\frac{\partial \text{O}_2}{\partial t} = 0 = D_{\text{O}_2} \frac{\partial^2 \text{O}_2}{\partial z^2} - w \frac{\partial \text{O}_2}{\partial z} - \frac{1-\phi}{\phi} \sum_i k_i \cdot [\text{O}_2\text{C} + 2\gamma_{\text{NH}_4} \text{NC}_i] \cdot \text{POC}_i(z) \quad (11)$$

410 which, using Eq. (8) and (9) for the depth-distribution of $\text{POC}_i(z)$, can be written as:

DH: comment Sandra,
which Section do you
mean here?

DH: you mean the way I
did it or in the solution?
I think it's easier to
understand (also how to
get the solution) if it's
done in the ODE

I Bioturbated zone ($z \leq z_{\text{bio}}$)

$$415 \quad \frac{\partial O_2^I}{\partial t} = 0 \stackrel{8}{=} D_{O_2}^I \frac{\partial^2 O_2}{\partial z^2} - w \frac{\partial O_2}{\partial z} - \frac{1-\phi}{\phi} \sum_i k_i \cdot [O_2 C + 2\gamma_{NH_4} NC_i] \cdot \left(A_{1i} \cdot [exp(a_{1i}z) - exp(b_{1i}z)] + POC_{0i} \cdot exp(b_{1i}z) \right)$$

II Non-bioturbated zone ($z_{\text{bio}} < z < z_{\text{ox}}$)

$$\frac{\partial O_2^{II}}{\partial t} = 0 \stackrel{9}{=} D_{O_2}^{II} \frac{\partial^2 O_2}{\partial z^2} - w \frac{\partial O_2}{\partial z} - \frac{1-\phi}{\phi} \sum_i k_i \cdot [O_2 C + 2\gamma_{NH_4} NC_i] \cdot \left(A_{2i} \cdot exp(a_{2i}z) \right)$$

420 where $D_{O_2}^I$ and $D_{O_2}^{II}$ denote the O_2 diffusion coefficient for the bioturbated and non-bioturbated zone, respectively. The term $\frac{1-\phi}{\phi}$ accounts for the volume conversion from solid to dissolved phase and NC_i is the nitrogen to carbon ratio in OM. **SA: explain all terms**

Integration yields the following analytical solution for each zone:

DH: Other terms are explained earlier in 2.2.2 or 2.2.1

425 I Bioturbated zone ($z \leq z_{\text{bio}}$):

$$O_2^I(z) = A_{O_2}^1 + B_{O_2}^1 \cdot exp(b_{O_2}^1 z) + \sum_i \Phi_{1,i}^I \cdot exp(a_{1i}z) + \sum_i \Phi_{1,i}^{II} \cdot exp(b_{1i}z) + \sum_i \Phi_{1,i}^{III} \cdot exp(b_{1i}z) \quad (12)$$

II Non-bioturbated zone ($z_{\text{bio}} < z < z_{\text{ox}}$)

$$430 \quad O_2^{II}(z) = A_{O_2}^2 + B_{O_2}^2 \cdot exp(b_{O_2}^2 z) + \sum_i \Phi_{i,2}^I \cdot exp(a_{2i}z) \quad (13)$$

with

$$435 \quad \begin{aligned} b_{O_2}^1 &= \frac{w}{D_{O_2}^I}, \quad b_{O_2}^2 = \frac{w}{D_{O_2}^{II}} \\ \Phi_{1,i}^I &= \frac{1-\phi}{\phi} \cdot \frac{k_i \cdot (O_2 C + 2\gamma_{NH_4} NC_i) \cdot A_{1i}}{D_{O_2}^I (-a_{1i})^2 - w \cdot (-a_{1i})}, \quad \Phi_{1,i}^{II} = -\frac{1-\phi}{\phi} \cdot \frac{k_i \cdot (O_2 C + 2\gamma_{NH_4} NC_i) \cdot A_{1i}}{D_{O_2}^I (-b_{1i})^2 - w \cdot (-b_{1i})} \\ \Phi_{1,i}^{III} &= \frac{1-\phi}{\phi} \cdot \frac{k_i \cdot (O_2 C + 2\gamma_{NH_4} NC_i) \cdot POC_{0i}}{D_{O_2}^I (-b_{1i})^2 - w \cdot (-b_{1i})} \\ \Phi_{i,2}^I &:= \frac{1-\phi}{\phi} \cdot \frac{k_i \cdot (O_2 C + 2\gamma_{NH_4} NC_i) \cdot A_{2i}}{D_{O_2}^{II} (-a_{2i})^2 - w \cdot (-a_{2i})} \end{aligned}$$

Determining the four integration constants ($A_{O_2}^1, B_{O_2}^1, A_{O_2}^2, B_{O_2}^2$, see Section 2.3 for details), as well as the *a priori* unknown oxygen penetration depth requires the definition of five boundary conditions (see Table 3). At the sediment-water interface, OMEN-SED applies a Dirichlet condition (i.e. known concentration) and assumes concentration and flux continuity across the bottom of the bioturbated zone, z_{bio} . The oxygen penetration depth z_{ox} marks the lower boundary and is dynamically calculated as the depth at which $O_2(z) = 0$. Therefore, OMEN-SED applies a Dirichlet boundary condition $O_2(z_{\text{ox}}) = 0$. In addition, a flux boundary is applied that implicitly accounts for the oxygen consumption by the partial oxidation of NH_4 and H_2S diffusing into the oxic zone

Table 3. Boundary conditions for oxygen. For the boundaries we define: $z_{\text{bio}}^- := \lim_{h \rightarrow 0} (z_{\text{bio}} - h)$ and $z_{\text{bio}}^+ := \lim_{h \rightarrow 0} (z_{\text{bio}} + h)$.

Boundary	Condition	
$z = 0$	known concentration	1) $O_2(0) = O_{20}$
$z = z_{\text{bio}}$	continuity	2) $O_2(z_{\text{bio}}^-) = O_2(z_{\text{bio}}^+)$
$z = z_{\text{ox}}$	O_2 consumption ($z_{\text{ox}} = z_\infty$)	3) $-(D_{O_2,0} + D_{\text{bio}}) \cdot \frac{\partial O_2}{\partial z} \Big _{z_{\text{bio}}^-} = -D_{O_2,0} \cdot \frac{\partial O_2}{\partial z} \Big _{z_{\text{bio}}^+}$
	$(z_{\text{ox}} < z_\infty)$	4) IF ($O_2(z_\infty) > 0$) 4.1) $\frac{\partial O_2}{\partial z} \Big _{z_{\text{ox}}} = 0$ ELSE
	with	4.2) $O_2(z_{\text{ox}}) = 0 \quad \text{and} \quad -D_{O_2} \cdot \frac{\partial O_2}{\partial z} \Big _{z_{\text{ox}}} = F_{\text{red}}(z_{\text{ox}})$ $F_{\text{red}}(z_{\text{ox}}) = \frac{1-\phi}{\phi} \cdot \int_{z_{\text{ox}}}^{\infty} \sum_i (2\gamma_{\text{NH}_4} \text{NC}_i + 2\gamma_{\text{H}_2\text{S}} \text{SO}_4 \text{C}) k_i \text{POC}_i dz$

445 from below (BC 4.2, Table 3). It is assumed that respective fractions (γ_{NH_4} and $\gamma_{\text{H}_2\text{S}}$) are directly reoxidised at the oxic/anoxic interface and the remaining fraction escapes reoxidation. OMEN-SED iteratively solves for z_{ox} by first testing if there is oxygen left at z_∞ (i.e. $O_2(z_\infty) > 0$) and, otherwise, by finding the root for the flux boundary condition 4.2 (Table 3). If $z_{\text{ox}} = z_\infty$, a zero flux boundary condition is applied as lower boundary condition.

DH: Edited explanation of finding z_{ox}

450 2.2.3 Nitrate and Ammonium

Nitrogen dynamics in OMEN-SED are controlled by the metabolic production of ammonium, nitrification, denitrification as well as ammonium adsorption. Ammonium is produced by organic matter degradation in both the oxic and anoxic zones, while denitrification consumes nitrate in the denitrification zone with a fixed $\text{NO}_3^- : \text{C}$ ratio ($\text{NO}_3^- \text{C}$, Tab. 10) **SA: need explanation**. The adsorption of 455 ammonium to sediment particles is formulated as an equilibrium process with constant equilibrium adsorption coefficient K_{NH_4} , thus assuming that the adsorption is fast compared with the characteristic time scales of transport processes (Wang and Van Cappellen, 1996). In addition, a defined fraction, γ_{NH_4} , of metabolically produced ammonium is directly nitrified to nitrate in the oxic zone, while the nitrification of upward diffusing ammonium produced in the sulfidic and methanic zones 460 is implicitly accounted for in the boundary conditions. The conservation equations for ammonium and nitrate are thus given by:

DH: explanation sufficient?

1. Oxic zone ($z \leq z_{\text{ox}}$)

$$465 \quad \frac{\partial \text{NO}_3^I}{\partial t} = 0 = D_{\text{NO}_3} \frac{\partial^2 \text{NO}_3^I}{\partial z^2} - w \frac{\partial \text{NO}_3^I}{\partial z} + \gamma_{\text{NH}_4} \frac{1-\phi}{\phi} \cdot \sum_i \text{NC}_i \cdot k_i \cdot \text{POC}_i(z) \quad (14)$$

$$465 \quad \frac{\partial \text{NH}_4^I}{\partial t} = 0 = \frac{D_{\text{NH}_4}}{1+K_{\text{NH}_4}} \frac{\partial^2 \text{NH}_4^I}{\partial z^2} - w \frac{\partial \text{NH}_4^I}{\partial z} + \frac{1-\gamma_{\text{NH}_4}}{1+K_{\text{NH}_4}} \cdot \frac{1-\phi}{\phi} \cdot \sum_i \text{NC}_i \cdot k_i \cdot \text{POC}_i(z) \\ (15)$$

2. Denitrification (or nitrogenous) zone ($z_{\text{ox}} < z \leq z_{\text{NO}_3}$)

$$470 \quad \frac{\partial \text{NO}_3^{II}}{\partial t} = 0 = D_{\text{NO}_3} \frac{\partial^2 \text{NO}_3^{II}}{\partial z^2} - w \frac{\partial \text{NO}_3^{II}}{\partial z} - \frac{1-\phi}{\phi} \text{NO}_3 \text{C} \cdot \sum_i k_i \cdot \text{POC}_i(z) \quad (16)$$

$$470 \quad \frac{\partial \text{NH}_4^{II}}{\partial t} = 0 = \frac{D_{\text{NH}_4}}{1+K_{\text{NH}_4}} \frac{\partial^2 \text{NH}_4^{II}}{\partial z^2} - w \frac{\partial \text{NH}_4^{II}}{\partial z} \quad (17)$$

3. Sulfidic and methanic zone ($z_{\text{NO}_3} < z \leq z_{\infty}$)

$$475 \quad \frac{\partial \text{NH}_4^{III}}{\partial t} = 0 = \frac{D_{\text{NH}_4}}{1+K_{\text{NH}_4}} \frac{\partial^2 \text{NH}_4^{III}}{\partial z^2} - w \frac{\partial \text{NH}_4^{III}}{\partial z} + \frac{1}{1+K_{\text{NH}_4}} \cdot \frac{1-\phi}{\phi} \cdot \sum_i \text{NC}_i \cdot k_i \cdot \text{POC}_i(z) \\ (18)$$

475 where D_{NO_3} and D_{NH_4} denote the diffusion coefficients for NO_3 and NH_4 which depend on the bioturbation status of the respective geochemical zone (compare Section 2.3.1). Integration of Eq. (14) - (18) yields the analytical solutions, which are not further developed here but follow the procedure outlined in Section 2.2.2 for oxygen (also see Section 2.3.1 for more details on how to find the analytical solution). Table 4 summarises the boundary conditions applied in OMEN-SED to solve Eq. (14) - (18) and to find the *a priori* unknown nitrate penetration depth, z_{NO_3} . The model assumes known bottom water concentrations for both NO_3 and NH_4 , the complete consumption of nitrate at the nitrate penetration depth (in case $z_{\text{NO}_3} < z_{\infty}$) and no change in nitrate and ammonium flux at z_{∞} . In addition, concentration and diffusive flux continuity across z_{bio} and z_{ox} is considered for NO_3 and NH_4 . Furthermore, the reoxidation of upward-diffusing reduced ammonium is accounted for in the oxic-anoxic boundary condition for nitrate and ammonium. OMEN-SED iteratively solves for z_{NO_3} by first testing if there is nitrate left at z_{∞} (i.e. $\text{NO}_3(z_{\infty}) > 0$) and, otherwise, by finding the root for the flux boundary condition 6.2 (Table 4).

DH: all other params explained earlier

2.2.4 Sulfate and Sulfide

Below the denitrification zone ($z > z_{\text{NO}_3}$), organic matter degradation is coupled to sulfate reduction, consuming sulfate and producing hydrogen sulfide with a fixed $\text{SO}_4 : \text{C}$ ratio ($\text{SO}_4 \text{C}$, Tab. 10). In addition, the anaerobic oxidation of upward diffusing methane (AOM) produced below the sulfate penetration and the associated consumption of sulfate and production of sulfide; as well as the production of sulfate and consumption of sulfide through sulfide oxidation are implicitly accounted for through the boundary conditions (Table 5). The conservation equations for sulfate and sulfide are thus given by:

Table 4. Boundary conditions for nitrate and ammonium. For the boundaries we define: $z_-^- := \lim_{h \rightarrow 0} (z_- - h)$ and $z_+^+ := \lim_{h \rightarrow 0} (z_- + h)$.

Boundary	Condition	
$z = 0$	known concentration	1) $\text{NO}_3(0) = \text{NO}_{30}$
$z = z_{\text{bio}}$	continuity	2) $\text{NO}_3(z_{\text{bio}}^-) = \text{NO}_3(z_{\text{bio}}^+)$
$z = z_{\text{ox}}$	continuity	3) $-(D_{\text{NO}_3,0} + D_{\text{bio}}) \cdot \frac{\partial \text{NO}_3}{\partial z} _{z_{\text{bio}}^-} = -D_{\text{NO}_3,0} \cdot \frac{\partial \text{NO}_3}{\partial z} _{z_{\text{bio}}^+}$
	where:	4) $\text{NO}_3(z_{\text{ox}}^-) = \text{NO}_3(z_{\text{ox}}^+)$
$z = z_{\text{NO}_3}$	NO_3 consumption ($z_{\text{NO}_3} = z_\infty$)	5) $-D_{\text{NO}_3} \cdot \frac{\partial \text{NO}_3}{\partial z} _{z_{\text{ox}}^-} + \gamma_{\text{NH}_4} \cdot F_{\text{NH}_4}(z_{\text{ox}}) = -D_{\text{NO}_3} \cdot \frac{\partial \text{NO}_3}{\partial z} _{z_{\text{ox}}^+}$ $F_{\text{NH}_4}(z_{\text{ox}}) = \frac{1}{1+K_{\text{NH}_4}} \cdot \frac{1-\phi}{\phi} \cdot \int_{z_{\text{NO}_3}}^\infty \sum_i \text{NC}_i \cdot k_i \cdot \text{POC}_i dz$
		6) IF ($\text{NO}_3(z_\infty) > 0$)
		6.1) $\frac{\partial \text{NO}_3}{\partial z} _{z_{\text{NO}_3}} = 0$
		ELSE
		6.2) $\text{NO}_3(z_{\text{NO}_3}) = 0 \quad \text{and} \quad \frac{\partial \text{NO}_3}{\partial z} _{z_{\text{NO}_3}} = 0$
$z = 0$	known concentration	1) $\text{NH}_4(0) = \text{NH}_{40}$
$z = z_{\text{bio}}$	continuity	2) $\text{NH}_4(z_{\text{bio}}^-) = \text{NH}_4(z_{\text{bio}}^+)$
$z = z_{\text{ox}}$	continuity	3) $-\frac{D_{\text{NH}_4,0} + D_{\text{bio}}}{1+K_{\text{NH}_4}} \cdot \frac{\partial \text{NH}_4}{\partial z} _{z_{\text{bio}}^-} = -\frac{D_{\text{NH}_4,0}}{1+K_{\text{NH}_4}} \cdot \frac{\partial \text{NH}_4}{\partial z} _{z_{\text{bio}}^+}$
	where:	4) $\text{NH}_4(z_{\text{ox}}^-) = \text{NH}_4(z_{\text{ox}}^+)$
$z = z_{\text{NO}_3}$	continuity flux	5) $-\frac{D_{\text{NH}_4}}{1+K_{\text{NH}_4}} \cdot \frac{\partial \text{NH}_4}{\partial z} _{z_{\text{ox}}^-} - \gamma_{\text{NH}_4} \cdot F_{\text{NH}_4}(z_{\text{ox}}) = -\frac{D_{\text{NH}_4}}{1+K_{\text{NH}_4}} \cdot \frac{\partial \text{NH}_4}{\partial z} _{z_{\text{ox}}^+}$ $F_{\text{NH}_4}(z_{\text{ox}}) = \frac{1}{1+K_{\text{NH}_4}} \cdot \frac{1-\phi}{\phi} \cdot \int_{z_{\text{NO}_3}}^\infty \sum_i \text{NC}_i \cdot k_i \cdot \text{POC}_i dz$
$z = z_\infty$	zero NH_4 flux	6) $\text{NH}_4(z_{\text{NO}_3}^-) = \text{NH}_4(z_{\text{NO}_3}^+)$
		7) $-\frac{D_{\text{NH}_4}}{1+K_{\text{NH}_4}} \cdot \frac{\partial \text{NH}_4}{\partial z} _{z_{\text{NO}_3}^-} = -\frac{D_{\text{NH}_4}}{1+K_{\text{NH}_4}} \cdot \frac{\partial \text{NH}_4}{\partial z} _{z_{\text{NO}_3}^+}$
		8) $\frac{\partial \text{NH}_4}{\partial z} _{z_\infty} = 0$

1. Oxic and nitrogenous zone ($z \leq z_{\text{NO}_3}$)

$$\frac{\partial \text{SO}_4^{II}}{\partial t} = 0 = D_{\text{SO}_4} \frac{\partial^2 \text{SO}_4^{II}}{\partial z^2} - w \frac{\partial \text{SO}_4^{II}}{\partial z} \quad (19)$$

$$500 \quad \frac{\partial \text{H}_2\text{S}^{II}}{\partial t} = 0 = D_{\text{H}_2\text{S}} \frac{\partial^2 \text{H}_2\text{S}^{II}}{\partial z^2} - w \frac{\partial \text{H}_2\text{S}^{II}}{\partial z} \quad (20)$$

2. Sulfidic zone ($z_{\text{NO}_3} < z \leq z_{\text{SO}_4}$)

$$\frac{\partial \text{SO}_4^{III}}{\partial t} = 0 = D_{\text{SO}_4} \frac{\partial^2 \text{SO}_4^{III}}{\partial z^2} - w \frac{\partial \text{SO}_4^{III}}{\partial z} - \frac{1-\phi}{\phi} \cdot \sum_i \text{SO}_4 \text{C} \cdot k_i \cdot \text{POC}_i(z) \quad (21)$$

$$505 \quad \frac{\partial \text{H}_2\text{S}^{III}}{\partial t} = 0 = D_{\text{H}_2\text{S}} \frac{\partial^2 \text{H}_2\text{S}^{III}}{\partial z^2} - w \frac{\partial \text{H}_2\text{S}^{III}}{\partial z} + \frac{1-\phi}{\phi} \cdot \sum_i \text{SO}_4 \text{C} \cdot k_i \cdot \text{POC}_i(z) \quad (22)$$

3. Methanic zone ($z_{\text{SO}_4} < z \leq z_\infty$)

$$\frac{\partial \text{H}_2\text{S}^{IV}}{\partial t} = 0 = D_{\text{H}_2\text{S}} \frac{\partial^2 \text{H}_2\text{S}^{IV}}{\partial z^2} - w \frac{\partial \text{H}_2\text{S}^{IV}}{\partial z} \quad (23)$$

where D_{SO_4} and D_{H_2S} denote the diffusion coefficients for SO_4 and H_2S which depend on the bioturbation status of the respective geochemical zone (compare Section 2.3.1). Integration of Eq. (19) - (23) yields the analytical solution and Table 5 summarises the boundary conditions applied. OMEN-SED assumes known concentrations at the sediment-water interface and continuity across the bioturbation depth and the nitrate penetration depth. The reoxidation of reduced H_2S to SO_4 is accounted for implicitly via the oxic-anoxic boundary condition for both species, while reduction of SO_4 and the associated production of H_2S via AOM is accounted for through the respective boundary conditions at z_{SO_4} . In case $z_{SO_4} < z_\infty$, OMEN-SED assumes zero sulfate concentration at z_{SO_4} and its diffusive flux must equal the amount of methane produced below (with a methane to carbon ratio of MC); or, in case $z_{SO_4} = z_\infty$, a zero flux condition for sulfate is considered. OMEN-SED iteratively solves for z_{SO_4} by first testing if there is sulfate left at z_∞ (i.e. $SO_4(z_\infty) > 0$) and, otherwise, by finding the root for the flux boundary condition 8.2 (Table 5). At the lower boundary z_∞ zero flux of H_2S is considered.

2.2.5 Phosphate

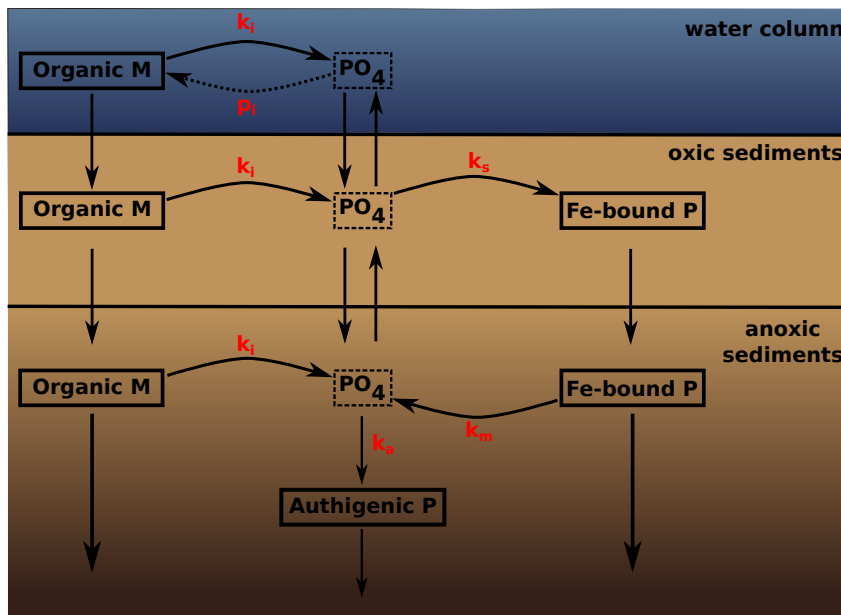


Figure 2. A schematic of the sedimentary P cycle in OMEN-SED. Red numbers represent kinetic rate constants for phosphorus dynamics (compare Table 10; p_i represents uptake rate of PO_4 via primary production in shallow environments). Adapted from Slomp et al. (1996).

The biogeochemical description of phosphorus (P) dynamics builds on the work of Slomp et al. (1996) and accounts for phosphorus recycling through organic matter degradation, adsorption onto sediments and iron(III) hydroxides (Fe-bound P), as well as carbonate fluorapatite (CFA or authi-

Table 5. Boundary conditions for sulfate and sulfide. For the boundaries we define: $z_-^- := \lim_{h \rightarrow 0} (z_- - h)$ and $z_-^+ := \lim_{h \rightarrow 0} (z_- + h)$.

Boundary	Condition	
$z = 0$	known concentration	1) $\text{SO}_4(0) = \text{SO}_{40}$
$z = z_{\text{bio}}$	continuity	2) $\text{SO}_4(z_{\text{bio}}^-) = \text{SO}_4(z_{\text{bio}}^+)$
	flux	3) $-(D_{\text{SO}_4,0} + D_{\text{bio}}) \cdot \frac{\partial \text{SO}_4}{\partial z} _{z_{\text{bio}}^-} = -D_{\text{SO}_4,0} \cdot \frac{\partial \text{SO}_4}{\partial z} _{z_{\text{bio}}^+}$
$z = z_{\text{ox}}$	continuity	4) $\text{SO}_4(z_{\text{ox}}^-) = \text{SO}_4(z_{\text{ox}}^+)$
	flux	5) $-D_{\text{SO}_4} \cdot \frac{\partial \text{SO}_4}{\partial z} _{z_{\text{ox}}^-} + \gamma_{\text{H}_2\text{S}} \cdot F_{\text{H}_2\text{S}}(z_{\text{ox}}) = -D_{\text{SO}_4} \cdot \frac{\partial \text{SO}_4}{\partial z} _{z_{\text{ox}}^+}$
	where:	$F_{\text{H}_2\text{S}}(z_{\text{ox}}) = \frac{1-\phi}{\phi} \cdot \left(\int_{z_{\text{NO}_3}}^{\text{SO}_4} \sum_i \text{SO}_4 \cdot k_i \cdot \text{POC}_i dz + \gamma_{\text{CH}_4} \cdot \int_{z_{\text{SO}_4}}^{\infty} \sum_i \text{MC} \cdot k_i \cdot \text{POC}_i dz \right)$
$z = z_{\text{NO}_3}$	continuity	6) $\text{SO}_4(z_{\text{NO}_3}^-) = \text{SO}_4(z_{\text{NO}_3}^+)$
	flux	7) $-D_{\text{SO}_4} \cdot \frac{\partial \text{SO}_4}{\partial z} _{z_{\text{NO}_3}^-} = -D_{\text{SO}_4} \cdot \frac{\partial \text{SO}_4}{\partial z} _{z_{\text{NO}_3}^+}$
$z = z_{\text{SO}_4}$	SO ₄ consumption ($z_{\text{SO}_4} = z_\infty$)	8) IF ($\text{SO}_4(z_\infty) > 0$) 8.1) $\frac{\partial \text{SO}_4}{\partial z} _{z_{\text{SO}_4}} = 0$ ELSE
	($z_{\text{SO}_4} < z_\infty$) with	8.2) $\text{SO}_4(z_{\text{SO}_4}) = 0 \quad \text{and} \quad -D_{\text{SO}_4} \cdot \frac{\partial \text{SO}_4}{\partial z} _{z_{\text{SO}_4}} = \gamma_{\text{CH}_4} \cdot F_{\text{CH}_4}(z_{\text{SO}_4})$ $F_{\text{CH}_4}(z_{\text{SO}_4}) = \frac{1-\phi}{\phi} \cdot \int_{z_{\text{SO}_4}}^{\infty} \sum_i \text{MC} \cdot k_i \cdot \text{POC}_i dz$
$z = 0$	known concentration	1) $\text{H}_2\text{S}(0) = \text{H}_2\text{S}_0$
$z = z_{\text{bio}}$	continuity	2) $\text{H}_2\text{S}(z_{\text{bio}}^-) = \text{H}_2\text{S}(z_{\text{bio}}^+)$
	flux	3) $-(D_{\text{H}_2\text{S},0} + D_{\text{bio}}) \cdot \frac{\partial \text{H}_2\text{S}}{\partial z} _{z_{\text{bio}}^-} = -D_{\text{H}_2\text{S},0} \cdot \frac{\partial \text{H}_2\text{S}}{\partial z} _{z_{\text{bio}}^+}$
$z = z_{\text{ox}}$	continuity	4) $\text{H}_2\text{S}(z_{\text{ox}}^-) = \text{H}_2\text{S}(z_{\text{ox}}^+)$
	flux	5) $-D_{\text{H}_2\text{S}} \cdot \frac{\partial \text{H}_2\text{S}}{\partial z} _{z_{\text{ox}}^-} - \gamma_{\text{H}_2\text{S}} F_{\text{H}_2\text{S}}(z_{\text{ox}}) = -D_{\text{H}_2\text{S}} \cdot \frac{\partial \text{H}_2\text{S}}{\partial z} _{z_{\text{ox}}^+}$
	where:	$F_{\text{H}_2\text{S}}(z_{\text{ox}}) = \frac{1-\phi}{\phi} \cdot \left(\int_{z_{\text{NO}_3}}^{\text{SO}_4} \sum_i \text{SO}_4 \cdot k_i \cdot \text{POC}_i dz + \gamma_{\text{CH}_4} \cdot \int_{z_{\text{SO}_4}}^{\infty} \sum_i \text{MC} \cdot k_i \cdot \text{POC}_i dz \right)$
$z = z_{\text{NO}_3}$	continuity	6) $\text{H}_2\text{S}(z_{\text{NO}_3}^-) = \text{H}_2\text{S}(z_{\text{NO}_3}^+)$
	flux	7) $-D_{\text{H}_2\text{S}} \cdot \frac{\partial \text{H}_2\text{S}}{\partial z} _{z_{\text{NO}_3}^-} = -D_{\text{H}_2\text{S}} \cdot \frac{\partial \text{H}_2\text{S}}{\partial z} _{z_{\text{NO}_3}^+}$
$z = z_{\text{SO}_4}$	continuity flux (with AOM) where:	8) $\text{H}_2\text{S}(z_{\text{SO}_4}^-) = \text{H}_2\text{S}(z_{\text{SO}_4}^+)$ 9) $-D_{\text{H}_2\text{S}} \cdot \frac{\partial \text{H}_2\text{S}}{\partial z} _{z_{\text{SO}_4}^-} + \gamma_{\text{CH}_4} \cdot F_{\text{CH}_4}(z_{\text{SO}_4}) = -D_{\text{H}_2\text{S}} \cdot \frac{\partial \text{H}_2\text{S}}{\partial z} _{z_{\text{SO}_4}^+}$ $F_{\text{CH}_4}(z_{\text{SO}_4}) = \frac{1-\phi}{\phi} \cdot \int_{z_{\text{SO}_4}}^{\infty} \sum_i \text{MC} \cdot k_i \cdot \text{POC}_i dz$
$z = z_\infty$	zero H ₂ S flux	10) $\frac{\partial \text{H}_2\text{S}}{\partial z} _{z_\infty} = 0$

genic P) formation (see Figure 2 for a schematic overview of the sedimentary P cycle). In the oxic zone of the sediment, PO_4 liberated through organic matter degradation can adsorb to iron(III) hydroxides forming Fe-bound P (or FeP, Slomp et al., 1998). Below the oxic zone, PO_4 is not only produced via organic matter degradation but can also be released from the Fe-bound P pool due to
 530 the reduction of iron(III) hydroxides under anoxic conditions. Furthermore, in these zones phosphate concentrations build up and pore waters can thus become supersaturated with respect to carbonate fluorapatite, thus triggering the authigenic formation of CFA (Van Cappellen and Berner, 1988). Phosphorus bound in these authigenic minerals represents a permanent sink for reactive phosphorus (Slomp et al., 1996). As for ammonium, the adsorption of P to the sediment matrix is treated as
 535 an equilibrium processes, parameterised with dimensionless adsorption coefficients for the oxic and anoxic zone, respectively ($K_{\text{PO}_4}^{\text{ox}}$, $K_{\text{PO}_4}^{\text{anox}}$ Slomp et al., 1998). The sorption and desorption of P to iron(III) hydroxides as well as the authigenic fluorapatite formation are described as first-order reactions with rate constants k_s , k_m and k_a , respectively (Table 10). The rate of the respective process is calculated as the product of the rate constant and the difference between the current concentration (of
 540 PO_4 and FeP) and an equilibrium or asymptotic concentration Slomp et al. (1996). The asymptotic Fe-bound P concentration is FeP^∞ and the equilibrium concentration for P sorption and authigenic fluorapatite formation are PO_4^s and PO_4^a , respectively (Table 10). The last term in Eq. (24) and (25) represents sorption of PO_4 to FeP in the oxic zone, the last term in Eq. (26) and (27) is the release of PO_4 from the FeP pool and the 4th term in Eq. (27) represents the permanent loss of PO_4
 545 to authigenic fluorapatite formation. The conservation equations for phosphate and Fe-bound P are thus given by:

1. Oxic zone ($z \leq z_{\text{ox}}$)

$$\frac{\partial \text{PO}_4^I}{\partial t} = \frac{D_{\text{PO}_4}}{1 + K_{\text{PO}_4}^{\text{ox}}} \frac{\partial^2 \text{PO}_4^I}{\partial z^2} - w \frac{\partial \text{PO}_4^I}{\partial z} + \frac{1-\phi}{\phi} \frac{1}{1 + K_{\text{PO}_4}^{\text{ox}}} \sum_i (\text{PC}_i \cdot k_i \cdot \text{POC}_i(z)) \\ - \frac{k_s}{1 + K_{\text{PO}_4}^{\text{ox}}} (\text{PO}_4^I - \text{PO}_4^s) \quad (24)$$

$$\frac{\partial \text{FeP}^I}{\partial t} = D_{\text{FeP}} \frac{\partial^2 \text{FeP}^I}{\partial z^2} - w \frac{\partial \text{FeP}^I}{\partial z} + \frac{\phi}{1-\phi} k_s (\text{PO}_4^I - \text{PO}_4^s) \quad (25)$$

2. Anoxic zones ($z_{\text{ox}} < z \leq z_\infty$)

$$\frac{\partial \text{FeP}^{II}}{\partial t} = D_{\text{FeP}} \frac{\partial^2 \text{FeP}^{II}}{\partial z^2} - w \frac{\partial \text{FeP}^{II}}{\partial z} - k_m (\text{FeP}^{II} - \text{FeP}^\infty) \quad (26)$$

$$\frac{\partial \text{PO}_4^{II}}{\partial t} = \frac{D_{\text{PO}_4}}{1 + K_{\text{PO}_4}^{\text{anox}}} \frac{\partial^2 \text{PO}_4^{II}}{\partial z^2} - w \frac{\partial \text{PO}_4^{II}}{\partial z} + \frac{1-\phi}{\phi} \frac{1}{1 + K_{\text{PO}_4}^{\text{anox}}} \sum_i (\text{PC}_i \cdot k_i \cdot \text{POC}_i(z)) \\ - \frac{k_a}{1 + K_{\text{PO}_4}^{\text{anox}}} (\text{PO}_4^{II} - \text{PO}_4^a) + \frac{(1-\phi)}{\phi} \frac{k_m}{1 + K_{\text{PO}_4}^{\text{anox}}} (\text{FeP}^{II} - \text{FeP}^\infty) \quad (27)$$

where D_{PO_4} denotes the diffusion coefficient for PO_4 which depends on the bioturbation status of the respective geochemical zone and $D_{\text{FeP}} = D_{\text{bio}}$ for $z \leq z_{\text{bio}}$ and $D_{\text{FeP}} = 0$ for $z > z_{\text{bio}}$ (compare

Table 6. Boundary conditions for phosphate and Fe-bound P (FeP). For the boundaries we define: $z_-^- := \lim_{h \rightarrow 0} (z_- - h)$ and $z_+^+ := \lim_{h \rightarrow 0} (z_- + h)$.

Boundary	Condition	
$z = 0$	known concentration	1) $\text{PO}_4(0) = \text{PO}_{40}$
$z = z_{\text{bio}}$	continuity	2) $\text{PO}_4(z_{\text{bio}}^-) = \text{PO}_4(z_{\text{bio}}^+)$
	flux	3) $(D_{\text{PO}_4,0} + D_{\text{bio}}) \cdot \frac{\partial \text{PO}_4}{\partial z} _{z_{\text{bio}}^-} = D_{\text{PO}_4,0} \cdot \frac{\partial \text{PO}_4}{\partial z} _{z_{\text{bio}}^+}$
$z = z_{\text{ox}}$	continuity	4) $\text{PO}_4(z_{\text{ox}}^-) = \text{PO}_4(z_{\text{ox}}^+)$
	flux	5) $-\frac{D_{\text{PO}_4}}{1 + K_{\text{PO}_4}^{2z}} \cdot \frac{\partial \text{PO}_4}{\partial z} _{z_{\text{ox}}^-} = -\frac{D_{\text{PO}_4}}{1 + K_{\text{PO}_4}^{\text{anox}}} \cdot \frac{\partial \text{PO}_4}{\partial z} _{z_{\text{ox}}^+}$
$z = z_\infty$	flux	10) $\frac{\partial \text{PO}_4}{\partial z} _{z_\infty} = 0$
$z = 0$	known concentration	1) $\text{FeP}(0) = \text{FeP}_0$
$z = z_{\text{bio}}$	continuity	2) $\text{FeP}(z_{\text{bio}}^-) = \text{FeP}(z_{\text{bio}}^+)$
	flux	3) $\frac{\partial \text{FeP}}{\partial z} _{z_{\text{bio}}^-} = \frac{\partial \text{FeP}}{\partial z} _{z_{\text{bio}}^+}$
$z = z_{\text{ox}}$	continuity	4) $\text{FeP}(z_{\text{ox}}^-) = \text{FeP}(z_{\text{ox}}^+)$
	flux	5) $\frac{\partial \text{FeP}}{\partial z} _{z_{\text{ox}}^-} = \frac{\partial \text{FeP}}{\partial z} _{z_{\text{ox}}^+}$
$z = z_\infty$	asymptotic concentration	10) $\text{FeP}(z_\infty) = \text{FeP}_\infty$

560 Section 2.3.1). Integration of Eq. (24) - (27) yields the analytical solution and Table 6 summarises the boundary conditions applied in OMEN-SED. The model assumes known bottom water concentrations and equal concentrations and diffusive fluxes at z_{bio} and z_{ox} for both species. Additionally OMEN-SED considers no change in phosphate flux and an asymptotic Fe-bound P concentration at z_∞ .

565 2.2.6 Dissolved Inorganic Carbon (DIC)

OMEN-SED accounts for the production of dissolved inorganic carbon (DIC) through organic matter degradation, as well as methane oxidation. Organic matter degradation produces dissolved inorganic carbon with a stoichiometric DIC : C ratio of 1:2 in the methanic zone and 1:1 in the rest of the sediment column (DICC^{II} and DICC^{I} respectively). DIC production through methane oxidation is implicitly taken into account through the boundary condition at z_{SO_4} . The conservation equations for DIC are thus given by:

1. Oxic, nitrogenous and sulfidic zone ($z \leq z_{\text{SO}_4}$)

$$575 \frac{\partial \text{DIC}^{\text{I}}}{\partial t} = 0 = D_{\text{DIC}} \frac{\partial^2 \text{DIC}^{\text{I}}}{\partial z^2} - w \frac{\partial \text{DIC}^{\text{I}}}{\partial z} + \frac{1-\phi}{\phi} \cdot \sum_i \text{DICC}^{\text{I}} \cdot k_i \cdot \text{POC}_i(z) \quad (28)$$

2. Methanic zone ($z_{\text{SO}_4} < z \leq z_\infty$)

$$\frac{\partial \text{DIC}^{\text{II}}}{\partial t} = 0 = D_{\text{DIC}} \frac{\partial^2 \text{DIC}^{\text{II}}}{\partial z^2} - w \frac{\partial \text{DIC}^{\text{II}}}{\partial z} + \frac{1-\phi}{\phi} \cdot \sum_i \text{DICC}^{\text{II}} \cdot k_i \cdot \text{POC}_i(z) \quad (29)$$

DH: I think what I wrote before also applies: a asymptotic Fe-bound P concentration at z_∞ is assumed! (but is the same as “no flux condition” as it is now?)

SA: need to say something about carbonates here

Table 7. Boundary conditions for DIC. For the boundaries we define: $z_-^- := \lim_{h \rightarrow 0} (z_- - h)$ and $z_+^+ := \lim_{h \rightarrow 0} (z_- + h)$.

Boundary	Condition	
$z = 0$	known concentration	1) $\text{DIC}(0) = \text{DIC}_0$
$z = z_{\text{bio}}$	continuity	2) $\text{DIC}(z_{\text{bio}}^-) = \text{DIC}(z_{\text{bio}}^+)$
	flux	3) $-(D_{\text{DIC},0} + D_{\text{bio}}) \cdot \frac{\partial \text{DIC}}{\partial z} _{z_{\text{bio}}^-} = -D_{\text{DIC},0} \cdot \frac{\partial \text{DIC}}{\partial z} _{z_{\text{bio}}^+}$
$z = z_{\text{SO}_4}$	continuity	4) $\text{DIC}(z_{\text{SO}_4}^-) = \text{DIC}(z_{\text{SO}_4}^+)$
	flux (with AOM)	5) $-D_{\text{DIC}} \cdot \frac{\partial \text{DIC}}{\partial z} _{z_{\text{SO}_4}^-} + \gamma_{\text{CH}_4} \cdot F_{\text{CH}_4}(z_{\text{SO}_4}) = -D_{\text{DIC}} \cdot \frac{\partial \text{DIC}}{\partial z} _{z_{\text{SO}_4}^+}$
	where:	$F_{\text{CH}_4}(z_{\text{SO}_4}) = \frac{1-\phi}{\phi} \cdot \int_{z_{\text{SO}_4}}^{\infty} \sum_i \text{MC} \cdot k_i \cdot \text{POC}_i dz$
$z = z_\infty$	zero DIC flux	6) $\frac{\partial \text{DIC}}{\partial z} _{z_\infty} = 0$

where D_{DIC} denotes the diffusion coefficient for DIC which depends on the bioturbation status of
580 the respective geochemical zone. Integration of Eq. (28) and (29) yields the analytical solution and
Table 7 summarises the boundary conditions applied in OMEN-SED. A Dirichlet condition is ap-
plied at the sediment-water interface. In addition, the model assumes a zero flux through the lower
boundary z_∞ and continuity across the bottom of the bioturbated zone, as well as the sulfate pene-
tration depth. An additional flux boundary condition at z_{SO_4} , implicitly accounts for DIC production
585 through anaerobic oxidation of methane (Table 7 Eq. 5).

2.2.7 Alkalinity

Organic matter degradation and secondary redox reactions exert a complex influence on alkalinity
(e.g. Jourabchi et al., 2005; Wolf-Gladrow et al., 2007; Krumins et al., 2013). To model alkalinity,
OMEN-SED divides the sediment column into four geochemical zones, where different equations
590 describe the biogeochemical processes using variable stoichiometric coefficients (compare values in
Table 10). Above z_{ox} , the combined effects of NH_4 and P release due to aerobic OM degradation in-
creases alkalinity according to ALK^{OX} whereas nitrification decreases alkalinity with stoichiometry
 ALK^{NIT} . In the remaining three zones anaerobic OM degradation generally results in an increase in
alkalinity, with the exact magnitude depending on the nature of the terminal electron acceptor used
595 (i.e. ALK^{DEN} , ALK^{SUL} , ALK^{MET}). In addition, the effect of secondary redox reactions, such as
nitrification, sulfide and methane oxidation are implicitly accounted for in the boundary conditions.

SA: TODO: again need to mention carboantes

In OMEN-SED, the conservation equations for alkalinity are thus given by:

1. Oxic zone ($z \leq z_{\text{ox}}$)

$$600 \quad \frac{\partial \text{ALK}^I}{\partial t} = 0 = D_{\text{ALK}} \frac{\partial^2 \text{ALK}^I}{\partial z^2} - w \frac{\partial \text{ALK}^I}{\partial z} + \frac{1-\phi}{\phi} \cdot \sum_i \left(\text{ALK}^{\text{NIT}} \cdot \frac{\gamma_{\text{NH}_4}}{1 + K_{\text{NH}_4}} \text{NC}_i + \text{ALK}^{\text{OX}} \right) \cdot k_i \cdot \text{POC}_i(z) \quad (30)$$

Table 8. Boundary conditions for alkalinity. For the boundaries we define: $z_-^- := \lim_{h \rightarrow 0} (z_- - h)$ and $z_-^+ := \lim_{h \rightarrow 0} (z_- + h)$.

Boundary	Condition	
$z = 0$	known concentration	1) $\text{ALK}(0) = \text{ALK}_0$
$z = z_{\text{bio}}$	continuity	2) $\text{ALK}(z_{\text{bio}}^-) = \text{ALK}(z_{\text{bio}}^+)$
	flux	3) $-(D_{\text{ALK},0} + D_{\text{bio}}) \cdot \frac{\partial \text{ALK}}{\partial z} _{z_{\text{bio}}^-} = -D_{\text{ALK},0} \cdot \frac{\partial \text{ALK}}{\partial z} _{z_{\text{bio}}^+}$
$z = z_{\text{ox}}$	continuity	4) $\text{ALK}(z_{\text{ox}}^-) = \text{ALK}(z_{\text{ox}}^+)$
	flux	5) $-D_{\text{ALK}} \cdot \frac{\partial \text{ALK}}{\partial z} _{z_{\text{ox}}^-} + F_{\text{ALK}}(z_{\text{ox}}) = -D_{\text{ALK}} \cdot \frac{\partial \text{ALK}}{\partial z} _{z_{\text{ox}}^+}$ $F_{\text{ALK}}(z_{\text{ox}}) = \frac{1-\phi}{\phi} \cdot \left(\text{ALK}^{\text{H}_2\text{S}} \cdot \gamma_{\text{H}_2\text{S}} \int_{z_{\text{NO}_3}}^{\text{SO}_4} \sum_i \text{SO}_4 \cdot k_i \cdot \text{POC}_i dz \right) + \frac{1-\phi}{\phi} \cdot \left(\text{ALK}^{\text{NIT}} \frac{\gamma_{\text{NH}_4}}{1+k_{\text{NH}_4}} \int_{z_{\text{NO}_3}}^{\infty} \sum_i \text{NC}_i \cdot k_i \cdot \text{POC}_i dz \right)$
	where:	
$z = z_{\text{NO}_3}$	continuity	6) $\text{ALK}(z_{\text{NO}_3}^-) = \text{ALK}(z_{\text{NO}_3}^+)$
	flux	7) $-D_{\text{ALK}} \cdot \frac{\partial \text{ALK}}{\partial z} _{z_{\text{NO}_3}^-} = -D_{\text{ALK}} \cdot \frac{\partial \text{ALK}}{\partial z} _{z_{\text{NO}_3}^+}$
$z = z_{\text{SO}_4}$	continuity	8) $\text{ALK}(z_{\text{SO}_4}^-) = \text{ALK}(z_{\text{SO}_4}^+)$
	flux (with AOM)	9) $-D_{\text{ALK}} \cdot \frac{\partial \text{ALK}}{\partial z} _{z_{\text{SO}_4}^-} + F_{\text{ALK}}(z_{\text{SO}_4}) = -D_{\text{ALK}} \cdot \frac{\partial \text{ALK}}{\partial z} _{z_{\text{SO}_4}^+}$ $F_{\text{ALK}}(z_{\text{SO}_4}) = \frac{1-\phi}{\phi} \cdot \left(\text{ALK}^{\text{AOM}} \gamma_{\text{CH}_4} \cdot \int_{z_{\text{SO}_4}}^{\infty} \sum_i k_i \cdot \text{POC}_i dz \right)$
	where:	
$z = z_{\infty}$	zero ALK flux	10) $\frac{\partial \text{ALK}}{\partial z} _{z_{\infty}} = 0$

2. Denitrification or nitrogenous zone ($z_{\text{ox}} < z \leq z_{\text{NO}_3}$)

$$\frac{\partial \text{ALK}^{II}}{\partial t} = 0 = D_{\text{ALK}} \frac{\partial^2 \text{ALK}^{II}}{\partial z^2} - w \frac{\partial \text{ALK}^{II}}{\partial z} + \frac{1-\phi}{\phi} \cdot \sum_i \text{ALK}^{\text{DEN}} \cdot k_i \cdot \text{POC}_i(z) \quad (31)$$

3. Sulfidic zone ($z_{\text{NO}_3} < z \leq z_{\text{SO}_4}$)

$$\frac{\partial \text{ALK}^{III}}{\partial t} = 0 = D_{\text{ALK}} \frac{\partial^2 \text{ALK}^{III}}{\partial z^2} - w \frac{\partial \text{ALK}^{III}}{\partial z} + \frac{1-\phi}{\phi} \cdot \sum_i \text{ALK}^{\text{SUL}} \cdot k_i \cdot \text{POC}_i(z) \quad (32)$$

4. Methanic zone ($z_{\text{SO}_4} < z \leq z_{\infty}$)

$$\frac{\partial \text{ALK}^{IV}}{\partial t} = 0 = D_{\text{ALK}} \frac{\partial^2 \text{ALK}^{IV}}{\partial z^2} - w \frac{\partial \text{ALK}^{IV}}{\partial z} + \frac{1-\phi}{\phi} \cdot \sum_i \text{ALK}^{\text{MET}} \cdot k_i \cdot \text{POC}_i(z) \quad (33)$$

where D_{ALK} denotes the diffusion coefficient for alkalinity which depends on the bioturbation status of the respective geochemical zone. Integration of Eq. (30) - (33) yields the analytical solution and Table 8 summarises the boundary conditions applied in OMEN-SED. A Dirichlet boundary

condition is applied at the sediment-water interface. The decrease of alkalinity due to oxidation of reduced species produced in the anoxic zones (with stoichiometry ALK^{NIT} and $\text{ALK}^{\text{H}_2\text{S}}$) is implicitly taken into account through the flux boundary condition at z_{ox} (Table 8 Eq. 5). Furthermore, the oxidation of methane by sulfate reduction increases alkalinity with stoichiometry ALK^{AOM} which is accounted for through the flux boundary condition at z_{SO_4} (Table 8 Eq. 9). At the lower boundary

z_{∞} a zero flux condition is applied.

2.3 Determination of Integration Constants

The integration constants of all general analytical solutions derived above change in response to changing boundary conditions. Thus, OMEN-SED has to re-determine integration constants for each dynamic zone (i.e. z_{ox} , z_{bio} , z_{NO_3} and z_{SO_4}) at every time step for all biogeochemical tracers. The
625 bioturbation boundary poses a particular challenge as it can theoretically occur in any of the dynamic geochemical zones (Fig. 3). Therefore, in order to generalise and simplify this recurring boundary matching problem, an independent, generic algorithm is implemented (rather than using multiple fully-worked-out algebraic solutions for each possible case and every biogeochemical tracer). The algorithm only has to solve a two-simultaneous-equation problem.

630 2.3.1 Generic Boundary Condition Matching (GBCM)

As discussed in Section 2.1, the solution of the general steady-state transport-reaction equation (Eq. (2)) for a generic tracer C is of the general form:

$$C(z) = A \exp(az) + B \exp(bz) + \sum_j \frac{\alpha_j}{D\beta_j^2 - w\beta_j - k} \cdot \exp(-\beta_j z) + \frac{Q}{k} \quad (34)$$

635 and can therefore be expressed as:

$$C(z) = A \cdot E(z) + B \cdot F(z) + G(z) \quad (35)$$

where $E(z)$, $F(z)$ are the homogeneous solutions of the ODE, $G(z)$ the particular integral (collectively called the basis functions), and A , B are the integration constants that must be determined with
640 the boundary conditions (shown in Fig. 3 for the whole sediment column).

Each internal boundary matching problem (i.e. excluding $z = 0$ and $z = z_\infty$) involves matching continuity and flux for the two solutions of the respective reaction-transport equation above, $C_U(z)$ (= 'upper'), and below, $C_L(z)$ (= 'lower'), the dynamic boundary at $z = z_b$:

$$C_U(z) = A_U \cdot E_U(z) + B_U \cdot F_U(z) + G_U(z) \quad (36)$$

645 $C_L(z) = A_L \cdot E_L(z) + B_L \cdot F_L(z) + G_L(z). \quad (37)$

OMEN-SED generally applies concentration continuity and flux boundary conditions at its internal, dynamic boundaries:

Continuity (where for generality we allow a discontinuity V_b)

650 $C_U(z_b) = C_L(z_b) + V_b \quad (38)$

Flux

$$D_U C'_U(z_b) + w C_U(z_b) = D_L C'_L(z_b) + w C_L(z_b) + F_b \quad (39)$$

655 where w is advection, D are the diffusion coefficients and F_b is any flux discontinuity (e.g. resulting from secondary redox reactions).

Considering that the advective flux above and below the boundary is equal (i.e. $wC_U(z_b) = wC_L(z_b)$) and substituting the general ODE solutions (36), (37), the boundary conditions can be represented as two equations connecting the four integration constants:

$$\begin{pmatrix} E_U & F_U \\ D_U E'_U & D_U F'_U \end{pmatrix} \begin{pmatrix} A_U \\ B_U \end{pmatrix} = \begin{pmatrix} E_L & F_L \\ D_L E'_L & D_L F'_L \end{pmatrix} \begin{pmatrix} A_L \\ B_L \end{pmatrix} + \begin{pmatrix} G_L - G_U + V_b \\ D_L G'_L - D_U G'_U + F_b - wV_b \end{pmatrix} \quad (40)$$

660

where the ODE solutions E , F , G are all evaluated at z_b .

Equation (40) can now be solved to give A_U and B_U as a function of the integration constants from the layer below (A_L and B_L), thereby constructing a piecewise solution for both layers, with just two integration constants (this is implemented in the function **benthic_utils.matchsoln** of OMEN-

665 SED):

$$\begin{pmatrix} A_U \\ B_U \end{pmatrix} = \begin{pmatrix} c_1 & c_2 \\ c_3 & c_4 \end{pmatrix} \begin{pmatrix} A_L \\ B_L \end{pmatrix} + \begin{pmatrix} d_1 \\ d_2 \end{pmatrix}. \quad (41)$$

Using Eq. (41), $C_U(z)$ in (36) can now be rewritten as a function of A_L and B_L (implemented in **benthic_utils.xformsoln**):

$$C_U(z) = (c_1 A_L + c_2 B_L + d_1) \cdot E_U(z) + (c_3 A_L + c_4 B_L + d_2) \cdot F_U(z) + G_U(z) \quad (42)$$

670 and hence define the “transformed” basis functions $E_U^*(z)$, $F_U^*(z)$, $G_U^*(z)$ such that:

$$C_U(z) = A_L \cdot E_U^*(z) + B_L \cdot F_U^*(z) + G_U^*(z) \quad (43)$$

where

$$\begin{aligned} E_U^*(z) &= c_1 E_U(z) + c_3 F_U(z) \\ F_U^*(z) &= c_2 E_U(z) + c_4 F_U(z) \end{aligned} \quad (44)$$

675 $G_U^*(z) = G_U(z) + d_1 E_U(z) + d_2 F_U(z)$

Equations (41), (43) and (44) can now be consecutively applied for each of the dynamic biogeochemical zone boundaries, starting at the bottom of the sediment column. The net result is a piecewise solution of the whole sediment column with just two integration constants (coming from 680 the lowest layer), which can then be solved for by applying the boundary conditions at the sediment-water interface and the bottom of the sediments .

2.3.2 Abstracting out the bioturbation boundary

The bioturbation boundary affects the diffusion coefficient of the modelled solutes, as well as the conservation equation of organic matter (and thereby the exact form of each reaction-transport equation). This boundary is particularly inconvenient as it can, in principle, occur in the middle of any of

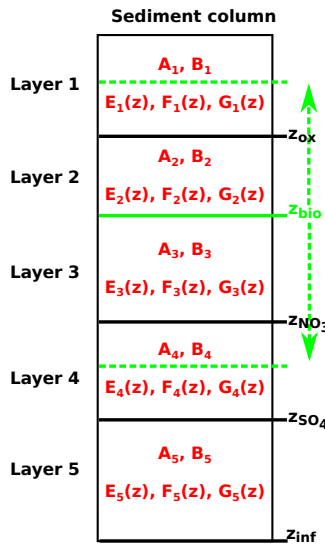


Figure 3. Schematic of the generic boundary condition matching (GBCM) problem. Showing the resulting integration constants (A_i, B_i) and ODE solutions (E_i, F_i, G_i) for the different sediment layers and the variable bioturbation boundary.

the dynamically shifting biogeochemical zones and therefore generate multiple cases (Fig. 3). The GBCM algorithm described above is thus not only used to construct a piecewise solution of the whole sediment column, but also to abstract out the bioturbation boundary. For each biogeochemical zone the "bioturbation-status" is initially tested (i.e. fully bioturbated, fully non-bioturbated, or crossing
690 the bioturbation boundary). Therefore, the upper and lower boundaries for the different zones (e.g. for the nitrogenous zone: $z_U = z_{\text{ox}}$, $z_L = z_{\text{NO}_3}$), as well as the respective reactive terms and diffusion coefficients (bioturbated and non-bioturbated) are passed over to the routine **zTOC.prepfg_l12** where the bioturbation-status is determined. In case the bioturbation depth is located within this zone (i.e. $z_U < z_{\text{bio}} < z_L$) a piecewise solution for this layer is constructed. Therefore, the reactive terms
695 and diffusion coefficients are handed over to the routines **zTOC.calcfg_l1** and **zTOC.calcfg_l2** which calculate the basis functions (E_U, F_U, G_U and E_L, F_L, G_L) and their derivatives for the bioturbated and the non-bioturbated part of this specific geochemical zone. The concentration and flux for both solutions at z_{bio} are matched and the coefficients $c_1, c_2, c_3, c_4, d_1, d_2$ (as in Eq. (41)) are calculated by the routine **benthic_utils.matchsoln**. These coefficients and the "bioturbation-status"
700 of the layer are passed back to the main GBCM algorithm where they can be used by the routine **benthic_utils.xformsoln** to calculate the "transformed" basis functions ($E_U^*(z), F_U^*(z), G_U^*(z)$) such that both layers are expressed in the same basis (compare Eq. (42 - 44)).

For instance, in the case of sulfate, **zTOC.prepfg_l12** is called three times before the actual profile is calculated (once per zone: oxic, nitrogenous, sulfidic) and hands back the information
705 about the "bioturbation-status" of the three layers and the coefficients $c_1, c_2, c_3, c_4, d_1, d_2$ for the

biogeochemical zone including the bioturbation depth. When calculating the complete piecewise solution for the sediment column, this information is passed to the function **zTOC.calcfg_I12** which sorts out the correct solution type to use. The main GBCM algorithm therefore never needs to know whether it is dealing with a piecewise solution (i.e. matched across the bioturbation boundary) or a
 710 “simple” solution (i.e. the layer is fully bioturbated or fully non-bioturbated).

2.4 Model Parameters

The following section provides a summary of global relationships used to constrain reaction and transport parameters in OMEN-SED. Table 9 synthesises sediment and transport parameters, while table 10 provides an overview of all biogeochemical parameters used in OMEN-SED.

715 2.4.1 Transport Parameters

The burial of sediments and porewater is directly related to the accumulation of new material on the seafloor (i.e. sedimentation, Burdige, 2006). This results in a downward advective flux of older sediment material and porewater in relation to the sediment-water interface. When coupled to an ocean model, its sedimentation flux can be readily used in OMEN-SED. The stand-alone version of
 720 OMEN-SED uses the empirical global relationship between sediment accumulation rate (cm yr^{-1}) and seafloor depth (m) of Middelburg et al. (1997):

$$w = 3.3 \cdot 10^{-0.87478367 - 0.00043512 \cdot \text{depth}}, \quad (45)$$

As mentioned before (Section 2.1), the diffusion coefficient of species i is calculated as $D_i = D_{i,0} + D_{\text{bio}} = D_{\text{mol},i} \cdot f_{ir} + D_{\text{bio}}$ for dissolved species and $D_i = D_{\text{bio}}$ for solid species. The bioturbation coefficient D_{bio} ($\text{cm}^2 \text{ yr}^{-1}$) is constant in the bioturbated zone and also follows the empirical relationship by Middelburg et al. (1997):
 725

$$D_{\text{bio}} = 5.2 \cdot 10^{0.76241122 - 0.00039724 \cdot \text{depth}} \quad (46)$$

Observations indicate that bioturbation is largely restricted to the upper 10 cm of the sediments and is only marginally related to seafloor depth (e.g. Boudreau, 1998; Teal et al., 2010). Therefore, OMEN-
 730 SED imposes a globally invariant bioturbation depth z_{bio} of 10 cm. In case the bottom water oxygen concentration is below 5 nanomole cm^{-3} infaunal activity is assumed to cease and $z_{\text{bio}} = 0.01$ cm. We choose a low value unequal to zero in order to simplify the implementation of the model. This approach ensures that the sediment column always consists of a bioturbated (even though very small for the low oxygen condition) and a non-bioturbated zone, thus the same GBCM algorithm
 735 can be used to solve the conservation equations. Furthermore, when OMEN-SED is coupled to an Earth system model the same method can be used to convert the POC depositional flux into a SWI concentration (i.e. the flux needs to be converted assuming bioturbation, see Section 4.1).

Bioirrigation (i.e. the pumping activity by burrow-dwelling animals) exchanges burrow water with overlying water and may enhance the SWI-flux of solutes (Aller, 1984, 1988). Several ap-

SA: need to explain why not 0; **DH:** Decent explanation?

740 proaches exist to incorporate this into a 1-D diagenetic model, for instance as a non-local trans-
 port/exchange process (Boudreau, 1984; Emerson et al., 1984) or as an enhancement factor of the
 molecular diffusion coefficient (Devol and Christensen, 1993; Soetaert et al., 1996). In OMEN-
 SED the latter approach is applied and the apparent “bio-diffusion” coefficient is calculated as
 $D_{i,0} = D_{\text{mol},i} \cdot f_{ir}$. Soetaert et al. (1996) derived an empirical relationship between f_{ir} and seafloor
 745 depth ($f_{ir} = \text{Min}\{1; 15.9 \cdot \text{depth}^{-0.43}\}$) based on observations from Archer and Devol (1992) and
 Devol and Christensen (1993). As this relationship just varies for depth below ~623 m (with a max-
 imum value of 3 at ~50 m) a constant value of $f_{ir} = 1$ is used in the default OMEN-SED config-
 750 uration. The specific molecular diffusion coefficients $D_{\text{mol},i}$ are corrected for sediment porosity ϕ ,
 tortuosity F and are linearly interpolated for an ambient temperature T using zero-degree coefficients
 D_i^0 and temperature-dependent diffusion coefficients D_i^T (Soetaert et al., 1996):

$$D_{\text{mol},i} = (D_i^0 + D_i^T \cdot T) \cdot \frac{1}{\phi \cdot F}.$$

Tortuosity can be expressed in terms of porosity as $F = \frac{1}{\phi^m}$ (Ullman and Aller, 1982) with the
 exponent m varying according to the type of sediment (here we use $m=3$). Values for D_i^T and D_i^0
 755 are summarised in Table 9 and are adapted from Li and Gregory (1974), Schulz (2006) and Gypens
 et al. (2008).

2.4.2 Reaction Parameters and Stoichiometries

Sandra: difficult to find a structure, I'd adapt to the order in the table and groups -as much as possible- according to chemical species, Also ALL parameters must be described and justified.
Let me take care of this section:

760 The first-order organic matter degradation constants of compound class i , k_i (yr^{-1}), are assumed
 invariant along the sediment column and therefore independent of the nature of the terminal electron
 acceptor. The rate constants can be altered manually to fit observed sediment profiles (compare Sec-
 tion 3.2) or related to a master variable (e.g. sedimentation rate or POC-flux) provided by a coupled
 Earth system model (compare Section ?? and ??). **until here, also need to mention f_i** Organic
 765 matter degradation consumes oxygen with a 1:1 stoichiometry.

N-related parameters: N/C, NO₃C, NH4, adsorption coefficient, gamma- explain nitrification

**SO₄-H₂S related parameters: SO₄C , gamma, AOM reduction of 1 mol organic matter addition-
 ally produces SO₄C = $\frac{138}{212}$ mol of hydrogen sulfide**

methane: MC, AOM MC = 0.5 mol of methane.

770 The rate constants sorption of PO₄ to Fe oxides, k_s , release of PO₄ from Fe-bound P due to Fe-oxide
 reduction k_m and authigenic CFA precipitation k_a are constrained on the basis of ???. The pore water
 equilibrium concentrations for P sorption and CFA precipitation (PO₄^s, PO₄^a) and the asymptotic
 concentration for Fe-bound P (FeP[∞]) are taken from Palastanga et al. (2011). The phosphorus to

Table 9. Sediment characteristics and transport parameters. **TODO: PO4 adsorption coefficients okay?**

Parameter	Unit	Value	Description/Source
ρ_{sed}	g cm^{-3}	2.6	Sediment density
w	cm yr^{-1}	Fct. of seafloor depth or from ESM	Advection/Sediment accumulation rate (Middelburg et al., 1997)
z_{bio}	cm	10 or 0.01	Bioturbation depth (Boudreau, 1998; Teal et al., 2010)
D_{bio}	$\text{cm}^2 \text{yr}^{-1}$	Fct. of seafloor depth	Bioturbation coefficient (Middelburg et al., 1997)
ϕ	-	0.85	Porosity
F	-	$\frac{1}{\phi^m}$	Tortuosity, here m=3
f_{ir}	-	1	Irrigation factor
Adsorption coefficients			
K_{NH_4}	-	1.3	NH_4 adsorption coefficient, (see Wang and Van Cappellen, 1996)
$K_{\text{PO}_4}^{\text{ox}}$	-	200.0	PO_4 adsorption coefficient (oxic), (see Slomp et al., 1998)
$K_{\text{PO}_4}^{\text{anox}}$	-	1.3	PO_4 adsorption coefficient (anoxic), (see Slomp et al., 1998)
Diffusion coefficients (Li and Gregory, 1974; Schulz, 2006; Gypens et al., 2008)			
$D_{\text{O}_2}^0$	$\text{cm}^2 \text{yr}^{-1}$	348.62	Molecular diffusion coefficient of oxygen at 0°C
$D_{\text{O}_2}^T$	$\text{cm}^2 \text{yr}^{-1} \text{°C}^{-1}$	14.09	Diffusion coefficient for linear temp. dependence of oxygen
$D_{\text{NO}_3}^0$	$\text{cm}^2 \text{yr}^{-1}$	308.42	Molecular diffusion coefficient of nitrate at 0°C
$D_{\text{NO}_3}^T$	$\text{cm}^2 \text{yr}^{-1} \text{°C}^{-1}$	12.26	Diffusion coefficient for linear temp. dependence of nitrate
$D_{\text{NH}_4}^0$	$\text{cm}^2 \text{yr}^{-1}$	309.05	Molecular diffusion coefficient of ammonium at 0°C
$D_{\text{NH}_4}^T$	$\text{cm}^2 \text{yr}^{-1} \text{°C}^{-1}$	12.26	Diffusion coefficient for linear temp. dependence of ammonium
$D_{\text{SO}_4}^0$	$\text{cm}^2 \text{yr}^{-1}$	157.68	Molecular diffusion coefficient of sulfate at 0°C
$D_{\text{SO}_4}^T$	$\text{cm}^2 \text{yr}^{-1} \text{°C}^{-1}$	7.88	Diffusion coefficient for linear temp. dependence of sulfate
$D_{\text{H}_2\text{S}}^0$	$\text{cm}^2 \text{yr}^{-1}$	307.48	Molecular diffusion coefficient of sulfide at 0°C
$D_{\text{H}_2\text{S}}^T$	$\text{cm}^2 \text{yr}^{-1} \text{°C}^{-1}$	9.64	Diffusion coefficient for linear temp. dependence of sulfide
$D_{\text{PO}_4}^0$	$\text{cm}^2 \text{yr}^{-1}$	112.91	Molecular diffusion coefficient of phosphate at 0°C
$D_{\text{PO}_4}^T$	$\text{cm}^2 \text{yr}^{-1} \text{°C}^{-1}$	5.59	Diffusion coefficient for linear temp. dependence of phosphate
D_{DIC}^0	$\text{cm}^2 \text{yr}^{-1}$	151.69	Molecular diffusion coefficient of DIC at 0°C
D_{DIC}^T	$\text{cm}^2 \text{yr}^{-1} \text{°C}^{-1}$	7.93	Diffusion coefficient for linear temp. dependence of DIC
D_{ALK}^0	$\text{cm}^2 \text{yr}^{-1}$	151.69	Molecular diffusion coefficient of ALK at 0°C
D_{ALK}^T	$\text{cm}^2 \text{yr}^{-1} \text{°C}^{-1}$	7.93	Diffusion coefficient for linear temp. dependence of ALK
Note: DIC and ALK coefficients are the values of HCO_3^- from Schulz (2006).			

carbon ratio represents the composition of organic matter and is chosen as ?? based on ??.

775

See Table 10 for a complete summary of the parameters and their values.

3 Stand-alone sensitivity analysis and case studies

3.1 Sensitivity Analysis

3.1.1 Methodology

780 Model parameters implicitly account for processes that are not explicitly resolved. Therefore, model parameters are notoriously difficult to constrain and a source of uncertainty for numerical and analytical models. A comprehensive sensitivity analysis (SA) can help quantify this uncertainty and identify the most sensitive parameters. More specifically, sensitivity analysis is used to investigate how the variations in the outputs (y_1, \dots, y_N) of a model can be attributed to variations in the different input parameters (x_1, \dots, x_M , Pianosi et al., 2016). Different types of sensitivity indices, which 785 quantify the relative influence of parameter x_i on output y_j with a scalar $S_{i,j}$ (for $i \in \{1, \dots, M\}$ and $j \in \{1, \dots, N\}$), can be calculated, ranging from simple one-at-a-time methods to statistical evaluations of the output distribution (e.g. variance-based or density-based approaches Pianosi et al., 2016). The latter indices take values between zero and one ($S_{i,j} \in [0, 1]$), where zero indicates a 790 non-influential parameter and a higher value a more influential parameter. Here, we use SA mainly to identify which parameters have the largest impact on the different model outputs and therefore require careful calibration. As the probability density functions of our model outputs (i.e. the resulting SWI-fluxes) are generally highly-skewed towards extreme organic matter degradation rates (not shown) variance-based sensitivity indices may not be a suitable proxy for output uncertainty 795 (Pianosi et al., 2016). Hence we employ the novel density-based PAWN method by Pianosi and Wagener (2015) which considers the entire conditional and unconditional Cumulative Distribution Function (CDF) of the model output rather than its variance only. The unconditional CDF, $F_y(y)$, of output y is obtained when all uncertain parameters (x_1, \dots, x_M) are varied simultaneously, and the conditional CDFs, $F_{y|x_i}(y)$, are obtained when all inputs but the i -th parameter are varied (i.e. 800 x_i is fixed to a so-called conditioning value). The sensitivity index of parameter i is measured by the distance between the two CDFs using the Kolmogorov-Smirnov statistic (Kolmogorov, 1933; Smirnov, 1939), i.e.:

$$S_i = \max_{x_i} \max_y |F_y(y) - F_{y|x_i}(y)|. \quad (47)$$

Since $F_{y|x_i}(y)$ accounts for what happens when the variability due to x_i is removed the distance 805 between the two CDFs provides a measure of the effects of x_i on the output y . Due to the model complexity it is impossible to compute the sensitivity indices analytically therefore they are approximated from a Latin-Hypercube sampling of parameter inputs and calculated outputs. For a brief

Table 10. Values for biogeochemical parameters used in OMEN-SED. The variables x , y and z denote the atomic ratio of carbon, nitrogen and phosphorus of the degrading organic matter (here set to $C : N : P = 106 : 16 : 1$). **P related coefficients okay?**

Parameter/Variable	Unit	Value	Description
Stoichiometric factors and molecular ratios			
NC _i	mol/mol	$\frac{y}{x} = \frac{16}{106}$	nitrogen to carbon ratio
PC _i	mol/mol	$\frac{z}{x} = \frac{1}{106}$	phosphorus to carbon ratio
MC	mol/mol	0.5	methane to carbon ratio
			produced during methanogenesis
DICC ^I	mol/mol	1.0	DIC to carbon ratio until z _{SO₄}
DICC ^{II}	mol/mol	0.5	DIC to carbon ratio below z _{SO₄}
O ₂ C	mol/mol	$\frac{x+2y}{x} = \frac{138}{106}$	oxygen to carbon ratio
NO ₃ C	mol/mol	$\frac{4x+3y}{5x} = \frac{94.4}{106}$	nitrate to carbon ratio
SO ₄ C	mol/mol	$\frac{1}{2}O_2C = \frac{138}{212}$	sulfate to carbon ratio
ALK ^{OX}	mol/mol	$\frac{y-2z}{x} = \frac{14}{106}$	ALK from aerobic degradation
ALK ^{NIT}	mol/mol	-2	ALK from nitrification
ALK ^{DEN}	mol/mol	$\frac{4x+3y-10z}{5x} = \frac{92.4}{106}$	ALK from denitrification
ALK ^{SUL}	mol/mol	$\frac{x+y-2z}{x} = \frac{120}{106}$	ALK from sulfate reduction
ALK ^{MET}	mol/mol	$\frac{y-2z}{x} = \frac{14}{106}$	ALK from methanogenesis
ALK ^{H₂S}	mol/mol	-2	ALK from H ₂ S oxidation
ALK ^{AOM}	mol/mol	2	ALK from AOM
Secondary reaction parameters			
γ _{NH₄}	-	0.9	fraction of NH ₄ that is oxidised in oxic zone
γ _{H₂S}	-	0.95	fraction of H ₂ S that is oxidised in oxic zone
γ _{CH₄}	-	0.99	fraction of CH ₄ that is oxidised at z _{SO₄}
P related parameters			
k _s	yr ⁻¹	1.0	Rate constant for PO ₄ sorption
k _m	yr ⁻¹	0.02	Rate constant for Fe-bound P release
k _a	yr ⁻¹	10.0	Rate constant for authigenic CFA precipitation
PO ₄ ^s	mol cm ⁻³	1 · 10 ⁻⁹	equilibrium conc. for P sorption (Slomp et al., 1996)
PO ₄ ^a	mol cm ⁻³	3.7 · 10 ⁻⁹	equilibrium conc. for authigenic P precipitation (Slomp et al., 1996)
FeP [∞]	mol cm ⁻³	1.99 · 10 ⁻¹⁰	asymptotic concentration for Fe-bound P (Slomp et al., 1996)

Table 11. Range of model parameters used for sensitivity analysis of model predicted output.

Parameter	Description	Units	Minimum	Maximum	Source
k_1	labile OM degradation constant	yr^{-1}	$1e^{-4}$	5.0	(1)
\tilde{k}_2	order of refractory OM degradation $(k_2 = \tilde{k}_2 \cdot k_1)$	-	$1e^{-4}$	$1e^{-1}$	(1)
f_1	fraction of labile OM	-	0.02	0.98	-
K_{NH_4}	Adsorption coefficient	-	0.8	1.7	(2)
γ_{NH_4}	NH_4 fraction oxidised		0.5	1.0	-
$\gamma_{\text{H}_2\text{S}}$	H_2S fraction oxidised		0.5	1.0	-
$K_{\text{PO}_4}^{\text{ox}}$	Adsorption coeff. oxic	-	100.0	400.0	(3)
$K_{\text{PO}_4}^{\text{anox}}$	Adsorption coeff. anoxic	-	1.3	2.0	(3)
k_s	kinetic P sorption	yr^{-1}	0.1	100.0	(4, 5)
k_m	Fe-bound P release	yr^{-1}	0.015	0.02	(4, 5)
k_a	authigenic P formation	yr^{-1}	0.001	10.0	(4, 6)

Sources: (1) Arndt et al. (2013); (2): Van Cappellen and Wang (1996); (3): Krom and Berner (1980)
(4): Gypens et al. (2008); (5): Slomp et al. (1996); (6): Van Cappellen and Berner (1988)

Table 12. Model boundary conditions for the two idealised sediment conditions used for the sensitivity analysis (Fig. 5 and 6). All solute concentrations are in nanomole cm^{-3} .

Depth (m)	Temp. ($^{\circ}\text{C}$)	OC (wt%)	O_2	NO_3	SO_4	PO_4	z_{bio} (cm)
400	8.0	2.0	0.0	40.0	28,000	40.0	0.001
4000	1.5	1.0	300.0	20.0	28,000	40.0	10.0

description of the methodology see Fig. 4. For more details we refer the interested reader to Pianosi and Wagener (2015).

810 The PAWN method, as implemented within the Sensitivity Analysis for Everyone (SAFE) matlab
toolbox (Pianosi et al., 2015), is used to investigate $M = 11$ model parameters for ranges as specified
in Table 11. Sensitivity indices for all resulting SWI-fluxes for two idealised sediment conditions
(i.e. anoxic at 400 m and oxic at 4000 m, see Table 12) are calculated. We use $NU = 200$ samples
to estimate the unconditional CDF, $NC = 100$ samples to estimate the conditional CDFs and $n = 10$
815 conditioning points, thus $N_{\text{eval}} = 200 + 100 \cdot 10 \cdot 11 = 11200$ model evaluations are performed for
each sediment condition. The resulting indices are then translated into a color code and summarised
in a pattern plot to simplify comparison (Fig. 5).

3.1.2 Results

Fig. 5 summarises results of the sensitivity analysis as a colour map. Results indicate that generally
820 the most significant parameters for all model outputs are the degradation rate constant for the labile

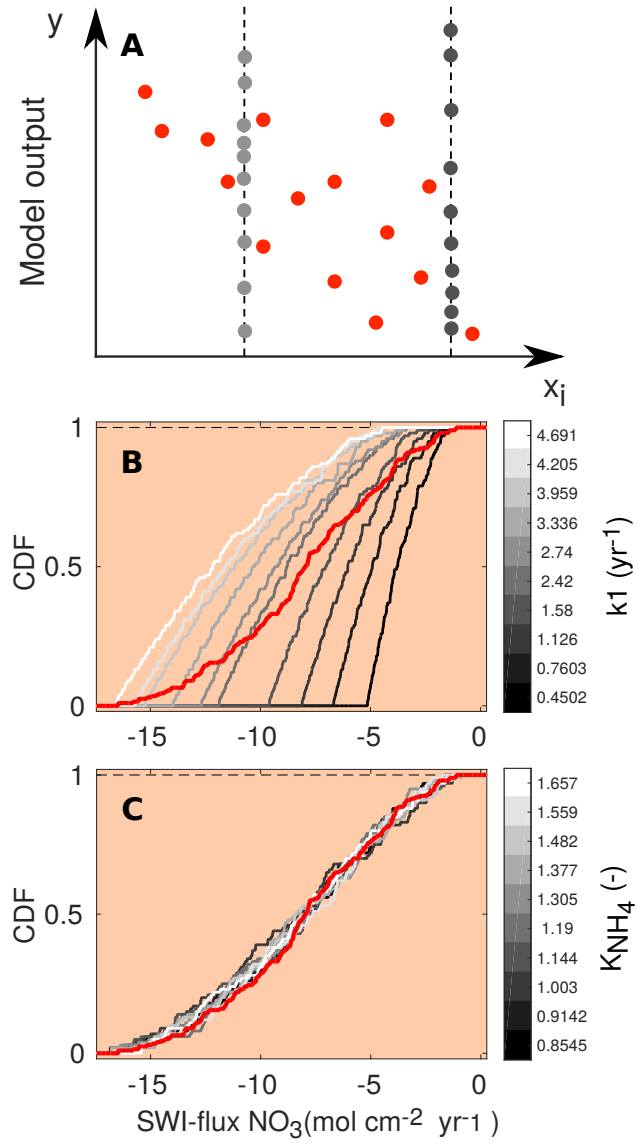


Figure 4. A: Schematic of the PAWN method, plotting an uncertain parameter (x_i) against a generic model output (y). Red dots represent points for calculating the unconditional CDF (NU, here 15), grey dots are points for calculating each conditional CDF (NC, here 10), here for $n = 2$ conditioning points. The user can change the values of NU, NC and n. The number of model evaluations equals $N_{\text{eval}} = \text{NU} + n \cdot \text{NC} \cdot M$, where M is the number of uncertain input parameters. B + C: Two examples of CDFs of the model calculated SWI-flux of NO_3 using NU = 200, NC = 100 and n = 10. The red lines are the unconditional distribution functions $F_y(\text{NO}_3)$ and the grey lines are the conditional distribution functions $F_{y|x_i}(\text{NO}_3)$ at different fixed values for input parameter k_1 (B) and K_{NH_4} (C). As the maximal distance between conditional CDFs and unconditional CDF is greater for k_1 this parameter is more influential for the model output (here SWI-flux of NO_3 , compare Fig. 5).

OM part (k_1) and the fraction of the labile pool in the total OM pool (f_1). Other parameters play a minor role for the SWI-fluxes, with the secondary redox parameters (i.e. γ_{NH_4} , $\gamma_{\text{H}_2\text{S}}$) in the oxic scenario being an exception. Here, NH_4 , SO_4 and H_2S are very sensitive to changes in γ_{NH_4} and $\gamma_{\text{H}_2\text{S}}$, as these parameters determine how much of the respective TEA is produced in situ via re-
825 oxidation of the corresponding reduced substance with O_2 , thus affecting the resulting SWI-fluxes. For the oxic setup, the reoxidation of H_2S produced in the sulfidic layer ($\gamma_{\text{H}_2\text{S}}$, Table 8 Eq. 5) also has a strong influence on alkalinity as it decreases alkalinity by 2 moles per mole of S ($\text{ALK}^{\text{H}_2\text{S}}$, Table 10). For the anoxic setup the secondary redox parameters are essentially non-influential as no O_2 is available for the reoxidation of reduced substances. Especially for the oxic condition the PO_4
830 SWI-flux appears to be insensitive to P-related parameters (i.e. $K_{\text{PO}_4}^{\text{ox}}$, $K_{\text{PO}_4}^{\text{anox}}$, k_s , k_m , k_a) as the majority is absorbed to Fe-oxides. The sensitivities change if other PO_4 related equilibrium concentrations PO_4^s , PO_4^a and FeP^∞ are used (not shown). Overall the results of the sensitivity analysis are in line with what one expects from a diagenetic model and thus provide ground to confirm that OMEN-SED is able to provide sensible results.

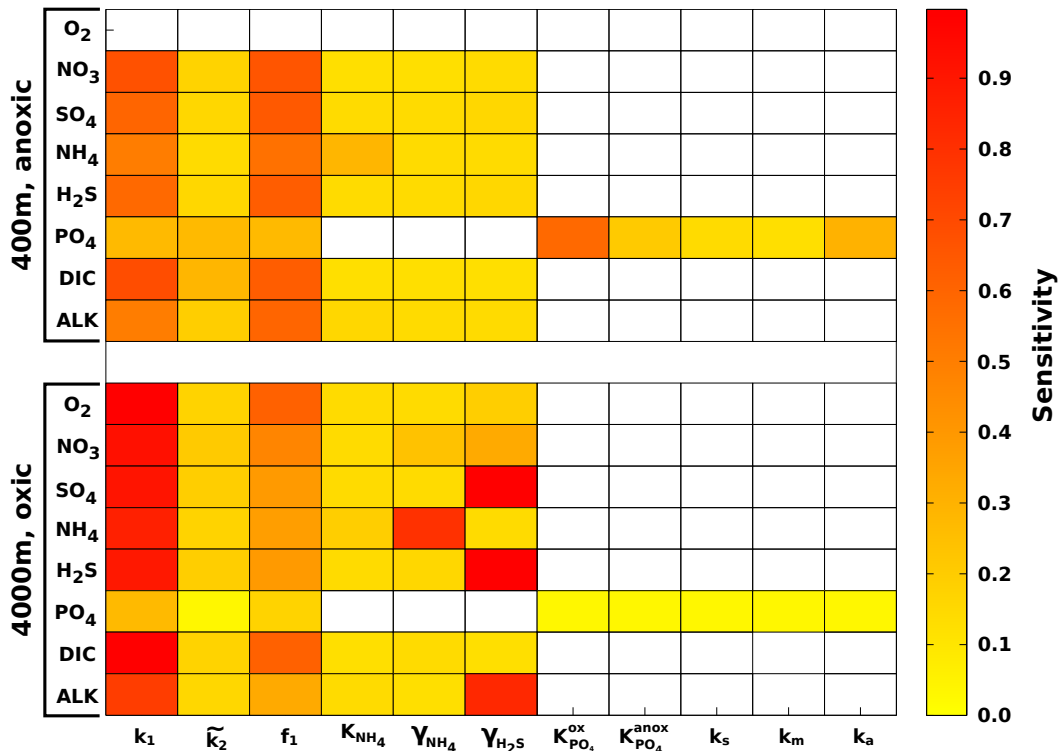


Figure 5. Pattern plot, showing the output sensitivity for each SWI flux (i.e. the chemical compounds on the vertical axis) and each input factor (i.e. the model parameters on the horizontal axis) for two idealised sediment cores. White patterns are assigned where the SWI flux is independent of the specific parameter.

DH: Rather low PO_4 sensitivity - bc of Equil. concentr.?

835 We further explore the sensitivity of simulated sediment-water exchange fluxes to variations in organic matter degradation parameters by varying k_1 , f_1 and \tilde{k}_2 while all other model parameters are set to their default values (Tables 9 and 10). For the deep sea condition we account for the presence of more refractory OM by sampling $f_1 \in [0.02, 0.3]$. Minimum and maximum values for k_1 , \tilde{k}_2 and f_1 in the shallow ocean are as in Table 11. The parameter space is sampled using another Latin-Hypercube
 840 approach with sample sizes of $N = 3500$ for each idealised sediment condition. Figure 6 summarises the results of the sensitivity study. In addition, the range of observed O_2 and NO_3^- sediment-water interface fluxes extracted from a global database (Bohlen et al., 2012) is indicated. Figure 6 shows that the observed fluxes fall well in the range of SWI-fluxes calculated with OMEN-SED. Also highlighted by the emergence of colour patterns in Figure 6 A+B are the strong interactions between
 845 the amount of labile OM f_1 and its degradation rate k_1 for the resulting SWI-fluxes of the most powerful TEA available. In general, a higher degradation rate in combination with more labile OM available leads to a higher SWI-flux.

SA: needs a more critical analysis, what is the msg you want the reader to understand here?

DH: How?

3.2 Case study: Simulations of sediment cores

3.2.1 Methodology

850 In order to illustrate the capabilities of OMEN-SED, comprehensive datasets from the Santa Barbara Basin (Reimers et al., 1996), as well as from the Iberian margin and the Nazaré Canyon (Epping et al., 2002) are modelled. Modelled profiles are compared with measured pore water data from different depths including the continental shelf (108 m) and the lower slope (2213 m) located at the Iberian margin, the upper slope (585 m) from the Santa Barbara Basin, and a deep sea site (4298 m)
 855 in the Nazaré Canyon. The Santa Barbara Basin is characterised by anoxic bottom waters, high POC concentrations and varved sediments (Reimers et al., 1990), therefore the depth of bioturbation in OMEN-SED is restricted to the upper 0.01 cm. In the uppermost sediments iron(III) hydroxides are reduced, releasing Fe^{2+} which reacts with sulfide to form iron sulfides. Thus, the Fe cycle exerts a strong control on sulfide concentrations in the sediments of this basin (Reimers et al., 1996). In
 860 addition, the sediments are generally supersaturated with respect to carbonate fluorapatite by and below 2 cm (Reimers et al., 1996). The Iberian margin, situated in the northeastern Atlantic, generally belongs to the more productive regions of the global ocean (Longhurst et al., 1995), however, seasonal changes in upwelling creates a strong temporal variability in primary productivity and organic carbon deposition and submarine canyons in this area (like the Nazaré Canyon) may deliver
 865 organic carbon from the shelf to the ocean interior (van Weering et al., 2002; Epping et al., 2002). For a more detailed description of the study areas and the experimental work, the interested reader is referred to the Reimers et al. (1996) and Epping et al. (2002).

SA: needs polishing

DH: Better like this?

In OMEN-SED sediment characteristics and boundary conditions are set to the observed values where available (Table 13). Other sediment characteristics (e.g. sedimentation rate, porosity,

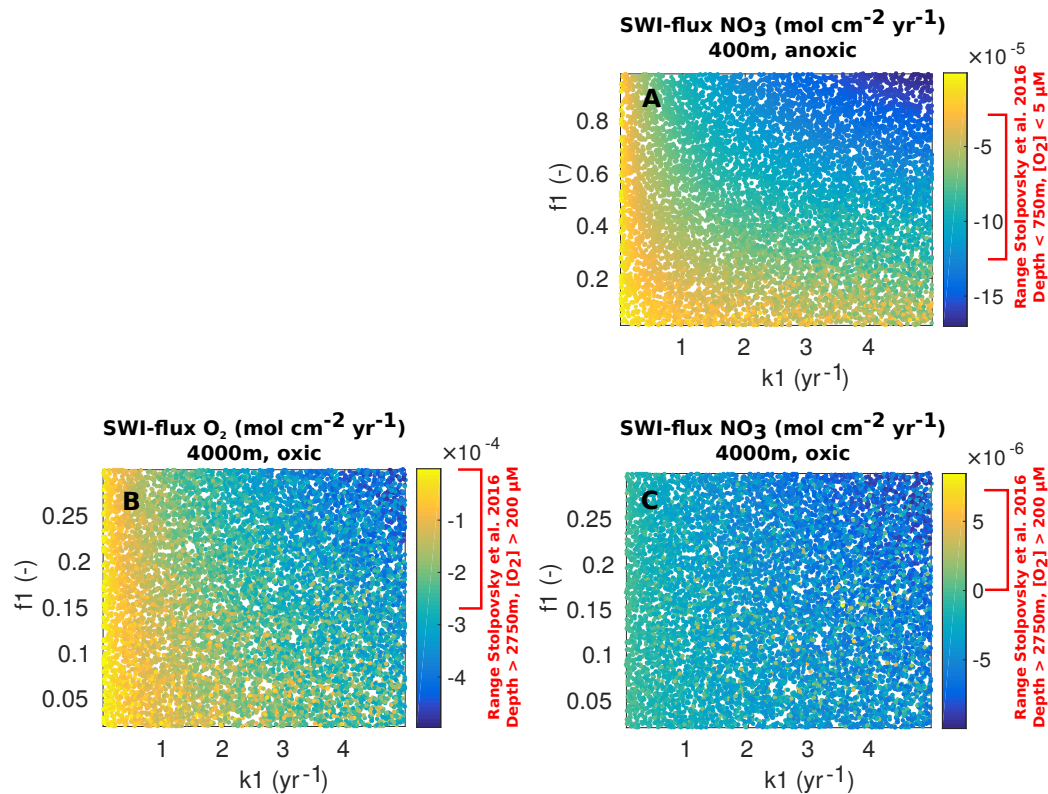


Figure 6. Coloured scatter plots (k_1 vs f_1) of resulting OMEN-SED SWI-fluxes for the 400m anoxic (A: NO_3) and 4000m oxic (B: O_2 , C: NO_3) scenario. Negative values representing a flux from the water column into the sediments. Indicated area in red at the respective colour scale represents the range of benthic fluxes in the global database of Bohlen et al. (2012).

DH: Why mainly negative
 NO_3 -flux 4000m in
 contrast to database!?...
 might change when using
 diff. gamma

density), stoichiometric factors and secondary reaction parameters are set to the default value (see Tables 9 and 10). Organic matter is modelled as two fractions, with different first-order degradation rate constants. The POC and pore water profiles were fitted by optimizing the POC partitioning into the fast and slow degrading pool and their respective first-order degradation rate constants (priority is given to reproduce the POC and O_2 profiles). For phosphorus the equilibrium concentration for authigenic P formation (PO_4^{a}) was adjusted to fit the PO_4 concentration at z_∞ .

3.2.2 Results

Fig. 7 compares modelled sediment profiles with measured pore water data for the Santa Barbara Basin and the Iberian margin. Results show that OMEN-SED is able to capture main features across a range of different environments without changing model parameters (e.g. stoichiometric ratios or secondary reaction parameters) to site specific conditions. For the two open Iberian margin stations

Table 13. Model boundary conditions for the sampling stations in Figure 7. (For all sites DIC bottom water concentration of 2,400 nanomole cm⁻³ is assumed.)

Sediment characteristics:							
Depth (m)	Temp. (°C)	z_{bio} (cm)	D_{bio} (cm ² yr ⁻¹)	POC ₁ (wt%)	POC ₂ (wt%)	k ₁ (yr ⁻¹)	k ₂ (yr ⁻¹)
108	12.5	1.0	0.02	2.64	1.8	0.65	$1.0e^{-5}$
585	5.85	0.01	0.02	2.0	3.5	0.2	$8.0e^{-4}$
2213	3.2	10.0	0.17	0.45	0.5	0.1	$4.0e^{-4}$
4298	2.5	4.2	0.18	0.83	1.2	0.052	$1e^{-5}$

Bottom water concentrations of solutes (all in nanomole cm ⁻³):								
Depth	O ₂	NO ₃	SO ₄	NH ₄	H ₂ S	PO ₄	PO ₄ ^a	Alkalinity
108	210	9.6	28,000	0.4	0.0	0.0	15.0	2,400
585	10	25.0	28,000	0.0	0.0	50.0	90.0	2,480
2213	250	25.0	28,000	0.6	0.0	0.0	5.0	2,400
4298	243	30.1	28,000	0.22	0.0	0.0	5.0	2,400

(108 and 2213 m) OMEN-SED fits all observations well. OMEN-SED does especially well at depth 2213 m by reproducing the deep O₂ penetration and the subsurface maximum in NO₃ concentration due to the nitrification of NH₄. For the anoxic Santa Barbara Basin (585 m) the decrease in SO₄ and the increase in ALK concentration with sediment depth is well represented, indicating the importance of sulfate reduction as the primary pathway of OM degradation at this site (compare Meysman et al., 2003). However, a misfit is observed for H₂S and PO₄ in the upper 20 cm of this sediment core. The discrepancy for H₂S can be explained by high iron(III) hydroxide concentrations, which is reduced to degrade organic matter (especially in the 2 – 4 cm depth interval), therefore placing the beginning of the sulfate reduction zone and the production of H₂S to the deeper sediments (Reimers et al., 1996). In addition, produced dissolved Fe reacts with H₂S to form iron sulfides (e.g. pyrite, FeS₂) and thus further inhibits the rise of H₂S (Reimers et al., 1990). The iron cycle also plays a critical role for phosphorus, as the reduction of iron(III) hydroxides in the surface sediments releases sorbed phosphate, leading to pore waters around and below 2 cm which are supersaturated with respect to fluorapatite, thus initiating CFA precipitation. Reimers et al. (1996) could even show that the accumulation of CFA is mainly restricted to the near-surface sediments (~ 5 cm) instead of throughout the sediment column. As OMEN-SED does not include an iron-cycle, and Fe-bound P and CFA processes are highly parameterised, the model is not able to capture these complex, non-steady state phosphorus dynamics at this specific site. For the Nazaré Canyon station (4298 m) satisfactory fits could be realised apart from NH₄. However, also Epping et al. (2002) could not obtain a better fit using a more complex diagenetic model. They suggested non-local solute exchange resulting from bioirrigation being responsible for the higher NH₄ concentrations at this site which is neglected in

their model, as well as in OMEN-SED. Furthermore, the fractured POC profile (indicating episodic depositional events through the canyon) could have been approximated using a different partitioning of the bulk POC into labile and refractory pool with different degradation rate constants. Thus, 905 leading to a better fit of the NH₄ profile. In general, better approximations of the data could have potentially been acquired by applying a sensitivity study using different NC-ratios (e.g. Epping et al., 2002, report different ratios from Redfield stoichiometry) and exploring the parameter space for the secondary reaction parameters (γ_{NH_4} , γ_{H_2S}). However, considering these generalisations and our assumption of steady-state, which might not be valid, particularly for the complex Santa Bar- 910 bara basin, the shallow core and the Nazaré Canyon, which are affected by seasonality and biology, OMEN-SED performs well in capturing the main dynamics.

3.3 Case study: Stand-alone simulations of global ocean transect

3.3.1 Methodology

In this section it is tested to which degree OMEN-SED is capable of capturing the dynamics of 915 organic matter degradation pathways and related TEA-fluxes as simulated with a complete, numerical diagenetic model. Therefore, we reproduce the simulations of typical conditions along a global ocean hypsometry of Thullner et al. (2009) and compare our modeled TEA-fluxes with the results of the complete model and observations from Middelburg et al. (1996). To explore the global degradation of OM in the seafloor Thullner et al. (2009) quantified various diagenetic processes using the 920 Biogeochemical Reaction Network Simulator (BRNS, Aguilera et al., 2005), a flexible simulation environment suitable for reactive transport simulations of complex biogeochemical problems (e.g. Jourabchi et al., 2005; Thullner et al., 2005). Thullner et al. (2009) use seafloor depth (SFD) as the master variable and calculate model parameters, such as w , D_{bio} and ϕ , from existing empirical relationships (e.g. Van Cappellen and Wang, 1995; Middelburg et al., 1997). Organic matter degra- 925 dation is described with a 1-G approach, thus assuming a single pool of organic matter of uniform reactivity. The first order rate constant is related to the burial velocity, w (cm year⁻¹), following the empirical relationship of Boudreau (1997):

$$k = 0.38 \cdot w^{0.59}. \quad (48)$$

This rate constant can be assumed as the mean reactivity of the organic matter fractions which 930 are degraded in the upper, bioturbated 10 – 20 cm of the sediments. Thus, more reactive fractions (degraded during days/weeks close to the SWI) and more refractory fractions (degraded on longer time scales deeper in the sediments) are not captured by this relationship (Boudreau, 1997). BRNS simulations were performed using boundary conditions and parameters for depths representative for shelf, slope and deep sea sediments (i.e. SFD of 100m, 200m, 500m, 1000m, 2000m, 3500m and 935 5000m). In order to reproduce these results, OMEN-SED is configured as a 1-G model and boundary conditions and model parameters are defined as in Thullner et al. (2009, see Table 14). As OMEN-

SA: needs polishing
DH: Better like this?

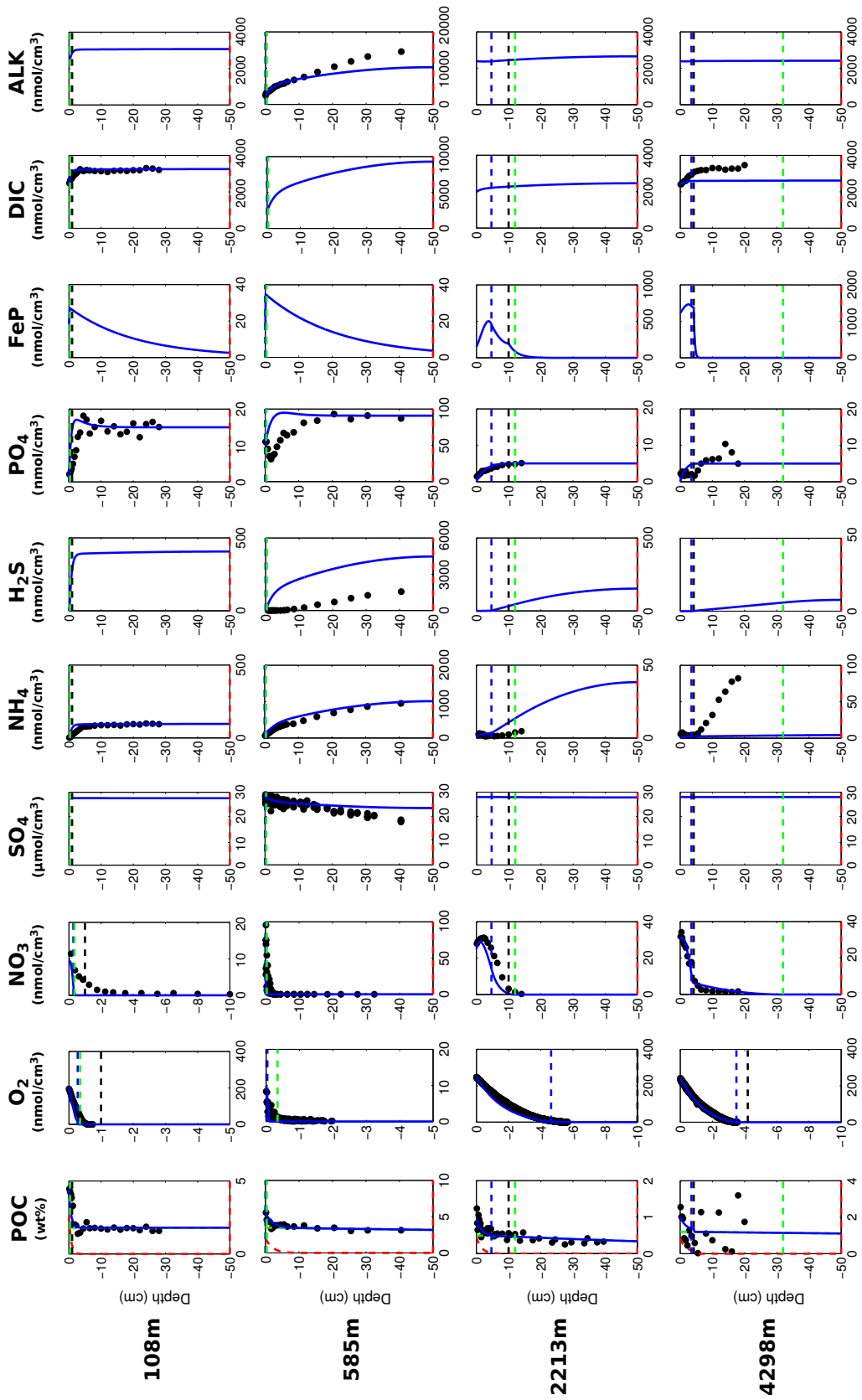


Figure 7. Modelled (curves) and measured (filled dots) dissolved and solid phase pore water profiles for four different sediment cores. Note that different scales are used for different stations. The blue POC curve represents the sum of the refractory (green) and labile (red) POC fraction.

SED assumes a fixed fraction of reduced substances to be reoxidised, which exerts a large impact on the resulting SWI-fluxes (compare Section 3.1), we perform two sets of simulations in order to show the range of possible model outputs. In the first setup 95% of the reduced substances are reoxidised
940 (i.e. $\gamma_{NH_4} = \gamma_{H_2S} = 0.95$) and in the second only 5% are reoxidised (all other model parameters and boundary conditions are equal).

Table 14. Seafloor depth dependency of key model parameters and boundary conditions (adapted from Thullner et al. (2009)).

	Seafloor depth						
	100 m	200 m	500 m	1000 m	2000 m	3500 m	5000 m
Model parameters							
w^a (cm yr ⁻¹)	3.98×10^{-1}	3.60×10^{-1}	2.67×10^{-1}	1.62×10^{-1}	5.94×10^{-2}	1.32×10^{-2}	2.94×10^{-3}
D_{bio}^a (cm ² yr ⁻¹)	27.5	25.1	19.0	12.1	4.83	1.23	0.310
ϕ^b	0.85	0.85	0.80	0.80	0.80	0.80	0.80
T ^c (°C)	10.3	9.7	8.1	5.8	3.0	1.5	1.4
ρ_{sed}^c (g cm ⁻³)	2.5	2.5	2.5	2.5	2.5	2.5	2.5
k^d (yr ⁻¹)	0.221	0.208	0.174	0.130	0.0718	0.0296	0.0122
Upper boundary conditions							
POC _{flux} ^a (μmol cm ⁻² yr ⁻¹)	510	467	357	228	93.0	24.3	6.33
POC ^e (wt%)	0.79	0.78	0.55	0.50	0.42	0.32	0.25
O ₂₀ ^c (nanomole cm ⁻³)	132	129	121	114	116	135	141
NO ₃₀ ^c (nanomole cm ⁻³)	17.3	18.6	22.1	26.5	31.0	31.6	31.6
SO ₄₀ ^b (nanomole cm ⁻³)	28,000	28,000	28,000	28,000	28,000	28,000	28,000

^a Derived from Middelburg et al. (1997).

^b Derived from Van Cappellen and Wang (1995).

^c Derived from Conkright et al. (2002).

^d Derived from Boudreau (1997).

^e Calculated with OMEN-SED from POC_{flux}.

3.3.2 Results

Figure 8 compares simulated SWI-fluxes of TEAs (i.e. O₂, NO₃ and SO₄) along the global hypsometry using OMEN-SED (black lines) with the results of Thullner et al. (2009) (red lines). Observations for O₂ and NO₃ fluxes are taken from Middelburg et al. (1996). Also plotted in Fig. 8A are the total oxygen uptake (TOU) estimates presented in Thullner et al. (2009) (filled red symbols), who assumed the organic matter flux to be equivalent to TOU. Due to the applied empirical relations organic matter flux to the seafloor decreases by 2 orders of magnitude from 100 to 5000 m and its degradation rate constant by 1 order of magnitude (Table 14). Therefore, the rate of organic matter degradation is about 50 times greater at 100 m than at 5000 m (compare Thullner et al., 2009), thus resulting in a decrease of TEA-fluxes along the hypsometry (Figure 8). The 95%-reoxidation exper-

iments (\bullet , in Fig. 8) show proportionally higher O_2 in-fluxes as the 5%-reoxidation experiments (\blacktriangledown) because more O_2 is utilised for in situ production of NO_3^- and SO_4^{2-} in the sediments. This is also mirrored by the increased NO_3^- out-flux and decreased SO_4^{2-} in-flux for shallower SFDs. This is in line with results of Thullner et al. (2009) who could show that in situ production is an important source for SO_4^{2-} and is responsible for $\sim 80\%$ of the total OM degradation rate at depths between 100 and 2000 m (SO_4^{2-} is not used for OM degradation in OMEN-SED below 2000m). In general, Figure 8 shows that OMEN-SED captures the main trends in observed TEA fluxes well and fluxes calculated with BRNS fall within the range of possible OMEN-SED results.

DH: Not sure, if this 80% is correct (seems to be pretty high)... but that's how I understand Thullner et al. (2009) - see pg. 12 for 80%!

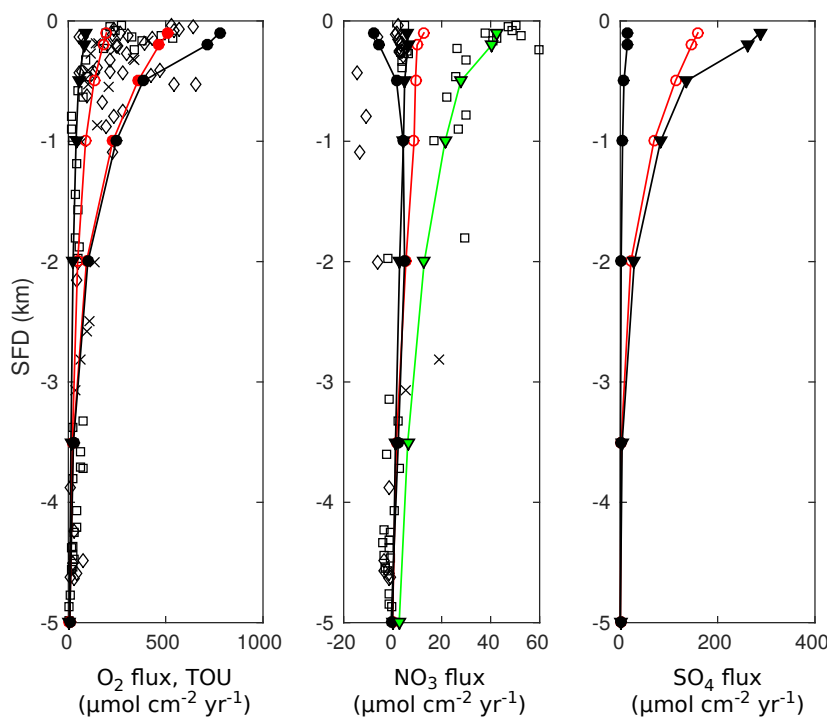


Figure 8. Fluxes of O_2 , NO_3^- and SO_4^{2-} to the sediment along the global hypsometry. Red lines (with open symbols) are modelled fluxes from Thullner et al. (2009) using BRNS; black lines are results from OMEN-SED (\bullet : $\gamma_{NH_4} = \gamma_{H_2S} = 0.95$; \blacktriangledown : $\gamma_{NH_4} = \gamma_{H_2S} = 0.05$). Observations of TEA fluxes are taken from Middelburg et al. (1996) (\diamond : Atlantic, \square : Pacific, \times : Arctic/Indian Ocean). Also plotted in Figure (A) are the total oxygen uptake (TOU) estimates of Thullner et al. (2009) (filled red symbols). The green line indicates OMEN-SED results for low oxygen/high nitrate levels and the lower NC-ratio. Negative values are directed out of the sediments.

In particular, the observed O_2 fluxes in the upper 2000m are well predicted by the two OMEN-SED simulations. Oxygen fluxes for the deep-sea sediments, however, are slightly underestimated. These deviations can presumably be related to the assumed 1-G description of organic matter degradation, which neglects the more labile OM pool. This highly reactive pool is degraded close to the

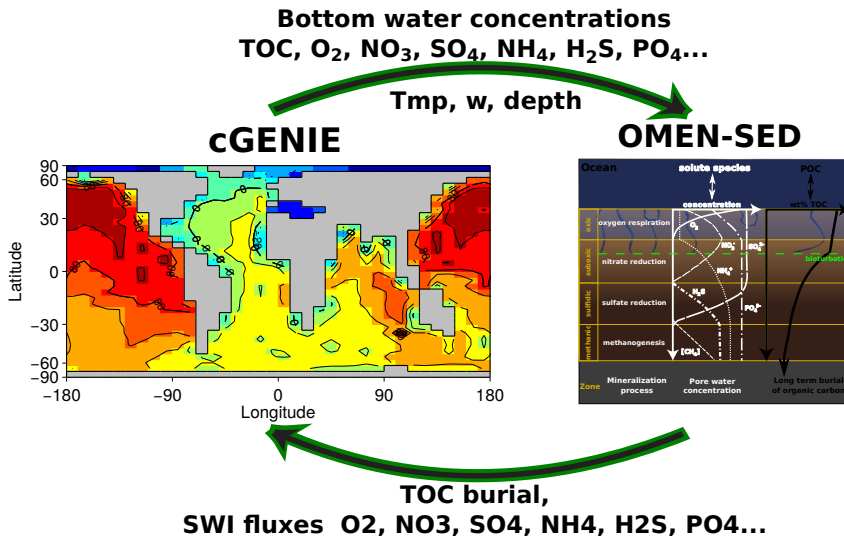


Figure 9. Schematic of the relationship between OMEN-SED and cGENIE. Arrows and accompanied text represent the information transferred between models.

sediment surface, thus promoting higher aerobic degradation rates and higher O₂ fluxes. Nitrate
965 fluxes in the upper 500m of the Atlantic Ocean are well predicted. However, as in Middelburg et al.
(1996) the direction of calculated nitrate fluxes in the upper 1000m of the Pacific Ocean differ from
the observations. Middelburg et al. (1996) related these discrepancies to the globally averaged model
parameters and the applied boundary conditions. They could reduce the disagreements significantly
by using more representative bottom water concentrations for the eastern Pacific and a higher flux of
970 labile organic matter for their 2-G model. By changing the boundary conditions and the NC-atomic
ratio of organic matter for the whole hypsometry, it is possible to obtain a better model-data fit with
OMEN-SED for the shallow Pacific Ocean (green line in Fig. 8B). Following Bohlen et al. (2012),
who could show that the atomic NC-ratio strongly deviates from Redfield stoichiometry (0.151) with
specifically lower values for the East Pacific Ocean, we adopt their globally averaged value of 0.067.
975 In addition, bottom water conditions are changed to low oxygen/high nitrate levels more likely to be
found in the shallow Pacific Ocean (O₂ = 10 nanomole cm⁻³ and NO₃ = 80 nanomole cm⁻³).

4 Coupled pre-industrial Earth system model simulations

4.1 Coupling to the cGENIE Earth system model

OMEN-SED is coupled to the carbon-centric version of the “GENIE” Earth system model (cGENIE,
980 Ridgwell et al., 2007) to illustrate the abilities of the newly developed model. The following
section provides a brief description of cGENIE and the coupling procedure (Fig. 9). cGENIE is a
model of Intermediate Complexity based on the efficient climate model “C-GOLDSTEIN” of Ed-

wards and Marsh (2005), featuring a frictional-geostrophic 3D-ocean circulation model coupled to a fast Energy-Moisture Balance 2D-atmosphere together with a dynamic-thermodynamic sea-ice component. The version of cGENIE used here includes the marine geochemical cycling of carbon, oxygen, phosphorus and sulfur (Ridgwell et al., 2007), preservation of carbonates in deep-sea sediments (SEDGEM, Ridgwell and Hargreaves, 2007) and terrestrial weathering (Colbourn et al., 2013). The ocean model is implemented on a 36×36 equal-area horizontal grid with 16 vertical levels using the pre-industrial continental configuration and bathymetry as in Archer et al. (2009). A finer grid (72×72) is used for the sediments (see Fig. 10C]. Instead of completely degrading POC at the seafloor, OMEN-SED is called by SEDGEM for each wet ocean grid point. Depending on the overlying biogeochemical ocean model, processes can be included or excluded in OMEN-SED and stoichiometric factors need to be adjusted to ensure preservation of mass. As nitrogen is not modelled explicitly in the employed cGENIE configuration, related stoichiometries in OMEN-SED are set to zero (i.e. NC_i , ALK^{NIT} and ALK^{DEN}). cGENIE, however, implicitly includes the effects of NH_4 release and its complete nitrification on alkalinity but neglects the impact of P release. Therefore, alkalinity stoichiometries from aerobic degradation and sulfate reduction are changed to $ALK^{OX} = -16/106$ and $ALK^{SUL} = 122/106$, respectively (compare to default in Table 10).

Several biogeochemical tracers and parameters are transferred from SEDGEM to OMEN-SED and have to be converted into the required units. Bottom water concentrations of solutes are converted from $mol\ kg^{-1}$ to $mol\ cm^{-3}$ and the depositional flux of POC (POC_{flux}) is converted from $cm^3\ cm^{-2}\ yr^{-1}$ to $mol\ cm^{-2}\ yr^{-1}$ assuming an average density of POC of $1.0\ cm^3\ g^{-1}$. Other parameters used from cGENIE are seafloor depth, local temperature and the partitioning of bulk POC into the slower and faster degrading pool (as cGENIE represents a labile and a refractory POC fraction, see Ridgwell et al., 2007). The advection/burial rate (w) is generally taken from cGENIE from the previous time-step, however, it is assured that w is not smaller than the detrital flux (Det_{flux}) to the sediments (e.g. $w < 0$ can occur if the sediments are being eroded during the spin-up of cGENIE). In case $w \leq Det_{flux} = 0.0$ all POC is remineralised at the ocean floor. Furthermore, a minimum value of $w = 0.4\ cm\ kyrs^{-1}$ is imposed as OMEN-SED tends to be unstable for lower values. The bulk POC_{flux} is separated into the labile and refractory component and the routine to find the steady-state solution for POC is called. Here, the two POC depositional fluxes are first converted into SWI concentrations (in $mol\ cm^{-3}$) by solving the flux divergence equation:

$$\frac{\partial F}{\partial z} = -\frac{\partial}{\partial z} \left(-\xi D_i \frac{\partial C_i}{\partial z} + \xi w C_i \right) \quad (49)$$

for $z=0$. OMEN-SED then computes the fraction of POC preserved in the sediment at a depth of 100 cm (POC_{pres}) and subsequently calls the routines to find the steady-state solutions for the solute substances. In case POC preservations leads to insane stuff ... all remineralised! Finally, POC_{pres} and the SWI-fluxes of solutes (in $mol\ cm^{-2}\ yr^{-1}$) are returned to cGENIE. In case no POC is deposited on the seafloor (i.e. $POC_{flux} = 0$), OMEN-SED is not called and the SWI-fluxes of solutes and POC_{pres} are set to zero. In order to reduce memory requirements the sediment profiles (e.g. as

1020 shown in Fig. 7) are not calculated in the FORTRAN version of OMEN-SED, however, the boundary conditions are saved at the end of the experiment and sediment profiles for specific grid-cells, ocean basins and ocean transects can be plotted using the stand-alone MATLAB version of OMEN-SED

4.2 Coupled pre-industrial simulations

4.2.1 Methodology

1025 All simulations presented here are run for 20,000 years to steady-state and OMEN-SED is called for each grid-cell in every time step, feeding back the resulting SWI-fluxes and the fraction of POC preserved in the sediments to cGENIE. As shown in our sensitivity analysis (Section 3.1) and discussed by Arndt et al. (2013) the degradation rate constants for OM (k_i) are the most influential parameters and strongly determine the SWI-flux of redox-sensitive elements as well as the preservation 1030 of organic matter. Yet, their spatial variability is unknown at the global scale and reported rate constants can vary by almost 10 orders of magnitude (Arndt et al., 2013). Thus defining appropriate OM degradation rate constants is a major challenge and source of uncertainty for diagenetic models. The rate constants in models are either determined through profile fitting for a specific site or, for global applications, they are related to a single, readily available characteristic (or master variable) 1035 of the local environmental conditions. For instance, considerable effort has been expended to relate the apparent rate constant for oxic and anoxic OM degradation to sedimentation rate (w) and various empirical relations have been proposed (Toth and Lerman, 1977; Tromp et al., 1995; Boudreau, 1997; Stolpovsky et al., 2015). Nevertheless, these relationships are generally based on limited data sets and their global applicability is questionable (Arndt et al., 2013).

1040 Modelled mean POC weight percentages (wt%) in the upper 5cm of the sediments are compared to the global distribution pattern of POC content in surface sediments (< 5cm sediment depth) of Seiter et al. (2004). Therefore, the original POC distribution pattern in $1^\circ \times 1^\circ$ grid resolution (interpolated from > 5500 measurements, compare Seiter et al., 2004) has been transformed onto the 72×72 SEDGEM grid (Figure 10). The regridding of the original POC distribution obviously affects the 1045 resolution of the data, especially for the continental margin, as some sites with higher POC wt% are lost due to the restricted SEDGEM grid-resolution (compare e.g. maximum values for the East Pacific and upwelling waters of the Namibian shelf, Figure 10A + B).

To parameterise the reactivity of organic matter we test two different approaches. First, the empirical relationship proposed by Boudreau (1997) is used (see also Section 3.3), which relates the 1050 apparent OM degradation rate constant in the bioturbated layer to the burial velocity, w (cm year $^{-1}$):

$$k_{\text{app}} = 0.38 \cdot w^{0.59}. \quad (50)$$

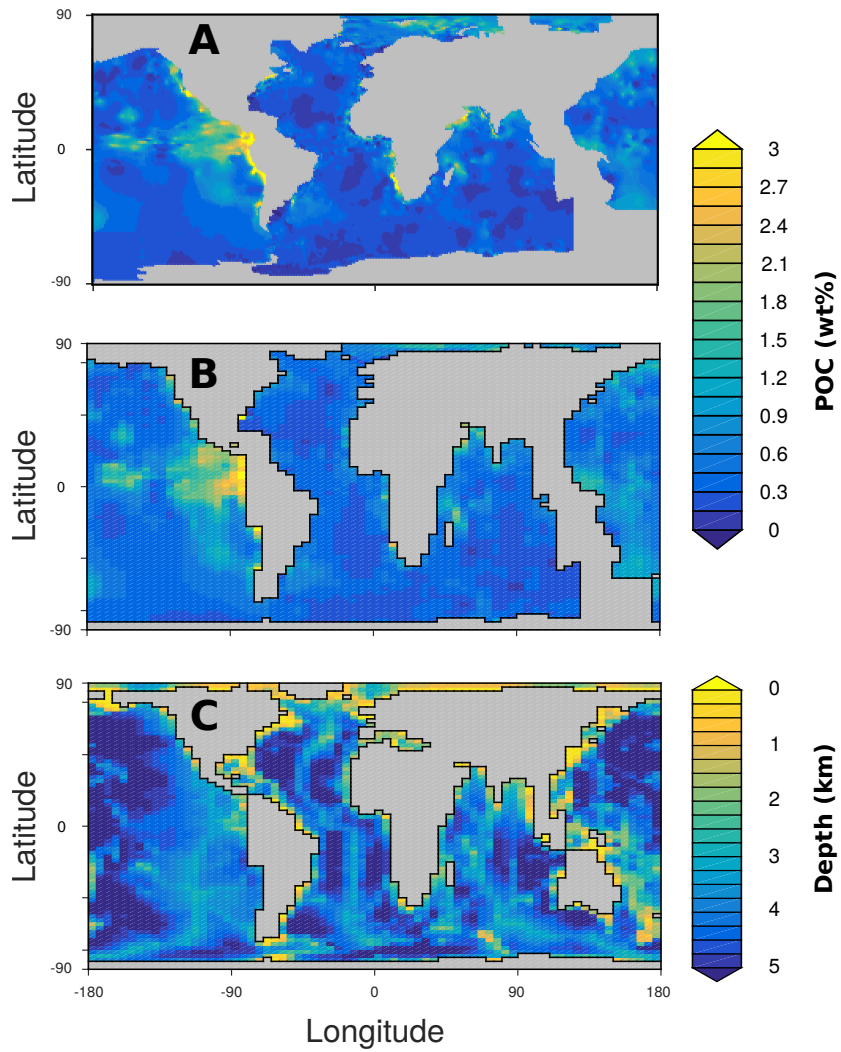


Figure 10. Observed distribution of sediment surface (< 5cm) POC wt% (A, B) and cGENIE bathymetry (C). (A) Original global distribution of POC wt% interpolated on a $1^\circ \times 1^\circ$ grid from more than 5500 individual data points (compare Seiter et al., 2004, for the interpolation procedure). (B) Observed POC wt% data transformed onto the 72 \times 72 SEDGEM grid. Grid points without any observations are left blank (grey). (C) Gridded continental configuration and ocean bathymetry of the 16-level, 72 \times 72 equal-area cGENIE grid.

We assume that k_{app} represents the mean OM reactivity in the bioturbated layer and make the following assumptions in order to calculate the two degradation rate constants for OMEN-SED:

1055 $k_{\text{app}} = f_1 \cdot k_1 + f_2 \cdot k_2$ (51)

$k_1 = x \cdot k_2$ (52)

where x describes the relation between k_1 and k_2 and is subject to sensitivity experiments (with values of $x \in \{2, 3, 4, 5, 10, 25, 50, 100\}$). As the fractions of labile and refractory OM reaching the sediments (f_1, f_2) is known from cGENIE we can calculate k_1 and k_2 independently for each grid-cell. For the second approach, we assume globally invariant degradation rate constants. The rate constants for the more refractory OM pool, k_2 , is systematically varied between 0.0045 and 0.007 year⁻¹ and the more labile OM component, described by k_1 , is assumed to degrade $x \in \{2, 3, 4, 5, 10\}$ times faster, respectively.

1065 **4.2.2 Results**

OMEN-SED is coupled to the global Earth system model cGENIE as described in Section 4.1. Our objective is not to perform and discuss a detailed calibration of the two models, as this is beyond the scope of this sediment model development paper. We rather want to showcase, that a coupling is possible and that the results show main sediment features one would expect to see on a global scale. The crossplots in this section (Figures 11 - 13) compare POC wt% from the regridded global distribution pattern of Seiter et al. (2004) with modelled POC wt% using different parameterisations for the degradation rate constants k_1 and k_2 . The colour of the points in Figures 11 - 13 represents the SFD of the respective cGENIE grid-cell. As the individual data-points are highly scattered and in order to see if a certain relation between k_1 and k_2 performs better for specific ocean depths, the data-points are binned into 6 uniform depth-classes of 1000m each (respective mean POC wt% and SFD are represented by the triangles). The regression line (and the corresponding R²-value) is calculated for the 6 bin-classes and included in the figures.

First, the relationship of Boudreau (1997) and the assumptions of Eq. (51) and (52) are used to calculate k_1 and k_2 . In Figure 11 (A-H) the relation between the two degradation rate constants (Eq. 1080 (52)) is changed globally, thus independent of the seafloor depth. The crossplots show that it is not possible to achieve a solution where all bin-classes fall onto, or close to, the 1:1 line. Also, the slope of the regression lines are generally much larger or smaller than 1.0 (with the exception of Figures 11C+D), indicating that the rate of change in modeled and observed POC wt% for the bin-classes is different. The R² values are strictly monotonically increasing for increasing x because a dependency is artificially imposed for the modelled POC wt% through the relation between k_1 and 1085 k_2 . When looking at the individual bin-classes it can be seen that shallow ocean depths are better represented by smaller differences between k_1 and k_2 (e.g. $k_1 = 2 \cdot k_2$ for SFD < 1000m, Figure 11A), and the deep ocean by a larger spread (e.g. $k_1 = 25 \cdot k_2$ for SFD > 3000m, Figure 11F). In a greatly

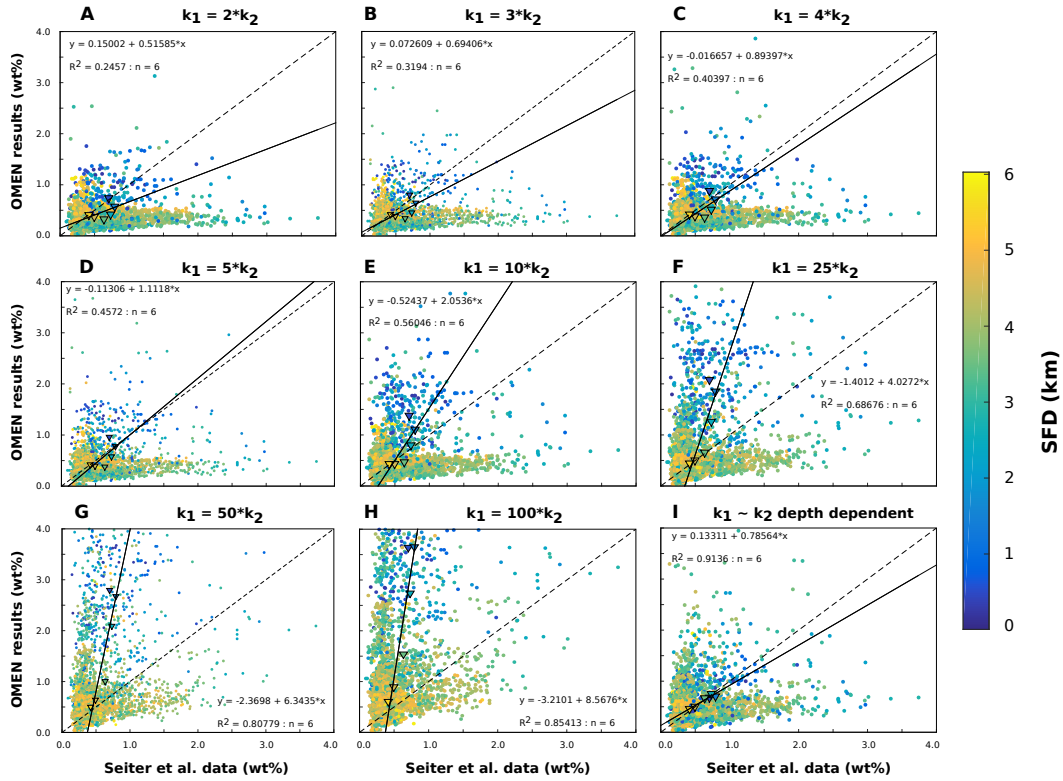


Figure 11. Crossplots comparing modelled and observed mean POC wt% in the upper 5 cm of the sediments using the relationship of Boudreau (1997) and the assumptions of Eq. (51) and (52) to calculate k_1 and k_2 . Data-points are binned into 6 uniform depth-classes of 1000m, each class is represented by a triangle. Grid-points with more than 4.0 POC wt% are not shown.

simplified way, this can be interpreted as bulk POC in the shallow ocean being more reactive (i.e. higher k_{app}) and consisting of fresher organic matter types, therefore the degradation rate constants of the two pools are more similar (i.e. $k_2 < k_1$). In the deeper ocean, bulk POC is generally less reactive (i.e. lower k_{app}) and due to the preferential degradation of more reactive organic matter types in the water-column (Wakeham et al., 1997; Lee et al., 2000) the refractory POC pool can be considered as being several orders of magnitude less reactive compared to the labile POC pool (i.e. $k_2 \ll k_1$). We use these observations to create a depth dependent relationship between the two degradation rate constants, where x in Eq. (52) takes values of $x = 2$ for $SFD < 1000\text{m}$, $x = 5$ for $1000\text{m} \leq SFD < 2000\text{m}$, $x = 10$ for $2000\text{m} \leq SFD < 3000\text{m}$ and $x = 25$ for $SFD \geq 3000\text{m}$ for the 6 SFD bin-classes, respectively. The resulting regression model (Figure 11I) accounts for 91% of the variance of the modeled POC wt% around the observed mean of the bin-classes. However, the slope of the regression line (0.786) indicates that the rate of change in modeled POC wt% for the bin-classes is smaller than in the observed POC wt%.

DH: more statistics, e.g.
p-value don't make
much sense right?

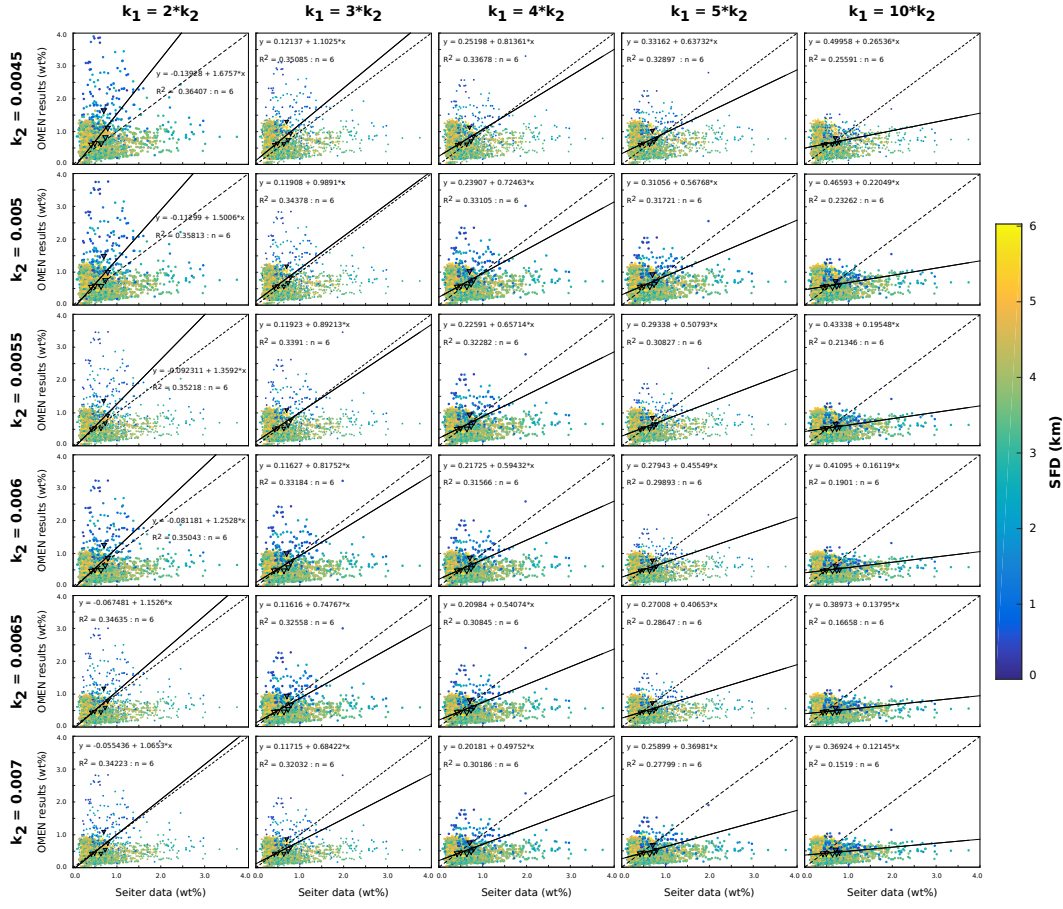


Figure 12. Crossplots comparing modelled and observed mean POC wt% in the upper 5 cm of the sediments using globally invariant degradation rate constants k_1 and k_2 . Data-points are binned into 6 uniform depth-classes of 1000m as in Fig. 11, each class is represented by a triangle. Grid-points with more than 4.0 POC wt% are not shown.

However, imposing the depth dependent relation of the degradation rate constants is rather arbitrary and the POC wt% data used for the comparison has their own limitations (compare Section 4.2). In addition, the empirical relationship used (Boudreau, 1997) and the regression model obtained is 1105 based on modern day observations and very likely not valid under different environmental conditions during Earth history (e.g. Hülse et al., 2017). Therefore, next the degradation rate constants are parameterised on model intrinsic information. By providing two pools of POC from the water-column characterised by different degradation rate constants, cGENIE accounts for the decrease 1110 in bulk POC degradability with water-depth. Therefore, the imposed depth dependent relation of the degradation rate constants presented in Figure 11 could also be regarded as double-accounting. Figure 12 presents results for the globally invariant degradation rate experiments, where k_2 is systematically varied between 0.0045 and 0.007 year⁻¹ and the more labile OM component, k_1 , is

assumed to degrade $x \in \{2, 3, 4, 5, 10\}$ times faster, respectively. In general, using globally invariant degradation rate constants 5 of the 6 bin-classes are located closer to the 1:1 line as in the previous experiments (with the exception of the shallow ocean bin-class). Also the slope of some regression lines is close to 1.0 (e.g. $(k_2, x) \in \{(0.0045, 3), (0.005, 3), (0.0055, 3), (0.0065, 2), (0.007, 2)\}$), indicating that the simpler parameterisation captures the rate of change in modeled and observed POC wt% for the bin-classes rather well. The shallowest bin-class (between 0 and 1000m) represents an exception, as OMEN-SED tends to overestimate POC preservation for this depth class. However, this could also be related to the regridding of the original POC distribution pattern of (Seiter et al., 2004) on to the SEDGEM grid, as some data grid-cells with higher POC wt% on the continental margin are lost due to the restricted SEDGEM resolution (compare Section 4.2). Overall, using this parameterisation a relationship where the labile POC fraction degrades 2 or 3 times faster than the refractory fraction fits the Seiter et al. (2004) data better than a larger spread between both POC pools (i.e. $x \in \{4, 5, 10\}$).

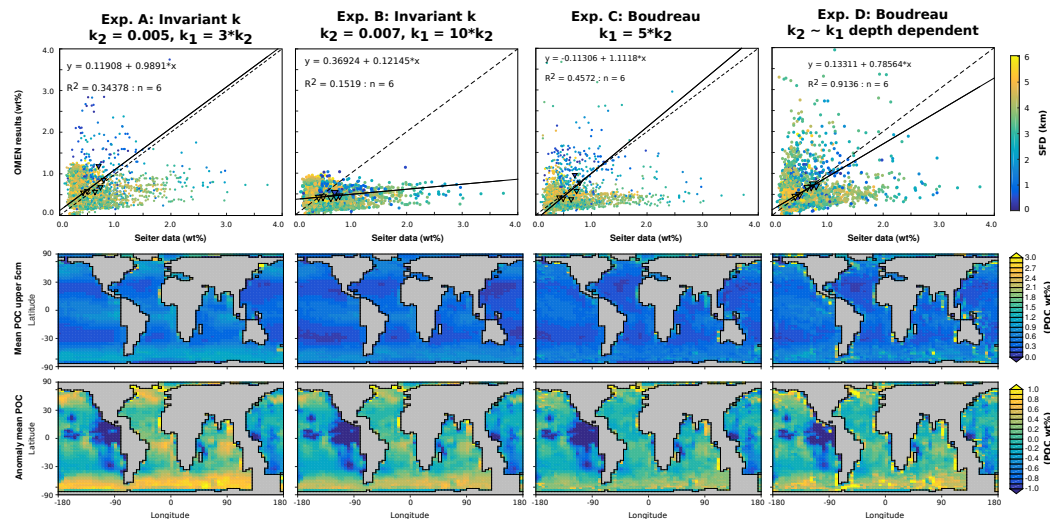


Figure 13. Mean POC concentrations in the upper 5cm of the sediments ($\text{POC}_{5\text{cm}}$) from the coupled OMEN-cGENIE model using representative parameterisations (invariant and after Boudreau, 1997) for the OM degradation rate constants (k_1, k_2 , compare Section 4.2). 1st row: Crossplots as shown in Fig. 11 and 12. 2nd row: $\text{POC}_{5\text{cm}}$ as calculated with OMEN-SED. 3rd row: Difference map of $\text{POC}_{5\text{cm}}$ as calculated with OMEN-SED and interpolated data from Seiter et al. (2004).

Figure 13 compares mean POC concentrations in the upper 5cm of the sediments ($\text{POC}_{5\text{cm}}$) from two globally invariant degradation rate constant approaches (experiments A and B, i.e. $(k_2, x) \in \{(0.005, 3), (0.007, 10)\}$) with two approaches using the relation of Boudreau (1997) (experiments C and D, with $k_2 = k_1/5$ and the depth dependent parameterisation). Within the globally invariant approaches of Figure 12 the depth bin-classes for experiment A fall closest to the 1:1 line whereas

experiment B is the parameterisation with the smallest POC preservation. Maybe use $(k_2, x) = (0.0045, 2)$ instead of $(k_2, x) = (0.007, 10)$, as we hopefully see more OM preservation and larger differences in Fig. 13 All 4 experiments reproduce minimal POC concentrations in the subtropical gyres and generally higher concentrations along the continental margins (Fig. 13, 2nd row). All experiments, however, underestimate mean POC wt% in the surface sediments of the equatorial east Pacific and overestimate POC concentrations in the North Pacific and Southern Oceans, especially experiment A and D (Fig. 13, 3rd row). The depth dependent approach of Boudreau (1997) shows more spatial variability in POC preservation than the other parameterisations. Mention that using slower, anaerobic degradation rate constants as in Palastanga et al. (2011) might help “to simulate more realistic POC concentrations in areas with high POC deposition”. For the globally invariant “best-fit” experiment A modelled total POC degradation (POC_{degr}) rates in the upper sediments decrease from the shelves to the deep sea by up to 2 orders of magnitude (Fig. 14). This is in agreement with data from the literature (e.g. Middelburg et al., 1993, 1997) and other model results (e.g. Thullner et al., 2009) which indicate that the highest degradation rates in marine sediments are found in the coastal ocean ($\text{SFD} < 200\text{m}$). The relative contribution of aerobic POC degradation in the upper sediments increases from the shelves to the deep sea (Fig. 14) which is also consistent with estimates from Thullner et al. (2009) who found that oxygen is responsible for less than 10% of POC_{degr} at 100m SFD and for more than 80% in the deep sea. The oxygen penetration depth in OMEN-SED for experiment A increases from below 1cm at the shelves to more than 10cm in the deep ocean (Fig. 14). Small oxygen penetration depths of a few millimeters are typical for bioturbated sediments at the coastal ocean (e.g. Wenzhöfer and Glud, 2002) and the oxygen penetration depth has been shown to increase exponentially with SFD to more than 10cm in the deep sea (Glud, 2008).

5 Scope of applicability and model limitations

Dominik: Needs polishing!? This is my first draft State-of-the art numerical models representing the full complexity of the diagenetic processes typically perform adequately at reproducing site-specific biogeochemical dynamics, however, tuning model parameters is laborious, the computational demand is high and, thus, their transferability to the global scale is limited. On the other hand, analytical models are very efficient, but existing approaches coupled to global models generally use highly simplified reaction networks, often restricted to oxic degradation with a limited number of explicit pore water tracers. However, our ability to assess the role of organic matter dynamics for global biogeochemical cycles and climate requires tools that resolve the most important biogeochemical processes and tracers explicitly, while at the same time are computationally efficient and have a degree of predictive capability to extrapolate knowledge to data poor areas. The new model OMEN-SED presented here is a legitimate compromise between complexity of biogeochemical processes and computational efficiency. Its scope of applicability covers the entire range

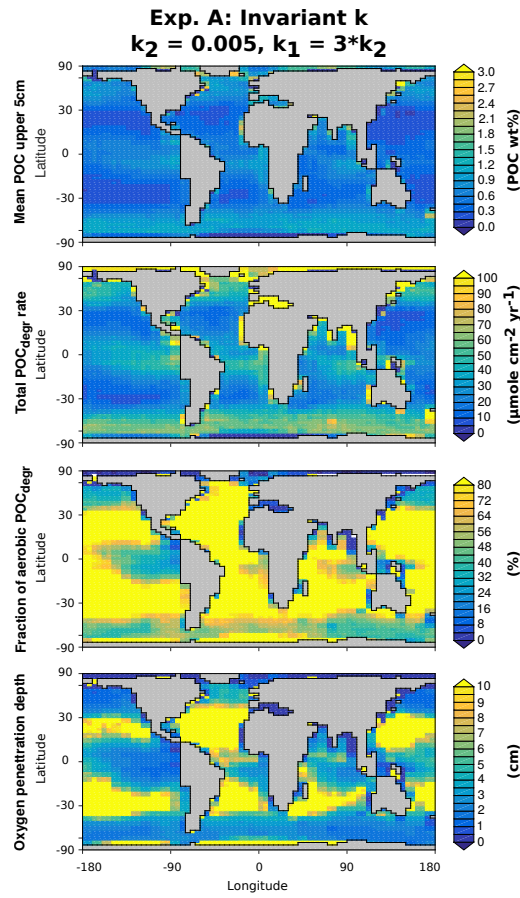


Figure 14. Sediment characteristics related to POC degradation and oxygen consumption for the globally invariant “best-fit” parameterisation (experiment A, $k_2 = 0.005$, $k_1 = 3 \cdot k_2$). Total POC_{degr} rate and fraction of aerobic POC_{degr} are the respective values for the first 5cm in the sediments.

from regional to global scales. OMEN-SED’s computational efficiency facilitates its use in two very different ways. Firstly, it can be coupled to global Earth system models and therefore allows the investigation of coupled global biogeochemical dynamics over different timescales. Secondly, it can be used to calculate quantitative sensitivity indices requiring large sample sizes such as variance- or density-based approaches. Therefore, OMEN-SED can help to quantitatively investigate how systematic variations in model parameters impact the model output, for instance when the model has been tuned to a site-specific problem. Due to the represented anaerobic processes and secondary-redox reactions, OMEN-SED is also useful to investigate the role of benthic-pelagic coupling on the development of ocean anoxia and euxinia for instance during extreme climate events such as OAEs.

1170 On more regional scales it can be applied to systems like continental margins or estuaries which are characterised by complex interactions between different pathways of organic matter degradation and

redox reactions. Here, the model can help to disentangle the complex process interplay that drives the biogeochemical dynamics and give quantifications for upper and lower constraints of carbon and nutrient budgets for these dynamic systems. In addition, OMEN-SED can be used to model eutrophication processes in shallow coastal waters as sediment-water oxygen and nutrient exchange fluxes are explicitly modelled and depend on reoxidation of reduced substances which causes a substantial part of oxygen consumption in these environments.

However, the model presented here, even more complete than previous analytical models, is still associated with a certain degree of simplifications. In order to solve the diagenetic equation analytically important assumptions have been made, which limit the general applicability of the model. One of the most important simplifications is assuming steady-state. When coupled to an Earth system model this assumption is only valid if the relevant variability in boundary conditions and fluxes is generally longer than the characteristic timescales of the reaction-transport processes. In that case the sediment column can be described by a series of pseudo steady-states as it is done in OMEN-SED. Consequently, the model can be used for investigating the long term effects of changes in boundary conditions such as input of OM or bottom water oxidation state on degradation and burial dynamics, for instance during OAEs. Yet, OMEN-SED is not able to predict the system response to short-term or seasonal variations of boundary conditions. Furthermore, the separation of the sediment column into distinct biogeochemical zones and the resulting lack of overlap in degradation pathways may cause distorted organic matter degradation rates for the different TEAs. For instance, in OMEN-SED denitrification does not occur in the oxic zone, while in reality, although inhibited by the presence of oxygen, denitrification can still occur in the oxic zone, even at shallow sediments depths with high OM contents. Manganese and iron are not represented and as such OMEN-SED is not able to model all processes important in coastal marine environments and highly accumulating upwelling regions. This can cause problems when modelling H₂S and PO₄ profiles in anoxic environments as their concentrations are affected by these metal ions (compare Section 3.2). In addition the depth invariant porosity limits the correct calculation of the sediment-water interface flux of dissolved species as in reality porosity decreases with sediment depth.

6 Conclusions

Dominik: Needs polishing!? This is my first draft In this paper we have described and tested a new, analytical early diagenetic model resolving organic matter cycling and associated biogeochemical dynamics called OMEN-SED. Our new model is the first of this class of analytical approaches to explicitly represent oxic degradation, denitrification, sulfate reduction and implicitly methanogenesis, as well as the reoxidation of reduced substances produced during organic matter degradation. Pore water tracers include O₂, NO₃, NH₄, SO₄, H₂S, DIC and ALK and the solid phase includes two fractions of organic matter, Fe-bound P and authigenic Ca-P minerals. We have shown that the

new analytical model is able to reproduce observed pore water profiles from different ocean depths when organic matter partitioning and degradation rate constants are tuned to site specific conditions. An extensive sensitive analysis, based on the novel density-based PAWN method (Pianosi and Wagener, 2015), has been performed to asses the importance of 11 internal model parameters for all resulting SWI-fluxes. The results reveal that the degradation rate constant for labile organic matter is the most influential parameter for all model outputs. Under anoxic conditions secondary redox parameters exert an important control on related SWI-fluxes of SO_4 , H_2S , NH_4 and alkalinity. In addition, the sensitivity analysis showed that globally observed benthic O_2 and NO_3 fluxes fall well into the range of produced model results. OMEN-SED is also used to quantify terminal electron acceptor fluxes across the sediment-water interface associated with organic matter degradation along a global ocean hysometry. The results demonstrate that OMEN-SED is capable of capturing most of the dynamics simulated with a complex, numerical diagentic model and observed fluxes fall well within the range of OMEN-SED results.

Furthermore, the coupling of OMEN-SED to the Earth system model cGENIE is described and the empirical relationship of Boudreau (1997) for the apparent first order degradation rate constant as well as globally invariant rate constants are tested to fit modelled to observed global organic matter concentrations. Generally, large scale patterns of modelled surface sediment organic matter concentrations are in agreement with observations of Seiter et al. (2004). Results show that invariant organic matter degradation rate constants are able to reproduce the observations as well or even better than the empirical relationship of Boudreau (1997). The coupled model is well suited to examine the role of sediments for global biogeochemical cycles and climate and its computational efficiency allows exploring feedbacks within the Earth system in response to a wide range of perturbations and over various timescales.

1235 7 Code Availability

The OMEN-SED source code (Fortran and Matlab) related to this article is provided as a supplementary package together with a ReadMe file, where hardware and software requirements, source code files and model output file management are fully described.

Appendix A: Reaction Network

1240 Appendix B: Sensitivity Analysis

B1

Acknowledgements. We thank Claire Reimers and Filip Meysman for supplying the dataset from the Santa Barbara Basin, as well as Martin Thullner and Jack Middelburg for making the BRNS results and observations in-

Table 15. Primary pathways of organic matter degradation, secondary redox reactions and stoichiometries implemented in the reaction network.

Pathway	Stoichiometry
Primary Redox reactions	
Aerobic degradation	$(\text{CH}_2\text{O})_x(\text{NH}_3)_y(\text{H}_3\text{PO}_4)_z + (\text{x}+2\text{y})\text{O}_2 + (\text{y}+2\text{z})\text{HCO}_3^- \rightarrow (\text{x}+\text{y}+2\text{z})\text{CO}_2 + \text{yNO}_3^- + \text{zHPO}_4^{2-} + (\text{x}+2\text{y}+2\text{z})\text{H}_2\text{O}$
Denitrification	$(\text{CH}_2\text{O})_x(\text{NH}_3)_y(\text{H}_3\text{PO}_4)_z + \frac{(\text{4x}+3\text{y})}{5}\text{NO}_3^- \rightarrow \frac{(2\text{x}+\text{3y})}{5}\text{N}_2 + \frac{(\text{x}-3\text{y}+10\text{z})}{5}\text{CO}_2 + \frac{(\text{4x}+3\text{y}-10\text{z})}{5}\text{HCO}_3^- + \text{zHPO}_4^{2-} + \frac{(\text{3x}+6\text{y}+10\text{z})}{5}\text{H}_2\text{O}$
Sulfate reduction	$(\text{CH}_2\text{O})_x(\text{NH}_3)_y(\text{H}_3\text{PO}_4)_z + \frac{\text{x}}{2}\text{SO}_4^{2-} + (\text{y}-2\text{z})\text{CO}_2 + (\text{y}-2\text{z})\text{H}_2\text{O} \rightarrow \frac{\text{x}}{2}\text{H}_2\text{S} + (\text{x}+\text{y}-2\text{z})\text{HCO}_3^- + \text{yNH}_4^+ + \text{zHPO}_4^{2-}$
Methanogenesis	$(\text{CH}_2\text{O})_x(\text{NH}_3)_y(\text{H}_3\text{PO}_4)_z + (\text{y}-2\text{z})\text{H}_2\text{O} \rightarrow \frac{\text{x}}{2}\text{CH}_4 + \frac{\text{x}-2\text{y}+4\text{z}}{2}\text{CO}_2 + (\text{x}-2\text{z})\text{HCO}_3^- + \text{yNH}_4^+ + \text{zHPO}_4^{2-}$
Secondary Redox reactions	
Nitrification	$\text{NH}_4^+ + 2\text{O}_2 + 2\text{HCO}_3^- \rightarrow \text{NO}_3^- + 2\text{CO}_2 + 3\text{H}_2\text{O}$
Sulfide oxidation	$\text{H}_2\text{S} + 2\text{O}_2 + 2\text{HCO}_3^- \rightarrow \text{SO}_4^{2-} + 2\text{CO}_2 + 2\text{H}_2\text{O}$
AOM	$\text{CH}_4 + \text{CO}_2 + \text{SO}_4^{2-} \rightarrow 2\text{HCO}_3^- + \text{H}_2\text{S}$
Adsorption reactions and mineral precipitation	
NH_4 adsorption	$\text{NH}_4^+ \xrightarrow{\text{K}_{\text{NH}_4}} \text{NH}_4^+$ (ads)
P ad-/desorption ???	$\text{PO}_4^{2-} \xrightarrow{\text{K}_{\text{PO}_4}^{\text{I},\text{II}}} \text{PO}_4^{2-}$ (ads); $\text{HPO}_4^{2-} \xrightarrow{\text{k}_s} \text{Fe-bound P} \xrightarrow{\text{k}_m} \text{HPO}_4^{2-}$
CFA precipitation	$\text{PO}_4^{2-} \xrightarrow{\text{k}_a} \text{CFA}$

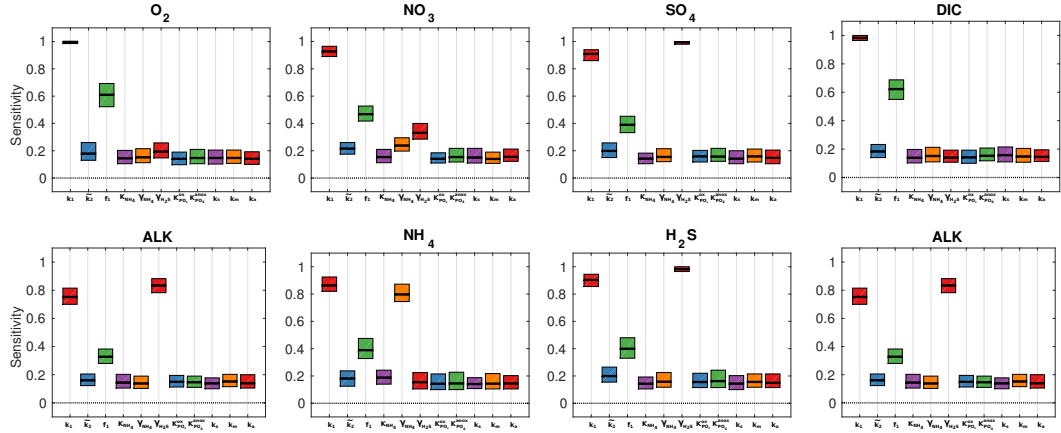


Figure 15. Move to Appendix Box plot of parameter sensitivities for the calculated SWI-fluxes for the 4000m oxic condition. Average sensitivities (black lines) and 90% confidence intervals using $N = 11200$ model evaluations and $Nboot = 100$ bootstrap resamples.

cluded in Section 3.3 available. We are also grateful to Andy Dale for providing the global flux database used in
1245 Section 3.1 and acknowledge BODC for the OMEXDIA dataset (check CD!). We are also grateful to Francesca Pianosi for helpful insights into sensitivity analysis. DH is supported by a graduate teaching studentship by the University of Bristol. SA is supported by funding from the European Unions Horizon 2020 research and innovation programme under the Marie Skłodowska-Curie grant agreement no. 643052 (C-CASCADES). AR acknowledge funding from the EU grant ERC-2013-CoG-617313.

1250 **References**

- Aguilera, D. R., Jourabchi, P., Spiteri, C., and Regnier, P. (2005). A knowledge-based reactive transport approach for the simulation of biogeochemical dynamics in Earth systems. *Geochemistry, Geophysics, Geosystems*, 6(7).
- Aller, R. C. (1984). The importance of relict burrow structures and burrow irrigation in controlling sedimentary solute distributions. *Geochimica et Cosmochimica Acta*, 48(10):1929–1934.
- Aller, R. C. (1988). Benthic fauna and biogeochemical processes in marine sediments: the role of burrow structures. In Blackburn, T. and Sorensen, J., editors, *Nitrogen cycling in coastal marine environments*, pages 301–338. Scope, Chichester.
- Archer, D. and Devol, A. (1992). Benthic oxygen fluxes on the Washington shelf and slope: A comparison of 1260 in situ microelectrode and chamber flux measurements. *Limnology and Oceanography*, 37(3):614–629.
- Archer, D., Eby, M., Brovkin, V., Ridgwell, A., Cao, L., Mikolajewicz, U., Caldeira, K., Matsumoto, K., Munhoven, G., Montenegro, A., and Tokos, K. (2009). Atmospheric Lifetime of Fossil Fuel Carbon Dioxide. *Annual Review of Earth and Planetary Sciences*, 37(1):117–134.
- Archer, D. and Maier-Reimer, E. (1994). Effect of Deep-Sea Sedimentary Calcite Preservation on Atmospheric 1265 CO₂ Concentration. *Nature*, 367(6460):260–263. 00506 WOS:A1994MR49400052.
- Archer, D., Winguth, A., Lea, D., and Mahowald, N. (2000). What caused the glacial/interglacial atmospheric pCO₂ cycles? *Reviews of Geophysics*, 38(2):159–189. 00414.
- Archer, D. E., Morford, J. L., and Emerson, S. R. (2002). A model of suboxic sedimentary diagenesis suitable 1270 for automatic tuning and gridded global domains. *Global Biogeochemical Cycles*, 16(1):17–1.
- Arndt, S., Jørgensen, B., LaRowe, D., Middelburg, J., Pancost, R., and Regnier, P. (2013). Quantifying the degradation of organic matter in marine sediments: A review and synthesis. *Earth-Science Reviews*, 123:53–86.
- Arthur, M. A., Dean, W. E., and Pratt, L. M. (1988). Geochemical and climatic effects of increased marine organic carbon burial at the Cenomanian/Turonian boundary. *Nature*, 335(6192):714–717.
- Berner, R. A. (1980). *Early Diagenesis: A Theoretical Approach*. Princeton University Press.
- Berner, R. A. (1991). A model for atmospheric CO₂ over Phanerozoic time. 291(4):339–376.
- Berner, R. A. (2004). *The Phanerozoic Carbon Cycle: CO₂ and O₂*. Oxford University Press. 00000.
- Billen, G. (1982). An idealized model of nitrogen recycling in marine sediments. *American journal of Science*, 282(4):512–541.
- Bohlen, L., Dale, A. W., and Wallmann, K. (2012). Simple transfer functions for calculating benthic fixed 1280 nitrogen losses and C:N:P regeneration ratios in global biogeochemical models. *Global Biogeochemical Cycles*, 26(3):GB3029.
- Boudreau, B. P. (1984). On the equivalence of nonlocal and radial-diffusion models for porewater irrigation. *Journal of Marine Research*, 42(3):731–735.
- Boudreau, B. P. (1986). Mathematics of tracer mixing in sediments; I, Spatially-dependent, diffusive mixing. *American Journal of Science*, 286(3):161–198.
- Boudreau, B. P. (1996). A method-of-lines code for carbon and nutrient diagenesis in aquatic sediments. *Computers & Geosciences*, 22(5):479–496.
- Boudreau, B. P. (1997). *Diagenetic models and their implementation*, volume 505. Springer Berlin.

- 1290 Boudreau, B. P. (1998). Mean mixed depth of sediments: The wherefore and the why. *Limnology and Oceanography*, 43(3):524–526.
- Boudreau, B. P., Mucci, A., Sundby, B., Luther, G. W., and Silverberg, N. (1998). Comparative diagenesis at three sites on the Canadian continental margin. *Journal of Marine Research*, 56(6):1259–1284.
- Boudreau, B. P. and Ruddick, B. R. (1991). On a reactive continuum representation of organic matter diagenesis. 1295 *American Journal of Science*, 291(5):507–538.
- Broecker, W. S. (1982). Ocean chemistry during glacial time. *Geochimica et Cosmochimica Acta*, 46(10):1689–1705.
- Burdige, D. J. (2006). *Geochemistry of marine sediments*, volume 398. Princeton University Press Princeton.
- Canfield, D. E., Kristensen, E., and Thamdrup, B. (2005). *Aquatic Geomicrobiology*. Gulf Professional Publishing.
- 1300 Colbourn, G., Ridgwell, A., and Lenton, T. M. (2013). The Rock Geochemical Model (RokGeM) v0.9. *Geosci. Model Dev.*, 6(5):1543–1573.
- Conkright, M. E., Locarnini, R. A., Garcia, H. E., O'Brien, T. D., Boyer, T. P., Stephens, C., and Antonov, J. I. (2002). *World Ocean Atlas 2001: Objective analyses, data statistics, and figures: CD-ROM documentation*.
- 1305 US Department of Commerce, National Oceanic and Atmospheric Administration, National Oceanographic Data Center, Ocean Climate Laboratory.
- Devol, A. H. and Christensen, J. P. (1993). Benthic fluxes and nitrogen cycling in sediments of the continental margin of the eastern North Pacific. *Journal of Marine Research*, 51(2):345–372.
- Edwards, N. R. and Marsh, R. (2005). Uncertainties due to transport-parameter sensitivity in an efficient 3-D 1310 ocean-climate model. *Climate Dynamics*, 24(4):415–433.
- Emerson, S. and Bender, M. L. (1981). Carbon fluxes at the sediment-water interface of the deep-sea: calcium carbonate preservation. *Journal of Marine Research*, 39:139–162.
- Emerson, S., Jahnke, R., and Heggie, D. (1984). Sediment-water exchange in shallow water estuarine sediments. *Journal of Marine Research*, 42(3):709–730.
- 1315 Epping, E., van der Zee, C., Soetaert, K., and Helder, W. (2002). On the oxidation and burial of organic carbon in sediments of the Iberian margin and Nazaré Canyon (NE Atlantic). *Progress in Oceanography*, 52(2–4):399–431.
- Glud, R. N. (2008). Oxygen dynamics of marine sediments. *Marine Biology Research*, 4(4):243–289.
- Goloway, F. and Bender, M. (1982). Diagenetic models of interstitial nitrate profiles in deep sea suboxic 1320 sediments1. *Limnology and Oceanography*, 27(4):624–638.
- Goosse, H., Brovkin, V., Fichefet, T., Haarsma, R., Huybrechts, P., Jongma, J., Mouchet, A., Selten, F., Barriat, P.-Y., Campin, J.-M., Deleersnijder, E., Driesschaert, E., Goelzer, H., Janssens, I., Loutre, M.-F., Morales Maqueda, M. A., Opsteegh, T., Mathieu, P.-P., Munhoven, G., Pettersson, E. J., Renssen, H., Roche, D. M., Schaeffer, M., Tartinville, B., Timmermann, A., and Weber, S. L. (2010). Description of the earth system model of intermediate complexity LOVECLIM version 1.2. *Geosci. Model Dev.*, 3(2):603–633.
- 1325 Gypens, N., Lancelot, C., and Soetaert, K. (2008). Simple parameterisations for describing n and p diagenetic processes: Application in the north sea. *Progress in Oceanography*, 76(1):89–110.
- Heinze, C., Maier-Reimer, E., Winguth, A. M. E., and Archer, D. (1999). A global oceanic sediment model for long-term climate studies. *Global Biogeochemical Cycles*, 13(1):221–250.

- 1330 Hensen, C., Zabel, M., and Schulz, H. N. (2006). Benthic Cycling of Oxygen, Nitrogen and Phosphorus. In Schulz, H. D. and Zabel, M., editors, *Marine Geochemistry*, pages 207–240. Springer Berlin Heidelberg.
- Hulse, D., Arndt, S., Wilson, J. D., Munhoven, G., and Ridgwell, A. (2017). Understanding the causes and consequences of past marine carbon cycling variability through models. *Earth-Science Reviews*, 171:349–382.
- 1335 Ilyina, T., Six, K. D., Segschneider, J., Maier-Reimer, E., Li, H., and Núñez-Riboni, I. (2013). Global ocean biogeochemistry model HAMOCC: Model architecture and performance as component of the MPI-Earth system model in different CMIP5 experimental realizations. *Journal of Advances in Modeling Earth Systems*, 5(2):287–315.
- Ingall, E. and Jahnke, R. (1994). Evidence for enhanced phosphorus regeneration from marine sediments overlain by oxygen depleted waters. *Geochimica et Cosmochimica Acta*, 58(11):2571–2575. 00302.
- 1340 Jarvis, I., Lignum, J. S., Gröcke, D. R., Jenkyns, H. C., and Pearce, M. A. (2011). Black shale deposition, atmospheric CO₂ drawdown, and cooling during the Cenomanian-Turonian Oceanic Anoxic Event. *Paleoceanography*, 26(3):n/a–n/a.
- Jenkyns, H. C. (2010). Geochemistry of oceanic anoxic events. *Geochemistry, Geophysics, Geosystems*, 11(3).
- 1345 Jørgensen, B. B. (1978). A comparison of methods for the quantification of bacterial sulfate reduction in coastal marine sediments: II Calculation from mathematical models. *Geomicrobiology Journal*, 1:29–47.
- Jourabchi, P., Cappellen, P. V., and Regnier, P. (2005). Quantitative interpretation of pH distributions in aquatic sediments: A reaction-transport modeling approach. *American Journal of Science*, 305(9):919–956.
- Jørgensen, B. B. and Kasten, S. (2006). Sulfur Cycling and Methane Oxidation. In Schulz, P. D. H. D. and 1350 Zabel, D. M., editors, *Marine Geochemistry*, pages 271–309. Springer Berlin Heidelberg.
- Kolmogorov, A. (1933). Sulla determinazione empirica di una legge di distribuzione. *Giorn. Ist Ital. Attuari*, 4, 91.
- Krom, M. D. and Berner, R. A. (1980). Adsorption of phosphate in anoxic marine sediments1. *Limnology and Oceanography*, 25(5):797–806.
- 1355 Krumins, V., Gehlen, M., Arndt, S., Van Cappellen, P., and Regnier, P. (2013). Dissolved inorganic carbon and alkalinity fluxes from coastal marine sediments: Model estimates for different shelf environments and sensitivity to global change. *Biogeosciences*.
- Lee, C., Wakeham, S. G., and I. Hedges, J. (2000). Composition and flux of particulate amino acids and chloropigments in equatorial Pacific seawater and sediments. *Deep Sea Research Part I: Oceanographic Research Papers*, 47(8):1535–1568.
- 1360 Lenton, T. M. and Watson, A. J. (2000). Redfield revisited: 1. Regulation of nitrate, phosphate, and oxygen in the ocean. *Global Biogeochemical Cycles*, 14(1):225–248.
- Li, Y.-H. and Gregory, S. (1974). Diffusion of ions in sea water and in deep-sea sediments. *Geochimica et Cosmochimica Acta*, 38(5):703–714.
- 1365 Longhurst, A., Sathyendranath, S., Platt, T., and Caverhill, C. (1995). An estimate of global primary production in the ocean from satellite radiometer data. *Journal of Plankton Research*, 17(6):1245–1271.
- Mackenzie, F. T. (2005). *Sediments, Diagenesis, and Sedimentary Rocks: Treatise on Geochemistry, Second Edition*. Elsevier. 00000.

- Meysman, F. J. R., Middelburg, J. J., Herman, P. M. J., and Heip, C. H. R. (2003). Reactive transport in surface
1370 sediments. II. Media: an object-oriented problem-solving environment for early diagenesis. *Computers & Geosciences*, 29(3):301–318. 00067.
- Middelburg, J. J., Soetaert, K., and Herman, P. M. (1997). Empirical relationships for use in global diagenetic models. *Deep Sea Research Part I: Oceanographic Research Papers*, 44(2):327–344.
- Middelburg, J. J., Soetaert, K., Herman, P. M. J., and Heip, C. H. R. (1996). Denitrification in marine sediments:
1375 A model study. *Global Biogeochemical Cycles*, 10(4):661–673.
- Middelburg, J. J., Vlug, T., Jaco, F., and van der Nat, W. A. (1993). Organic matter mineralization in marine systems. *Global and Planetary Change*, 8(1):47–58.
- Mort, H. P., Adatte, T., Föllmi, K. B., Keller, G., Steinmann, P., Matera, V., Berner, Z., and Stüben, D. (2007).
1380 Phosphorus and the roles of productivity and nutrient recycling during oceanic anoxic event 2. *Geology*, 35(6):483–486. 00135.
- Munhoven, G. (2007). Glacial-interglacial rain ratio changes: Implications for atmospheric and ocean–sediment interaction. *Deep Sea Research Part II: Topical Studies in Oceanography*, 54(5–7):722–746.
- Najjar, R. G., Jin, X., Louanchi, F., Aumont, O., Caldeira, K., Doney, S. C., Dutay, J.-C., Follows, M., Gruber,
1385 N., Joos, F., Lindsay, K., Maier-Reimer, E., Matear, R. J., Matsumoto, K., Monfray, P., Mouchet, A., Orr, J. C., Plattner, G.-K., Sarmiento, J. L., Schlitzer, R., Slater, R. D., Weirig, M.-F., Yamanaka, Y., and Yool, A. (2007). Impact of circulation on export production, dissolved organic matter, and dissolved oxygen in the ocean: Results from Phase II of the Ocean Carbon-cycle Model Intercomparison Project (OCMIP-2). *Global Biogeochemical Cycles*, 21(3):GB3007.
- Palastanga, V., Slomp, C. P., and Heinze, C. (2011). Long-term controls on ocean phosphorus and oxygen in a global biogeochemical model. *Global Biogeochemical Cycles*, 25(3):GB3024.
- Pianosi, F., Beven, K., Freer, J., Hall, J. W., Rougier, J., Stephenson, D. B., and Wagener, T. (2016). Sensitivity analysis of environmental models: A systematic review with practical workflow. *Environmental Modelling & Software*, 79:214–232.
- Pianosi, F., Sarrazin, F., and Wagener, T. (2015). A Matlab toolbox for Global Sensitivity Analysis. *Environmental Modelling & Software*, 70:80–85.
- Pianosi, F. and Wagener, T. (2015). A simple and efficient method for global sensitivity analysis based on cumulative distribution functions. *Environmental Modelling & Software*, 67:1–11.
- Regnier, P., Dale, A. W., Arndt, S., LaRowe, D. E., Mogollon, J., and Van Cappellen, P. (2011). Quantitative
1400 analysis of anaerobic oxidation of methane (AOM) in marine sediments: A modeling perspective. *Earth-Science Reviews*, 106(1):105–130.
- Reimers, C. E., Lange, C. B., Tabak, M., and Bernhard, J. M. (1990). Seasonal spillover and varve formation in the Santa Barbara Basin, California. *Limnology and Oceanography*, 35(7):1577–1585.
- Reimers, C. E., Ruttenberg, K. C., Canfield, D. E., Christiansen, M. B., and Martin, J. B. (1996). Porewater
1405 pH and authigenic phases formed in the uppermost sediments of the Santa Barbara Basin. *Geochimica et Cosmochimica Acta*, 60(21):4037–4057.
- Ridgwell, A. and Hargreaves, J. C. (2007). Regulation of atmospheric CO₂ by deep-sea sediments in an Earth system model. *Global Biogeochemical Cycles*, 21(2):n/a–n/a.

- Ridgwell, A., Hargreaves, J. C., Edwards, N. R., Annan, J. D., Lenton, T. M., Marsh, R., Yool, A., and Watson, A. (2007). Marine geochemical data assimilation in an efficient Earth System Model of global biogeochemical cycling. *Biogeosciences*, 4(1):87–104. 00090.
- Ridgwell, A. and Zeebe, R. E. (2005). The role of the global carbonate cycle in the regulation and evolution of the Earth system. *Earth and Planetary Science Letters*, 234(3–4):299–315. 00172.
- Ruttenberg, K. C. (1993). Reassessment of the oceanic residence time of phosphorus. *Chemical Geology*, 107(3):405–409.
- Schulz, H. D. (2006). Quantification of Early Diagenesis: Dissolved Constituents in Pore Water and Signals in the Solid Phase. In Schulz, P. D. H. D. and Zabel, D. M., editors, *Marine Geochemistry*, pages 73–124. Springer Berlin Heidelberg.
- Seiter, K., Hensen, C., Schröter, J., and Zabel, M. (2004). Organic carbon content in surface sediments—defining regional provinces. *Deep Sea Research Part I: Oceanographic Research Papers*, 51(12):2001–2026.
- Shaffer, G., Malskær Olsen, S., and Pepke Pedersen, J. O. (2008). Presentation, calibration and validation of the low-order, DCESS Earth System Model (Version 1). *Geosci. Model Dev.*, 1(1):17–51. 00007.
- Slomp, C., Malschaert, J., and Van Raaphorst, W. (1998). The role of adsorption in sediment-water exchange of phosphate in north sea continental margin sediments. *Limnology and Oceanography*, 43(5):832–846.
- Slomp, C. P., Epping, E. H., Helder, W., and Van Raaphorst, W. (1996). A key role for iron-bound phosphorus in authigenic apatite formation in north atlantic continental platform sediments. *Journal of Marine Research*, 54(6):1179–1205.
- Smirnov, N. V. (1939). On the estimation of the discrepancy between empirical curves of distribution for two independent samples. *Bull. Math. Univ. Moscou*, 2(2).
- Soetaert, K., Herman, P. M. J., and Middelburg, J. J. (1996). A model of early diagenetic processes from the shelf to abyssal depths. *Geochimica et Cosmochimica Acta*, 60(6):1019–1040.
- Soetaert, K., Middelburg, J. J., Herman, P. M. J., and Buis, K. (2000). On the coupling of benthic and pelagic biogeochemical models. *Earth-Science Reviews*, 51(1–4):173–201.
- Stein, R., Rulkötter, J., and Welte, D. H. (1986). Accumulation of organic-carbon-rich sediments in the Late Jurassic and Cretaceous Atlantic Ocean — A synthesis. *Chemical Geology*, 56(1–2):1–32.
- Stolpovsky, K., Dale, A. W., and Wallmann, K. (2015). Toward a parameterization of global-scale organic carbon mineralization kinetics in surface marine sediments. *Global Biogeochemical Cycles*, 29(6):2015GB005087.
- Stumm, W. and Morgan, J. J. (2012). *Aquatic Chemistry: Chemical Equilibria and Rates in Natural Waters*. John Wiley & Sons.
- Teal, L., Bulling, M., Parker, E., and Solan, M. (2010). Global patterns of bioturbation intensity and mixed depth of marine soft sediments. *Aquatic Biology*, 2(3):207–218.
- Thullner, M., Dale, A. W., and Regnier, P. (2009). Global-scale quantification of mineralization pathways in marine sediments: A reaction-transport modeling approach. *Geochemistry, Geophysics, Geosystems*, 10(10).
- Thullner, M., Van Cappellen, P., and Regnier, P. (2005). Modeling the impact of microbial activity on redox dynamics in porous media. *Geochimica et Cosmochimica Acta*, 69(21):5005–5019.

- Tjiputra, J. F., Roelandt, C., Bentsen, M., Lawrence, D. M., Lorentzen, T., Schwinger, J., Seland, Ø., and Heinze, C. (2013). Evaluation of the carbon cycle components in the Norwegian Earth System Model (NorESM).
 1450 *Geosci. Model Dev.*, 6(2):301–325. 00057.
- Toth, D. J. and Lerman, A. (1977). Organic matter reactivity and sedimentation rates in the ocean. *American Journal of Science*, 277(4):465–485.
- Tromp, T. K., Van Cappellen, P., and Key, R. M. (1995). A global model for the early diagenesis of organic carbon and organic phosphorus in marine sediments. *Geochimica et Cosmochimica Acta*, 59(7):1259–1284.
 1455 00164.
- Tsandev, I. and Slomp, C. (2009). Modeling phosphorus cycling and carbon burial during Cretaceous Oceanic Anoxic Events. *Earth and Planetary Science Letters*, 286(1–2):71–79.
- Ullman, W. J. and Aller, R. C. (1982). Diffusion coefficients in nearshore marine sediments. *Limnology and Oceanography*, 27(3):552–556.
- 1460 Van Cappellen, P. and Berner, R. A. (1988). A mathematical model for the early diagenesis of phosphorus and fluorine in marine sediments; apatite precipitation. *American Journal of Science*, 288(4):289–333.
- Van Cappellen, P. and Ingall, E. D. (1994). Benthic phosphorus regeneration, net primary production, and ocean anoxia: A model of the coupled marine biogeochemical cycles of carbon and phosphorus. *Paleoceanography*, 9(5):677–692.
- 1465 Van Cappellen, P. and Wang, Y. (1995). Metal cycling in surface sediments: modeling the interplay of transport and reaction. *Metal contaminated aquatic sediments*, pages 21–64.
- Van Cappellen, P. and Wang, Y. (1996). Cycling of iron and manganese in surface sediments; a general theory for the coupled transport and reaction of carbon, oxygen, nitrogen, sulfur, iron, and manganese. *American Journal of Science*, 296(3):197–243.
- 1470 van Weering, T. C. E., de Stigter, H. C., Boer, W., and de Haas, H. (2002). Recent sediment transport and accumulation on the NW Iberian margin. *Progress in Oceanography*, 52(2):349–371.
- Vanderborght, J.-P. and Billen, G. (1975). Vertical distribution of nitrate concentration in interstitial water of marine sediments with nitrification and denitrification. *Limnology and Oceanography*, 20(6):953–961.
- Vanderborght, J.-P., Wollas, R., and Bitten, G. (1977). Kinetic models of diagenesis in disturbed sediments.
 1475 Part 2. Nitrogen diagenesis. *Limnology and Oceanography*, 22(5):794–803.
- Wakeham, S. G., Hedges, J. I., Lee, C., Peterson, M. L., and Hernes, P. J. (1997). Compositions and transport of lipid biomarkers through the water column and surficial sediments of the equatorial Pacific Ocean. *Deep Sea Research Part II: Topical Studies in Oceanography*, 44(9):2131–2162.
- Wang, Y. and Van Cappellen, P. (1996). A multicomponent reactive transport model of early diagenesis: Application to redox cycling in coastal marine sediments. *Geochimica et Cosmochimica Acta*, 60(16):2993–3014.
 1480 00283.
- Wenzhöfer, F. and Glud, R. N. (2002). Benthic carbon mineralization in the Atlantic: a synthesis based on in situ data from the last decade. *Deep Sea Research Part I: Oceanographic Research Papers*, 49(7):1255–1279.
- Wolf-Gladrow, D. A., Zeebe, R. E., Klaas, C., Körtzinger, A., and Dickson, A. G. (2007). Total alkalinity:
 1485 The explicit conservative expression and its application to biogeochemical processes. *Marine Chemistry*, 106(1–2):287–300.